

UNIVERSITY OF KWAZULU-NATAL

PMSG-BASED WIND POWER INTEGRATION— modelling and  
analysis of impacts on the dynamic performances of a power system and  
mitigation under stochastic wind disturbances

Ayele Nigussie Legesse



October 2017

Supervisor: Dr Akshay Kumar Saha

Co-supervisor: Dr Rudiren Pillay Carpanen

**PMSG-BASED WIND POWER INTEGRATION— modelling and  
analysis of impacts on the dynamic performances of a power system and  
mitigation under stochastic wind disturbances**

Ayele Nigussie Legesse

In fulfilment of the Degree of Doctor of Philosophy in Electrical  
Engineering, College of Agriculture, Engineering and Science,  
University of KwaZulu-Natal, Durban, South Africa



October 2017

Supervisor:

As the candidate's supervisor, I agree to the submission of this thesis

Dr Akshay Kumar Saha\_\_\_\_\_

Date\_\_\_\_\_

Co-supervisor:

As the candidate's co-supervisor, I agree to the submission of this thesis


Dr Rudiren Pillay Carpanen\_\_\_\_\_

Date\_\_\_\_\_

## DECLARATION 1 - PLAGIARISM

I, Ayele Nigussie Legesse, with Student Number 214584668, with the thesis entitled "PMSG-BASED WIND POWER INTEGRATION— modelling and analysis of impacts on the dynamic performances of a power system and mitigation under stochastic wind disturbances," declare that

1. The research reported in this thesis, except where otherwise indicated, is my original research.
2. This thesis has not been submitted for any degree or examination at any other university.
3. This thesis does not contain other person's data, pictures, graphs or other information, unless specifically acknowledged as being sourced from other persons.
4. This thesis does not contain other persons' writing, unless specifically acknowledged as being sourced from other researchers. Where other written sources have been quoted, then:
  - a. Their words have been re-written but the general information attributed to them has been referenced
  - b. Where their exact words have been used, then their writing has been placed in italics and inside quotation marks, and referenced.
5. This thesis does not contain text, graphics or tables copied and pasted from the Internet, unless specifically acknowledged, and the source being detailed in the thesis and in the References sections.

Signed..........Date .....08 Dec  
2017.....

## DECLARATION 2 - PUBLICATIONS


DETAILS OF CONTRIBUTION TO PUBLICATIONS that form part and/or include research presented in this thesis (include publications in preparation, submitted, in press and published and give details of the contributions of each author to the work and writing of each publication).

### JOURNAL PUBLICATIONS

1. Ayele N. Legesse, Akshay K. Saha and Rudiren Pillay Carpanen, “Damping local oscillations of a direct-drive PMSG wind turbine”, *International Journal of Engineering & Technology*, Vol. 9 No. 1, Feb—March 2017, pp. 158—168, DOI: 10.21817/ijet/2017/v9i1/170901411. [published]
2. Ayele N. Legesse, Akshay K. Saha and Rudiren Pillay Carpanen, “Characterisation of Wind Speed Series and Power in Durban”, *Journal of Energy in South Africa*, Vol. 28 No. 1, August 2017, pp. 66—78, DOI: <http://dx.doi.org/10.17159/2413-3051/2017/v28i3a1683>. [published]
3. Ayele N. Legesse, Akshay K. Saha and Rudiren Pillay Carpanen, “Enhancing the dynamic performance of a wind turbine driven PMSG using compensators”, submitted to *Electric Power Systems Research*, July 2015. [Under review]
4. Ayele N. Legesse, Akshay K. Saha and Rudiren Pillay Carpanen, “Factors affecting the small-signal stability of a power system with a direct-driven PMSG wind turbine and mitigation of detrimental effects”, submitted to *IETE Journal of Research*, September 2016. [Under review]
5. Ayele N. Legesse, Akshay K. Saha and Rudiren Pillay Carpanen, “Improving the Dynamic Performance of a Direct-Drive PMSG Wind Turbine Using Stator Damper Windings”, submitted to *Indian Journal of Science and Technology*, October 2016. [Under review]

### CONFERENCE PROCEEDINGS

6. Ayele N. Legesse, Akshay K. Saha and Rudiren Pillay Carpanen, “Generating wind speed time series for time domain simulation of wind turbines”, Proceedings of the 25<sup>th</sup> Southern African Universities Power Engineering Conference, SAUPEC 2017, Stellenbosch University, South Africa, January 30 — February 01, 2017, pp. 453—459. [Published]
7. Ayele N. Legesse, Akshay K. Saha and Rudiren Pillay Carpanen, “Enhancing the Dynamic Performance of a Direct-Drive PMSG Wind Turbine Using Damping Controllers”, Proceedings of the 24<sup>th</sup> Southern African Universities Power Engineering Conference, SAUPEC 2016, Vaal University of Technology, South Africa, 26—28 January 2016, pp. 684—689. [Published]

Signed..........Date .....08 Dec 2017.....

## ACKNOWLEDGMENTS

I am highly grateful to my supervisor, Dr Akshay Kumar Saha, as without his encouragement, insight, guidance, and professional expertise, the completion of this research would not have been possible. My special thanks go to my co-supervisor, Dr Rudiren Pillay Carpanen. Dear my supervisors, your support, professional guidance and constructive criticism during my study are highly appreciated.

I would also like to take this opportunity to sincerely thank the University of KwaZuluNatal, South Africa, Haramaya University, Ethiopia, and the Federal Democratic Republic of Ethiopia Ministry of Education for giving me the chance and fund for my doctoral study in Electrical Engineering.

I sincerely appreciate the South African Weather Services (SAWS) for providing wind speed data used in this research.

I would also like to express my appreciation to my dear friends and colleagues, both at the University of KwaZulu-Natal and back at home, who have been supportive throughout my doctoral study in one way or the other.

Finally, my deepest thanks go to my beloved wife, Selam Mekonen and my lovely children, Ruhama, Soyam and Abenezer for their unreserved affection, love, understanding, and patience during my three years' study.

## ABSTRACT

Because of the ever-growing demand for electrical energy and environmental challenges of fossil fuel consumption, a priority has been given to the development of wind energy systems, among which, currently, permanent magnet synchronous generator (PMSG)-based wind power is receiving much attention from researchers, engineers, and turbine manufacturers. However, high PMSG-based wind power integration into a power system brings several challenges to transmission system operators. One of the challenges is its impacts on the dynamic performances of a power system due to the presence of stochastic wind disturbances. Thus, for a thorough investigation of the influences of stochastic wind speed disturbances, a proper wind speed model should be adopted. Therefore, this thesis proposes the use of Markov chain model for modelling wind speed series in dynamic simulations of wind turbines. In this regard, comparison of statistical quantities of measured wind speed data from Durban and Markov model generated ones confirms the accuracy of the model adopted.

The results have shown that the dynamic performances of a power system deteriorate with the presence of stochastic wind speed disturbances, and thus the need for improving poor dynamic performances. Wind gusts cause stress, over currents, over voltages and instability in a power system. This thesis, therefore, introduces novel mitigation techniques based on virtual controls stemming from real resistors, compensators, and damper windings, and supplementary controllers to enhance the dynamic performances of a wind turbine directdriven PMSG, the main component of a PMSG-based wind farm. In the proposed schemes, the virtual controllers adjust the terminal d- and q-axis reference voltages in the generator side converter controller and their influences on the dynamic performances of the wind turbine are investigated. MATLAB/Simulink simulations on a wind turbine connected to an infinite bus show that virtual controls are effective in enhancing the dynamic performances of the PMSG. Local oscillations caused by wind disturbances are efficiently suppressed. Overall, the proposed mitigation techniques smooth the rotor speed and power of a PMSG, and hence reducing the influences of the stochastic wind speed disturbances.



Furthermore, the results have demonstrated that stochastic wind speed disturbances affect the dynamic performances of a power system containing a PMSG-based wind farm as the dynamics of synchronous machines within the system depend on power balance, which is influenced by the power response of the wind farm. Finally, investigations in this thesis have confirmed that virtual controls and FACTS devices such as STATCOM and SVC are efficient in improving the dynamic performances of a power system containing PMSG-based wind farms under stochastic wind disturbances.

## CONTENTS

DECLARATION 1 - PLAGIARISM.....	
ii	DECLARATION 2 - PUBLICATIONS
.....	iii ACKNOWLEDGMENTS
.....	v ABSTRACT
.....	vi
CONTENTS .....	
vii	LIST OF FIGURES
.....	xi LIST OF TABLES
.....	xiv
LIST OF ABBREVIATIONS AND VARIABLES .....	
xv	
1	GENERAL INTRODUCTION .....
	1
	1.1 Introduction .....
1	
	1.2 Problem Formulation .....
	2
	1.3 Scope of the Thesis .....
	5
	1.4 Contributions to Knowledge .....
	6
	1.5 Thesis Overview .....
	7
2	LITERATURE REVIEW .....
	8
	2.1 Introduction .....
8	
	2.2 Power System Dynamics .....
	9
	2.3 Power System Disturbances .....
	11
	2.4 Wind Process.....
	12

2.4.1	General	12
2.4.2	Review of Wind Speed Modelling	13
2.5	Review of Wind Power Integration	15
2.5.1	Wind Turbines	15
2.5.2	Principle of Operation	16
2.5.3	Classification of Wind Turbines	18
2.5.4	Wind Turbine Direct-Driven PMSG	19
2.6	General Overview	20
2.7	Impacts of Wind Turbine Direct-Driven PMSGs: Review	22
2.7.1	Dynamic Stability of Wind Turbine Direct-Driven PMSG	22
2.7.2	System-Wide Dynamic Stability	24
2.8	Review of Mitigation Techniques for Dynamic Performances	26
2.8.1	Active Power Control	26
2.8.2	Reactive Power Control	28
2.8.3	FACTS Devices	29
2.8.4	Virtual Control	29
2.9	Conclusion	30
3	MODELLING AND ANALYSIS OF WIND SPEED SERIES	31
3.1	Introduction	31
3.2	Markov Chain Wind Speed Model	32
3.2.1	Introduction	32
3.2.2	Data Analysis and Markov Chain Model (MCM)	33

3.2.2.1	Wind Speed Data .....	33	
3.2.2.2	Data Analysis .....	33	
3.2.3	Developing .....	35	MCM
3.2.3.1	TPM and Limiting Probabilities .....	36	
3.2.3.2	Generation of Wind Speed Series Using MCM .....	39	
3.2.4	Validation of the Markov Model .....	42	
3.2.5	Weibull Distribution.....	43	
3.2.6	Intermediate Wind Speeds .....	43	
3.2.7	Wind Power Density (WPD) Distribution .....	44	
3.2.8	Results and Discussion .....	45	
3.2.8.1	Wind Speed Analysis .....	45	
3.2.8.2	MCM and Weibull Wind Speed Distributions .....	46	
3.2.8.3	Intermediate Wind Speed Series .....	47	
3.2.8.4	Power Density Distribution .....	47	
3.3	Composite Wind Speed Model .....	49	
3.4	Fourier Series Wind Speed Model .....	50	
3.5	Conclusion .....	51	
4	MODELLING A WIND TURBINE DIRECT-DRIVEN PMSG FOR DYNAMIC SIMULATIONS.....	52	
4.1	Introduction .....	52	

4.2	Wind Turbine Direct-Driven PMSG .....	52
4.2.1	Drive .....	53
4.2.2	Pitch Angle and Speed Controllers .....	54
4.2.3	DC-Link .....	55
4.2.4	Grid Side Converter Controller .....	56
4.3	Power Grid Model .....	57
4.4	Proposed Mitigation Method (Using Compensators) .....	58
4.4.1	PMSG Model with Compensators .....	58
4.4.2	Modified Generator Side Converter Controller (MGSCC) .....	61
4.5	Simulation Results and Discussion .....	62
4.5.1	Large Load Changes .....	63
4.5.1.1	Effect of a Lag Compensator .....	63
4.5.1.2	Effects of a Lead Compensator .....	67
4.5.1.3	Effect of a Lead-Lag Compensator .....	68
4.5.2	Wind Speed Disturbances .....	68
4.5.3	Effectiveness of Compensators over Range of Wind Speeds .....	70
4.5.4	Response to Stochastic Wind Speed Series.....	71
4.6	Conclusion .....	73
5	ENHANCING THE DYNAMIC PERFORMANCES OF A WIND TURBINE DIRECT-DRIVEN PMSG .....	75
5.1	Introduction .....	75
5.2	Mitigation Using VRs .....	76
5.2.1	PMSG Model Including VRs .....	76

5.3 Mitigation Using FFAs .....	78
5.3.1 PMSG Model with Fictitious Damper Windings .....	78
5.4 Modified Generator Side Converter Controllers (MGSCC) .....	85
5.4.1 MGSCC with VRs .....	85
5.4.2 MGSCC with FFA .....	86
5.4.3 MGSCC with SDCs .....	87
5.5 Simulation Results and Discussion .....	88
5.5.1 Response to Constant Wind Speed and Large Load Changes.....	89
5.5.2 Response to Stochastic Wind Speed Series.....	94
5.6 Conclusion .....	98
6 IMPACTS OF A PMSG-BASED WIND FARM ON POWER SYSTEM DYNAMICS .....	100
6.1 Introduction .....	100
6.2 The Test System .....	101
6.3 Modelling the Test System .....	102
6.3.1 PMSG-Based Wind Farm Model .....	102
6.3.2 Synchronous Machine Model .....	105
6.3.2.1 The Swing Equation .....	105
6.3.2.2 Governor Model .....	107
6.3.2.3 Exciter Model .....	107
6.3.3 Load Model .....	108
6.4 Mitigation Techniques .....	108
6.4.1 Enhancing the Dynamic Performances of the PMSG .....	108
6.4.2 Conventional Methods .....	109

6.4.3	FACTS Devices .....	112
6.4.3.1	SVC Model .....	112
6.4.3.2	STATCOM Model .....	112
6.5	Results and Discussion .....	114
6.5.1	Effects of Dynamic Characteristics of PMSG-Based Wind Farm on Power System Dynamics .....	114
6.5.2	Effects of an SVC on the Dynamic performances of the Test System .....	119
6.5.3	Effects of a STATCOM on the Dynamic Performances of the Test System .....	120
6.5.4	Effects of Power System Disturbances on the PMSG-Based Wind Farm ... ..	122
6.5.5	Effects of Stochastic Wind Speed Series .....	123
6.6	Conclusion .....	125
7	CONCLUSIONS AND RECOMMENDATIONS.....	127
7.1	Introduction .....	127
7.2	Conclusions .....	128
7.2.1	Chapter 3: Modelling and Analysis of Wind Speed Series .....	128
7.2.2	Chapter 4: Modelling a Wind Turbine Direct-Driven PMSG for Dynamic Simulations.....	129
7.2.3	Chapter 5: Enhancing the Dynamic Performances of a Wind Turbine Direct-Driven PMSG .....	129
7.2.4	Chapter 6: Impacts of a PMSG-Based Wind Farm on Power System Dynamics .....	131
7.3	Suggestions for Future Research .....	131
8	REFERENCES.....	133
		8
		APPENDIX
		A

.....	146	9 APPENDIX
B .....	148	

## LIST OF FIGURES

Figure 2.1. Horizontal axis wind turbine [79] .....	16
Figure 2.2. Forces on the blade of a wind turbine .....	16
Figure 2.3. Power coefficient vs. tip-speed ratio curve for a typical wind turbine .....	17
Figure 2.4: Typical wind turbine power curve .....	18
Figure 2.5. A wind turbine driven PMSG connected to a grid [83] .....	19
Figure 2.6. A wind turbine direct-drive PMSG connected to an infinite bus.....	23
Figure 2.7. IEEE 3-generator 9-bus test system with a wind farm .....	24
Figure 2.8. Pitch angle control .....	27
Figure 2.9. Active power damping scheme .....	27
Figure 2.10. Active power supplementary loop .....	28
Figure 2.11. Reactive power supplementary loop .....	28
Figure 3.1. Observed wind speed series at DSM .....	33
Figure 3.2. Monthly hourly mean wind speeds at DSM at 8 m hub height .....	34
Figure 3.3. Monthly hourly mean wind speeds at DSM at 70 m hub height .....	34
Figure 3.4. Annual mean wind speeds at different hub heights .....	35
Figure 3.5. Synthetic wind speed data .....	40
Figure 3.6. PDFs of measured, generated wind speeds and Weibull distribution .....	42
Figure 3.7. Wind speeds generated using a Weibull distribution based on MCM data .....	44
Figure 3.8. Wind speeds generated using Gaussian distribution .....	44
Figure 3.9. Cumulative density probability for (a) wind speeds (b) wind power density in Durban .....	45

Figure 3.10. Wind power density over a year at 70 m hub height .....	48
Figure 3.11. Wind power density at 100 m hub height .....	48
Figure 3.12. Mean wind power density at different hub heights .....	48
Figure 3.13. Typical composite wind speed series .....	50
Figure 3.14. Wind speed series represented by a Fourier series method .....	51
Figure 4.1. A wind turbine direct-driven PMSG connected to a grid .....	53
Figure 4.2. $C_p$ -TSR-pitch curves of the wind turbine at 11 m/s wind speed .....	54
Figure 4.3. Grid-side controller structure .....	57
Figure 4.4. One-line diagram of the grid, transmission line and transformer .....	57
Figure 4.5. (a) d-axis and (b) q-axis equivalent circuits of a PMSG with proposed compensator .....	58
Figure 4.6. Block diagram of the PMSG (a) d-axis and (b) q-axis equivalent circuits with $H(s)$ .....	59
Figure 4.7. Generator side controller with virtual compensators (a) $i_d$ controller (b) $i_q$ controller .....	61
Figure 4.8. Effect of a lag compensator on rotor speed .....	64
Figure 4.9. Effect of a lag compensator on (a) real power (b) reactive power responses .....	65
Figure 4.10. (a) Mechanical torque response (b) Electromagnetic torque response .....	66
Figure 4.11. Effect of a lag compensator on (a) DC- link voltage (b) terminal voltage responses .....	66
Figure 4.12. Effect of lead compensator on rotor speed .....	67
Figure 4.13. (a) electromagnetic torque (b) terminal voltage responses .....	67
Figure 4.14. Effect of a lead-lag compensator on electromagnetic torque response .....	68
Figure 4.15. Rotor speed response for small disturbances .....	69
Figure 4.16. (a) Real power (b) electromagnetic torque responses for wind speed disturbances .....	69
Figure 4.17. Effects of lag and lead compensators on the damping ratio of rotor speed .....	70
Figure 4.18. Effects of lag and lead compensators on the settling time of rotor speed .....	71
Figure 4.19. Electromagnetic torque response for stochastic wind speed series .....	72
Figure 4.20. Real power response for stochastic wind speed series .....	72



.....	72	Figure 5.1. Equivalent circuits of a PMSG with VRs (a) d-axis circuit with series VR (b) q-axis circuit with series VR (c) d-axis circuit with parallel VR (d) q-axis circuit with parallel
VR .....	77	
Figure 5.2. Block diagrams of the PMSG equivalent circuits (a) d-axis circuit with series VR (b) q-axis circuit with series VR (c) d-axis circuit with parallel VR (d) q-axis circuit with parallel VR .....	77	
Figure 5.3. Windings of the PMSG and fictitious damper windings .....	78	
Figure 5.4. Block diagram of (a) d-axis and (b) q-axis of the PMSG with fictitious damper windings .....	84	
Figure 5.5. Proposed generator side controller (a) $i_d$ controller (b) $i_q$ controller with VR scheme .....	85	
Figure 5.6. Proposed generator side controller (a) $i_{sd}$ (b) $i_{sq}$ controller with FFA .....	86	
Figure 5.7. Proposed generator side controller with (a) d-axis SDC and (b) q-axis SDC.....	87	
Figure 5.8. (a) Rotor speed (b) electromagnetic torque for step wind speed .....	90	
Figure 5.9. (a) Real (b) reactive power responses to a step wind speed .....	92	
Figure 5.10. (a) DC-link (b) terminal voltage responses to a step wind speed .....	93	
Figure 5.11. Effect of parallel VRs on (a) rotor speed (b) DC- link voltage .....	93	
Figure 5.12. Stochastic wind speed series .....	94	
Figure 5.13. (a) Rotor speed (b) electromagnetic torque responses for stochastic wind speed .....	95	
Figure 5.14. (a) Real (b) reactive power responses for stochastic wind speed .....	96	
Figure 5.15. (a) DC-link (b) terminal voltage responses for stochastic wind speed .....	97	
Figure 6.1. Modified IEEE 14-bus test system .....	101	
Figure 6.2. A typical PMSG-based wind farm .....	103	
Figure 6.3. Equivalent wind turbine direct-driven PMSG .....	104	
Figure 6.4. A steady state circuit model of a synchronous machine .....	105	
Figure 6.5. Three-phase star-connected shunt capacitor bank .....	109	
Figure 6.6. A shunt capacitor and three filter banks [143] .....	110	
Figure 6.7. A STATCOM connected		

to the CCP .....	113	Figure 6.8. Dynamic responses of generator 2 .....	115
of test system with FFAs .....	116	Figure 6.10. Effects of the PMSG-based wind farm on bus voltages .....	117
Dynamic responses of the test system with capacitor bank and filters connected to bus 1 .....	117	Figure 6.12. Typical dynamic responses .....	118
.....	120	Figure 6.13. Effects of SVC .....	120
Figure 6.14. Comparison of Effects of Conventional method, SVC and STATCOM on dynamic performances .....	121	Figure 6.15. Dynamic responses of the PMSG-based wind farm .....	122
.....	124	Figure 6.16. Impact of stochastic wind speed series on power dynamics .....	124

## LIST OF TABLES

Table 2.1 Sources of electromagnetic disturbances as classified by the IEC [65] .....	12
Table 3.1. Wind speed states and corresponding frequencies at 70 m hub height .....	36
Table 3.2. TPM .....	38
Table 3.3. The limiting vector .....	39
Table 3.4. CTPM .....	41
Table 3.5. Comparison of measured and generated wind speeds .....	42
Table 4.1. Dynamic performances of rotor speed response .....	42

.....	63	Table 4.2. Dynamic performances of PMSG with and without a lag compensator .....	64
.....	64	Table 4.3. Effect of movement of zero of a lead compensator on the damping ratio of the rotor	
speed .....			678
Table 5.1. Dynamic performance of the wind turbine direct-driven PMSG .....			90
Table A1. Wind turbine driven PMSG parameters .....	146	Table A2. Control parameters of the PMSG .....	146
.....	146	Table A3. Virtual control parameters .....	146
.....	146		
Table B1. IEEE-14 bus line data .....			148
Table	B2.	IEEE-14	bus data
.....			147
Table B3. Synchronous machine parameters .....			149
Table B4. Governor and turbine model parameters .....	149	Table B5. Exciter model parameters .....	149
.....	149	Table B6. Capacitor and filter banks parameters .....	149
.....	149	Table B7. SVC parameters .....	149
.....	149		
Table B8. STATCOM parameters .....			149

## LIST OF ABBREVIATIONS AND VARIABLES

A	Area
a	scale parameter
b	Shape parameter
B	Band width
CCP	Common connection point
CTPM	cumulative TPM
D	Damping coefficient
DFIG	Doubly-fed induction generator
DSM	Durban South Merebank
E	Induced voltage
$E_i$	dataset from measurement

FACTS	Flexible AC transmission system
FFA	Feed forward algorithm
$F_i$	dataset from generated series
Fotf	First order transfer function
GTO	Gate turn off
H	Hub height
H(s)	Transfer function
H	Inertia constant
IEC	International electrotechnical commission
IEEE	International electrical and electronics engineers
K	Kelvin
KE	Kinetic energy
kPa	Kilo paskal
KVL	Kirchhoff's voltage law
L	Length
LPF	Low pass filter
M	Mass
MCM	Markov Chain Model
MGSCC	Modified generator side converter controller
MVA	Mega volt ampere
MW	Mega-watt
N	Number of samples
P	Pressure
P	Real power
PDF	probability density function
PI	Proportional integral
PID	Proportional integral derivative
PMSG	Permanent magnet synchronous generator
$P_{ref}$	Reference power
PSS	Power system stabilizer
PWM	Pulse with modulator
R	Radius
RL	Resistance inductance
RLC	Resistance inductance capacitance
RMSE	Root-Mean-Square Error

S	Apparent power
SAWS	South African Weather Services
SCIG	Squirrel-cage induction generator
SDC	Supplementary damping controller
SSSC	series compensators
STATCOM	Static synchronous compensator
SVC	Static var compensator
T	Temperature
TCSC	thyristor controlled series capacitors
TPM	transition probability matrix
TSO	Transmission system operator
TSR	Tip speed ratio
TW	Wind turbine
UPFC	unified power flow controllers
V	Speed or voltage
VR	Virtual resistor
w[n]	Background noise
WPD	Wind power density
WRIG	Wound rotor induction generator
X	Disturbance
Z	Elevation
Z	Impedance
ZN	Zeigler-Nicholas Moment of inertia reactive power Torque D-axis grid voltage Angle of attack Firing angle Pitch angle Tip speed ratio Mean wind speed Density Standard deviation

Angular speed

Power coefficient

d-axis current

\* reference d-axis current

grid q-axis current

grid d-axis current

\* grid q-axis reference current

q-axis current

grid inductance

q-axis inductance

Wind turbine power

Wind power

\* reference reactive power

generator torque

\* reference torque

compensating torque

rotor torque

AC voltage of the PMSG

\* reference AC voltage

D-axis grid current

Q-axis grid current

Number of jumps from state i to j

Probability of transition from state i to j

Q-axis grid voltage

d-axis voltage

\* d-axis reference voltage

grid-quadrature axis voltage

\* grid q-axis reference voltage

Wind speed

Limiting probability

Flux linkage

grid angular frequency

Rotor speed

Reference rotor speed

Permanent magnet flux

1/R

Droop





# CHAPTER 1

## GENERAL INTRODUCTION

The fuel in the earth will be exhausted in a thousand or more years, and its mineral wealth, but man will find substitutes for these in the winds, the waves, the sun's heat, and so forth.

John Burroughs (1837 – 1921)

### 1.1 Introduction

Modern life is unthinkable without electricity— over the last 136 years, since the operation of the first power system [1], there have been astonishing developments in the civilization of mankind because of incredible achievements in the electric industry. The information and communication technology, entertainment industry, works, transportation, lighting, food processing and storages, and industrial processes, from which humans have tremendously benefited, are all geared by electrical energy. Today, electric power systems have become complex systems ever made by man, with major concerns of serving customers through seamless, cost-effective, and dynamically stable systems. They have become large, sophisticated and span throughout a continent; even there are plans for connecting continental power systems, and thus making them further complex. Practically, the cost-effectiveness and dynamic performances of power systems depend on the technologies and energy sources employed in the systems. Thus, much attention has been given to cutting-edge technologies and less polluting energy sources to achieve cost-effective, magnificent, and reliable power systems.

Conventionally, the world heavily depends on fossil fuels and radioactive minerals to meet its ever-growing energy requirements. The same fuels are vastly employed in electrical energy production in conventional power plants. However, this approach is facing alarming challenges, including depletion of reserves, global warming because of carbon emissions, security concerns related to the disposal of radioactive waste materials, and rising cost of fossil fuels [2]. In tackling these challenges, the world is giving much attention to the development of renewable energy resources, among which harnessing wind energy is one of the cheapest alternatives [3].

Wind is a renewable source of energy, which provides electrical energy with low environmental pollution, and thus receiving much attention during the last three decades. In the wind industry, fixed and variable speed wind turbines are used. Fixed speed wind turbines use squirrel-cage induction generators (SCIG) whereas the latter employ either doubly-fed induction generators (DFIG) or synchronous generators. Variable speed wind turbines are advantageous over the fixed speed ones as they can capture more wind energy and operate at a maximum power point possible [4, 5]. Moreover, they are efficient and have improved power quality. Currently, the most popular variable speed wind turbines used in large-scale wind farms are DFIG-based wind turbines [6].

Nevertheless, recently, wind turbine direct-driven permanent magnet synchronous generators (PMSGs) are gaining momentum among researchers, engineers and turbine manufacturers due to their high-efficiency, low power loss and relatively small size [7—12]. However, transmission system operators (TSOs) face several challenges as the level of penetration of this type of wind power rises in a power system. One of the challenges is the impact on the dynamic stability of the power system, caused by the stochastic nature of wind, control technology and power electronic converters [13]. Indeed, a power system should be stable when subjected to disturbances. Otherwise, synchronous machines will fall out of step, causing disastrous power interruptions or even blackouts [14, 15]. The dynamic stability problems of wind power plants invariably affect the dynamics of a power system. Moreover, the concomitant problems become worse when the wind power plants operate in areas having high wind disturbances with a potential capacity of disturbing the whole power system.

In view of this, this thesis will investigate the impacts of stochastic wind disturbances, control technology and power converters on a power system having high PMSG-based wind power penetration. When wind power takes much portion of the generation, the influences of the stochastic wind disturbances on the dynamic performances of a power system can no more be neglected. Thus, the random behaviour of wind and its impacts on system dynamics, and possible mitigation techniques are the subject of discussions in this thesis, especially from the perspective of stochastic wind speed series.

## 1.2 Problem Formulation

Different factors influence the dynamic performances of a power system. In this regard, wind power integration has become one of the critical factors as its level of

penetration is steadily growing in today's power systems. Hence, several authors have investigated the impacts of the integration of wind power, especially wind power generated by variable speed wind turbines, on the dynamic performances of a power system. As a result, it is found that high wind power penetration has both negative and positive impacts depending on the level of wind power penetration, location of wind farms, level of loading, frequency of system oscillation, operating point of wind farm, generator technology, grid configuration, unit commitment of conventional units, amount of conventional generation replaced by wind power, stress level of a power system, and contingency [16—27]. Especially, PMSG-based wind power integration hardly affects the dynamic performances of a power system directly because of the decoupling effect of back-to-back converters. Yet, it indirectly affects the dynamic performances of a power system through replacing conventional generators, changes in power flow, displacement of synchronous generators with power system stabilizers (PSS) and wind power controllers [28—30].

Nevertheless, hitherto, the impacts of stochastic wind speed series, which determine the output power of a PMSG-based wind farm affecting the dynamic performances of a power system, and the characteristics of wind turbines on the dynamic performances of a power system have been overlooked by authors for two reasons: (1) when the level of wind power generation in the concerned power system is low, it hardly affects the corresponding dynamic performances and (2) the total output power of large number of wind turbines is smoothed by the variation in wind speed series over the geographical location [28].

However, with increasing penetration and steady growing of the capacities of wind turbines, the impacts of PMSG-based wind power on the dynamic performances of a power system become significantly evident. Naturally, wind is a random process that exhibits variations over the geographical location of a wind farm. A typical distribution may not necessarily represent the cumulative wind behaviour of all locations in a region [31]. Hence, the wind speed series of a farm site should be appropriately characterised for the investigation of the dynamic performances of a power system with high penetration of wind power [31—33]. Traditionally, Weibull distribution is used to represent wind speed series at a given site [33—35]. However, the main disadvantage of the Weibull distribution is that it does not retain chronology [33]. Nevertheless, naturally, wind speed series show chronology. Different from existing efforts, therefore, this thesis adopts a Markov chain model, which retains chronology and consumes less computation time [36—39], in synthesizing wind speed time series for the investigation of the influences of stochastic wind speed disturbances

on the dynamic performances of a power system. Thus, the Markov chain model is developed based on the wind speed data in Durban.

In this thesis, wind speed series generated by a Markov chain model have been considered, and therefore, the study of the impacts of PMSG-based wind power on the dynamics of a power system is extended one step further. The influences of the stochastic wind speed disturbances on the dynamic performances of a power system containing PMSG-based wind farms can be observed from two perspectives: (1) dynamic stability problems within wind turbine direct-driven PMSGs and (2) system-wide stability problems. Undeniably, these problems should be addressed employing some mitigation techniques that enhance the dynamic performances of the system.

In view of this, various efforts have been made to enhance the dynamic performances of a wind turbine direct-driven PMSG through active power control [29, 40—45] and reactive power control [7, 29, 45—49]. For instance, in [41], a mechanical method, using springs and dampers, has been used to give the PMSG a damping capacity. It is obvious to an electrical engineer that real compensators and resistors can also damp oscillations and enhance the dynamic performances of a wind turbine direct-driven PMSG. However, in addition to making a bulky system, this approach incurs extra cost and power loss. It also requires extra space. Moreover, in conventional generators, damper windings are proven to be effective in damping oscillations [14]. However, a multi-pole PMSG, by its very nature, has no damper windings. In enhancing the dynamic performances of a PMSG, the concept of fictitious stator damper windings is not yet investigated. Therefore, this thesis proposes the use of virtual control, a novel approach, stemming from compensators, resistors and damper windings to enhance the dynamic performances of a wind turbine direct-driven PMSG. This work virtually extends the traditional effectiveness of real components to a wind turbine direct-driven PMSG and illustrates the comprehensive benefits obtained by employing their fictitious cousins. The fictitious ones do not incur extra cost and power loss and do not make a bulky system. In addition, supplementary controllers, which improve the dynamic performances of a PMSG further, are also proposed.

Furthermore, this thesis investigates the use of FACTS devices along with virtual control techniques in tackling system-wide stability problems associated with stochastic wind speed disturbances.

In general, this research tries to give answers to the following questions:

- What are the appropriate wind speed models for dynamic simulation of a wind turbine direct-driven PMSG?
- How do stochastic wind speed disturbances affect the dynamic performances of a wind turbine direct-driven PMSG?
- How are the negative effects of stochastic wind speed disturbances on a PMSG dynamics improved?
- What are the effects of stochastic wind speed disturbances, characteristics of a wind turbine direct-driven PMSG and power converters on the dynamics of a power system having PMSG-based wind farms?
- How are the dynamic problems associated with stochastic wind speed disturbances tackled?

The research assists in expanding the knowledge of the influences of stochastic wind speed disturbances on the dynamic performances of a power system and possible mitigation techniques thereof.

### 1.3 Scope of the Thesis

This research focuses on:

- Developing a localized wind speed series model using Markov Chain, where intermediate wind speeds between hours and minutes are considered as Weibull and Gaussian distributions respectively, for dynamic simulation of a wind turbine direct-driven PMSG based on wind speed data from Durban
- Investigating the impacts of stochastic wind speed disturbances on the dynamic performances of a wind turbine direct-driven PMSG
- Proposing mitigation models that enhance the dynamic performances of a wind turbine direct-driven PMSG under stochastic wind disturbances
- Investigating the impacts of PMSG-based wind power on the dynamic performances of a power system under stochastic wind speed disturbances
- Proposing mitigation methods for poor dynamic performances in a power system with a PMSG-based wind power
- Comparing different dynamic performance mitigation techniques

## 1.4 Contributions to Knowledge

The contributions of this work to the existing literature are given as follows:

- Wind speed series retain chronology, and thus the conventional wind speed modelling used in dynamic simulation of wind turbines, Weibull distribution, lacks this capability. The results in this thesis have demonstrated that the characteristics of stochastic wind speed disturbances over a wind farm geographical location can be reasonably preserved using a Markov chain model. Therefore, in this work, the Markov model for the wind speed series are developed using wind speed data from Durban and are used in the dynamic analysis of the impacts of PMSG-based power on the dynamic performances of a power system.
- The influences of stochastic wind speed disturbances modelled by a Markov chain model on the dynamic performances of a wind turbine direct-driven PMSG and a power system have been analysed and discussed in this thesis.
- Development of virtual controls stemming from resistors, real compensators and damper windings for tackling poor dynamic performances caused by stochastic wind disturbances in a power system has been established in this thesis. These approaches are novel and advance the virtual control concept, which is currently confined to virtual inertia control in wind power, one step further.
- The use of a supplementary control based on rotor speed deviation and DC-link voltage deviation, which enhances the dynamic performances of a wind turbine direct-driven PMSG, is another contribution of this work.
- Furthermore, to reduce the negative impacts of stochastic wind speed disturbances, the virtual controls can be employed along with FACTS devices. This thesis has demonstrated that the dynamic performances of a power system encompassing PMSG-based wind power under stochastic wind speed disturbances can significantly be enhanced by using virtual controls along with FACTS devices.

## 1.5 Thesis Overview

Overall, this thesis has been organized in seven chapters. This chapter deals with the background of the thesis, problem formulation, scope of the research, and the contribution of the research. Whereas, chapter two is totally dedicated to the review of related works. Therefore, chapter two presents a brief review of power system dynamics, power system disturbances and the wind process. It also addresses the review of the impacts of wind power integration, especially PMSG-based power in detail, on the dynamic performances of a power system. Moreover, it reviews mitigation techniques for tackling the negative impacts of wind power.

Subsequently, Chapter three presents the results of modelling of wind speed series and wind power in Durban employing Markov chain, Weibull and Gaussian distributions. The results will be used in the subsequent chapters for the dynamic simulations of a wind turbine direct-driven PMSG and a power system having a PMSG-based wind farm.

The modelling and analysis of a wind turbine direct-driven PMSG are discussed in Chapter four. Furthermore, the chapter presents modelling and analysis of a virtual mitigation technique stemming from real RLC compensators. Time domain analysis results are also presented in detail.

Chapter five extends the investigations of novel mitigation techniques involving virtual control to enhance the dynamic performances of a wind turbine direct-driven PMSG. Virtual control techniques emulating resistors and damper windings are modelled and analysed. Moreover, a supplementary control method based on rotor speed deviation and DC-link voltage deviation is proposed in this chapter.

Chapter six presents the modelling, analysis and investigation of the impacts of high penetration of PMSG-based wind power on the dynamic performances of a power system based on the IEEE 14-bus test system. The chapter also suggests mitigation techniques to improve the dynamics of the test system.

Finally, Chapter seven presents conclusions and recommendations arising from the research undertaken. In the chapter, the conclusions are organised chapter wise and possible future research works emanating from this thesis are suggested.

## CHAPTER 2

### LITERATURE REVIEW

#### 2.1 Introduction

Several disturbances contribute to the dynamic instability of wind farms, which may, in fact, lead an interconnected power system to a stability problem. Among them are short circuits, open circuits, loss of permanent magnetic fields and wind disturbances. The continuous disturbance occurring in the wind speed series is one of the major challenges in controlling and operating a power system with high penetration of wind farms [50, 51]. Indeed, wind gusts contribute to large disturbances in power systems consisting of large wind power penetration. On the other hand, the loss of wind speed for few seconds leads to much part of generation loss, which significantly affects the dynamic stability of the system. Wind is also responsible for continuous small-signal disturbances because of its stochastic nature [52—54]. Transmission system operators are concerned with the dynamic stability of power plants connected to their power systems [51]. Unless controlled, a dynamic stability problem in the wind farm may lead to load shedding or even blackout. Analysis of wind power integration using different models has demonstrated that the dynamic performances of a power system depend on the degree of wind power penetration [13, 55—57].

So far the influences of wind speed disturbances and the characteristics of the corresponding wind turbines on the dynamic stability of a power system have been overlooked for two reasons: (1) when the level of wind power generation in the concerned power system is low, its influence on the dynamic performances of a power system is negligible and (2) in large wind farms there are a number of wind turbines and the total output power is smoothed because of the variation in wind speed series over the geographical location of the wind farms [28]. However, today, technological development has further pushed the capacity of wind turbines. For instance, the capacity of a single wind turbine direct-driven PMSG has reached 8 MW [58, 59]. Nevertheless, a limited number of wind turbines in a wind farm leads to fluctuations in the power output of the farm due to the stochastic wind speed series. For this reason, with the ever-growing technology in the wind



industry, the dynamic stability problems associated with wind speed series and the dynamic characteristics of wind turbines can no longer be neglected, and therefore, mitigation techniques should be sought to enhance the dynamic performances of a power system consisting of high penetration of wind power.

This chapter reviews power system dynamics, sources of disturbances in power systems, wind process, challenges of wind power integration, and the impacts of large-scale wind farms, especially PMSG-based wind farms, on power system dynamic stability. Additionally, mitigation techniques for improving the local and system-wide dynamic performances of a wind turbine direct-driven PMSG connected to a power system are reviewed.

## 2.2 Power System Dynamics

An interconnected power system is the most complex dynamic system ever made by man. Its dynamic performances depend on the dynamics of components such as synchronous machines, controllers, dynamic loads, and wind power controllers. Traditionally, power system stability is defined as the ability to return to stable operation after being subjected to disturbances. In contrast, instability shows loss of synchronism of synchronous generators. Stability analysis is a crucial step in power system planning. Renewable power integration, continuous growth of the power system itself, vast extension over wide geographical regions, and the inclusion of new technologies such as FACTS devices have made maintaining synchronism between different parts of an interconnected system increasingly difficult [14, 15, 60].

Power system dynamics are characterised by the following features [60]:

- (1) In a power system, real power cannot be transferred indefinitely without a limit; in fact, there is a limit beyond which the system becomes unstable.
- (2) A power system acts like a spring-inertia oscillatory system, where the mechanical power into the system corresponds to the inertia and the output electrical power transfer, which is proportional to the sin of the power angle, corresponds to the spring. This relationship is expressed by the swing equation.
- (3) As expressed by the swing equation, the equation deciding the power system dynamics is nonlinear for disturbances causing changes in the power angles

(rotor angles) of synchronous machines. Power system dynamic stability depends on the size of the power system disturbance.

Power system stability problems can be categorised into steady-state, dynamic and transient problems [14, 61]. Steady-state stability study determines the maximum loading of a machine through gradually increasing the load. Small disturbances such as wind speed disturbances continuously occur in a power system. These disturbances are not large enough to cause abrupt changes so that the machines in the system lose synchronism. However, they do excite the system into a state of natural oscillation. If these natural oscillations do not go beyond certain limits and die out quickly, then the system is said to be dynamically stable; otherwise, the system is dynamically unstable. In power systems having wind power, dynamic instability occurs more often than steady-state instability. In a dynamically unstable system, the amplitudes of the natural oscillations are large and persist for a long duration. Undeniably, this kind of instability behaviour brings a serious security issue and creates a challenging operating condition. And these kinds of problems should be mitigated using power system stabilisers. To investigate the dynamics of a power system, dynamic stability studies should be done for 5 to 10 seconds and rarely up to 30 seconds using digital computers. Indeed, digital computer simulation is the effective way of dynamic stability study. The same simulation software can be used for transient stability study [60].

In stability studies, the boundary between small and large disturbances is not bold [14, 15, 60]. The severity of a disturbance is determined by changes it brings to the rotor speeds or the power angles of synchronous machines. If the disturbance is sufficiently small and doesn't disturb the rotor speeds of the synchronous machines, the power system can be linearized around an operating point, and eigenvalue analysis can be applied to analyse the dynamic stability of the system [14, 15]. If the disturbance brings significant changes in the rotor speeds and the power angles, it is considered to be a large disturbance [60], and time domain analysis is the best option in analysing the dynamic stability of the system. Large and sudden disturbances cause transient stability problems, which are fast and usually occur within a second.

Wind speed disturbances, the focus of this thesis, cause both small-signal and transient stability problems depending on the degree of wind power penetration in a power system. Usually, the changes due to wind speed disturbance are not sufficiently small to linearize the system around an operating point. In this work, dynamic stability includes stability issues

related to a range of wind speed disturbances including gusts, i.e. it includes both small-signal and transient stability problems due to wind speed disturbances. As the penetration grows high, it is a bare fact that wind disturbances will be responsible for disastrous instability problems, and hence the need for the investigation of such problems and the corresponding mitigation techniques. Due to the vague demarcation between small and large disturbances and the stochastic nature of the wind, as suggested by [60] time domain simulation is the best option in analysing the impacts of wind speed disturbances on the dynamic performances of a wind turbine direct-driven PMSG.

### 2.3 Power System Disturbances

The aim of any power system is to ensure the supply of electric power to customers with unwavering voltage, excellent power quality and without interruptions. However, this cannot be achieved with 100% efficiency as disturbances impair the quality of power by distorting the voltage and even leading to instability and power shedding through changing the rotor speeds and angles of synchronous generators. A power system is fully exposed and can never be shielded from disturbances.

In general, power system disturbances can be classified into two groups: natural disturbances and manmade (or artificial) power system disturbances, which are commonly known as cyber-attacks [62, 63]. In this digital era, cyber-attacks on power systems are becoming common. However, this thesis focuses on natural power system disturbances. There is a range of natural disturbances which occur in power systems and are responsible for the deterioration of power quality. A disturbance can be modelled as [64]:

$$\begin{aligned}
 x[n] = & \quad x_s[n] + \quad x_t[n] + \quad x_w[n] + \quad x_d[n] + \quad x_h[n] + \quad x_n[n] \\
 & + \quad x_w[n] \quad = 0, 1, 2, 3, \dots,
 \end{aligned}
 \tag{2.1}$$

where  $N$  is number of samples,  $x_s$  is the power supply signal (or fundamental component),  $x_t$  is transient component of the disturbance,  $x_w$  represents waveform variations (including sag, swell and momentary interruption components),  $x_d$ ,  $x_h$ , and  $x_n$  denote waveform distortions (including DC-offset, harmonics, inter-harmonics, notching and spike components). And  $w[n]$  represents the background noise.

The IEC categorises electromagnetic disturbances as shown in Table 2.1 [65]. Most disturbances causing dynamic stability problems in a power system such as faults, generation

tripping, load shedding, wind speed disturbances, line trip and oscillation lie under the first (low frequency) category. Naturally, the wind is a low frequency stochastic phenomenon which affects the dynamic performances of a power system and its disturbance is expressed as shown in (2.1). The intermittent wind speed can also cause generation loss and leading to load shedding through controller actions. Therefore, the dynamic performances of a power system having large wind power penetration can be severely affected by wind disturbances, which are not sufficiently addressed in the existing academic literature.

Table 2.1. Sources of electromagnetic disturbances as classified by the IEC [65]

Group	Examples
low-frequencies through conductance	Harmonic, interharmonic
	Signal system
	Voltage fluctuation
	Voltage dip and interruption
	Voltage imbalance
	Power-frequency variation
	Induced low-frequency voltage
	DC in AC network
low-frequencies through radiance	Magnetic field
	Electric field
high-frequencies through conductance	Induced continuous wave (CW) voltage or current
	Unidirectional transient
	Oscillatory transient
high-frequencies through radiance	Magnetic field
	Electric field
	Electromagnetic field
	Continuous wave
	Transient

## 2.4 Wind Process

### 2.4.1 General

The origin of any form of renewable energy on this planet is the sun. The uneven heating of the surface of the earth by solar radiation results in pressure differences in the lower atmosphere, which in turn results in the movement of large mass of air, wind, as hot air rises and cold air falls. In fact, air moves from high pressure to low pressure. Besides, the

rotation of the earth around its own axis highly influences this movement of air [66]. Moreover, seasonal variations in the distribution of solar energy give rise to variations in the wind. Usually, the wind blows in a horizontal plane because of horizontal pressure gradient as the earth's gravitational force counterbalances the vertical wind component.

Winds can be either global or regional. Orographic conditions such as the surface of the area and global phenomena have their own influences on regional winds. The wind close to the ground, which wind power plants exploit, is known as boundary layer [28]. This wind is turbulent due to the roughness of the earth. Wind speed varies continuously with time and height because of gusts, time of the day and weather condition. Consequently, unless controlled, the power output of a wind power plant continuously fluctuates, resulting in poor power quality.

The kinetic energy of wind flowing at a speed  $v$  is given by [28]:

$$= \frac{1}{2} \quad (2.2)$$

where  $m$  is mass of air. The mass is the product of the density of the air,  $\rho$ , and its volume, which is in turn the product of the area,  $A$ , through which the air is flowing and the length,  $l$ , the air travels in a second. Hence, equation (2.2) can be rewritten as shown in (2.3).

$$= \frac{1}{2} \quad [ \quad ] \quad (2.3)$$

The power of the wind is the rate of its kinetic energy and is given by [66, 67]:

$$= \frac{1}{2} \quad [ \quad ] \quad (2.4)$$

In (2.4), the rate of the length is the same as the speed of the wind.

The surrounding temperature ( $T$ ) and pressure ( $p$ ) affect the density of air. Indeed, both temperature and pressure vary with height. Hence, the density of dry air is approximately given by [66]:

$$= 3.4837 \_ \quad (2.5)$$

Pressure is measured in kPa, temperature in K and density in kg/m<sup>3</sup>. In general, pressure decreases with elevation. Up to 5,000 m elevation, the surrounding pressure can approximately be given by [66]:

$$= 101.29 - 0.01183 z + 4.793(10^{-5} z^2) \quad (2.6)$$

where  $z$  is elevation in meters. In wind farms, the wind turbines convert the power in (2.4) into electrical power.

#### 2.4.2 Review of Wind Speed Modelling

Challenges such as depletion of reserves, global warming, security concerns, and rising cost are pushing the world to go green. Currently, much attention is given to the development of renewable energy, among which harnessing wind energy is the cheapest alternative [2, 3, 68]. Feasibility studies related to wind power require an appropriate wind speed model of a site [33]. These models are also important in planning and operating wind turbines. Hence, the wind speed series of a specified site should be appropriately characterized to determine wind energy potential and attain comprehensive results in the investigations of the dynamics of wind turbines [31—33]. Moreover, a good characterization of wind speed series helps transmission system operators (TSOs) in scheduling their power dispatch [33].

Wind is a random stochastic process whose dynamic behaviour can be represented by a stochastic model [53]. Naturally, it depends on pressure gradient, waves, jet streams, and local weather conditions [69]. Its stochastic modelling is a complicated task because of its strong variability in time and land terrains. Over a year, wind speed is periodic, showing seasonal variations; however, hourly average wind speed is a stochastic process with a Weibull probability density function; whereas within minutes, it follows a Gaussian random process [36].

Different methods have been employed for time series characterization of wind processes. Conventionally, for dynamic simulation of wind turbines, Weibull distribution is used to represent wind speed series at a given site [33—35]. Normal, Gamma, Lognormal or combination of these distributions with Weibull distribution [31, 70—71] can also be used to model wind speed series in metrological wind forecasting. Kernel density method is used in [73]. A typical distribution may not necessarily represent the cumulative wind behaviour of all locations in a region [31]. Thus, the wind speeds for a location need to be modelled.

However, the above distributions cannot be used when chronology is considered [33]. In reality, the current wind speed depends on the previous wind speed indicating chronology should be considered in modelling wind speed series. Evolutionary algorithms such as genetic algorithm and local search technique are also used in wind speed modelling [74]. However, these algorithms are time consuming during simulations [33].

Therefore, the Markov chain model, which retains chronology and consumes less computation time, could be employed to synthesize wind speed time series [36—39] for dynamic simulation and wind power forecasting. This model is not adopted for dynamic simulation of wind turbines in the existing literature. The accuracy of a Markov model increases with its order [37]. The first-order model is often adopted for its simplicity and computing time [39]. A modified Markov model [75] may show better performances than the corresponding normal model in preserving the properties of wind speed series. Particularly, the second order semi-Markov process is more suitable for processes including state and duration [36].

Few efforts have been done to characterize wind speed series and power for electric generation in South Africa using computer algorithms and frequency distribution methods [76—78]; however, the Markov model has never been used, particularly, in Durban, South Africa. As wind speed model series strongly depend on location, an investigation into the wind speed series in each site is vital. Therefore, in Chapter 3, the Markov chain model is employed to characterize the wind speed series in Durban, South Africa. The model is also compared with the corresponding Weibull distribution. The comparison shows that the Markov Model is more effective than the Weibull distribution. Finally, Weibull and Gaussian probability density functions, along with the Markov model, are employed to produce synthetic wind speed series over minute and second intervals respectively. Generation of artificial wind speed series is crucial for dynamic simulations of wind turbines.

## 2.5 Review of Wind Power Integration

### 2.5.1 Wind Turbines

A wind turbine, a machine designed to capture wind energy, converts the kinetic energy of wind into electrical energy by slowing down the stream of air flowing past it [79]. In practice, a wind turbine transforms the kinetic energy into mechanical energy first, and

then, a generator in the nacelle converts the mechanical energy into electrical energy, which can be supplied to either a power grid or customers.

There are two types of wind turbines based on the direction of their rotor axes: namely, vertical axis and horizontal axis wind turbines. A horizontal axis wind turbine catches more wind energy than a vertical one. Nevertheless, it is complex as it requires long tower and complex blade design. In addition, a yaw control system is required in these types of turbines. Maintenance is also difficult. However, it offers a better performance than the vertical axis one. Since the 1990s, in large-scale wind farms, which are the core of this study, horizontal axis wind turbines have been widely employed [28, 66]. Figure 2.1 shows a typical horizontal axis wind turbine.

Commercial horizontal axis wind turbines have a wide range of sizes. For instance, there are small standalone turbines with capacities less than or equal to 10 kW [66]. On the other hand, utility-grade turbines capable of generating up to 5 MW [80] power are joining the wind energy market in the USA, Europe and China; even huge ones with capacities up to 8 MW [81] are under investigation.



Figure 2.1. Horizontal axis wind turbine [79]

### 2.5.2 Principle of Operation

A wind turbine cannot completely extract the power from the wind. According to [28], equation (2.7) gives the power that can be extracted.

$$= \tag{2.7}$$



$C_P$  is the power coefficient. The theoretical maximum value of the power coefficient is 0.59 [79].

The principle of operation of a wind turbine is similar to that of an aircraft. The wind flowing past a turbine exerts a force on the blades as shown in Figure 2.2. The resultant wind force has vertical and horizontal components. The vertical component, which is known as aerodynamic lift force, drives the rotor. Thus, wind turbine designers usually try to maximize the lift force. In contrast, they want to reduce the drag force, which is the result of air friction. In fact, it is impossible to eliminate this force [82].

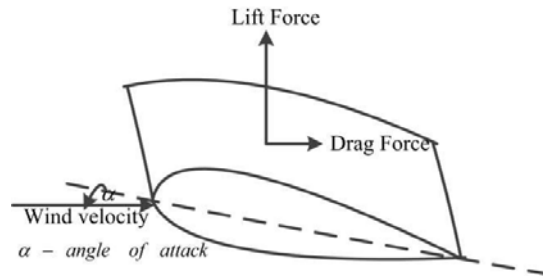


Figure 2.2. Forces on the blade of a wind turbine

The aerodynamic lift force depends on the angle of attack,  $\alpha$ , of the wind velocity. There is an optimum angle of attack which creates the maximum lift to drag force ratio. Tip-speed ratio is a common term in wind turbine design and is given by [82]:

$$\lambda = \frac{R \omega}{v} \quad (2.8)$$

where  $R$  is the radius of the wind turbine in metre,  $v$  is wind speed, and  $\omega$  is the angular speed of the rotor of the wind turbine in radians per second. Usually, a wind turbine has twisted blades to optimize the angle of attack. As given in [28, 79], the power coefficient varies with tip-speed ratio as shown in Figure 2.3.

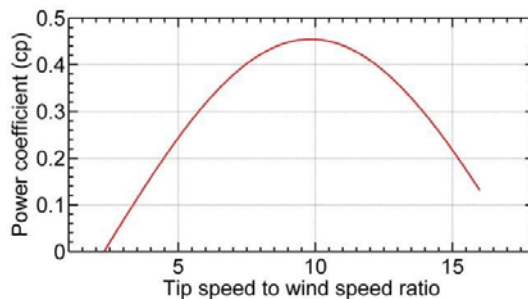


Figure 2.3. Power coefficient vs. tip-speed ratio curve for a typical wind turbine

Horizontal axis wind turbines with two and three blades have become famous in the wind industry because of design considerations of aerodynamic efficiency, component costs, system reliability and aesthetics. Aerodynamic efficiency increases as the number of blades increases, but manufacturing cost also increases. Consequently, optimization is binding. And thus, the current trend is to use wind turbines with three-blades [28].

Wind turbines cannot be operational for the whole range of wind speeds. If the wind speed is too low for generating power, the rotor will be locked. The minimum operational wind speed is called cut-in speed, whereas the maximum is known as cut-out speed. At rated speed, the turbine generates its rated power [79].

Figure 2.4 shows the power curve of a typical wind turbine, which is obtained at a pitch angle of 5 degrees. In the figure, the cut-in wind speed is around 2.5 m/s, while the cut-out speed is 18 m/s. From 12 to 18 m/s, the machine operates at its rated power. Usually, manufacturers offer power curves for their wind turbines.

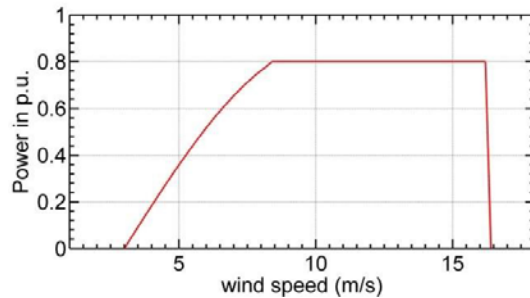


Figure 2.4. Typical wind turbine power curve

### 2.5.3 Classification of Wind Turbines

For synchronization with a power system, like conventional synchronous generators, a wind turbine generator should have the same voltage amplitude, phase angle and frequency as that of the power system. Since the 1980s, the rotor diameter of wind turbines has increased dramatically. Today, it is common to see rotors having blades longer than 50 m. In fact, an astonishing development has also taken place on the electrical side of grid-connected wind turbines. Earlier the rotational speeds of wind turbines were directly coupled to the

speed of the power system. However, now, the rapid development of power electronics has solved this problem, and the speeds of the wind turbine and the power system should not necessarily be the same [83]. Wind farms and grids are decoupled by power converters and are controlled separately.

The major configurations of grid-connected wind turbines based on their ability to control speed are [28]:

1. Squirrel Cage Induction Generator (SCIG)-Based Wind Turbine
2. Wound Rotor Induction Generator (WRIG)-Based Wind Turbine
3. Doubly Fed Induction Generator (DFIG)-Based Wind Turbine and
4. Wind Turbine Direct-Driven PMSG

Though there are different types of wind turbine configurations based on different criteria, only the above standard types of wind turbines are commonly employed in modern wind farms. Currently, wind turbine manufacturers are highly interested in wind turbine directdriven PMSG, which is the core of this thesis, for its higher generation efficiency, gearless structure, lower maintenance cost and higher operation and reliability [7—12]. This would be the future wind turbine. The next subsection deals with the discussion of a wind turbine directdriven PMSG.

#### 2.5.4 Wind Turbine Direct-Driven PMSG

In this configuration, the wind turbine employs a PMSG instead of an induction generator as shown in Figure 2.5. The PMSG is connected to the utility grid through a fullscale power converter (back-to-back converter), a low pass filter and a transformer. The power converter converts the variable frequency output voltage of the generator into a voltage having a fixed frequency. Essentially, the fixed frequency should be the same as the grid frequency. The low pass filter filters out the harmonics created by the power electronic converter, while the transformer steps up the output voltage to the grid voltage level [28, 84, 85].

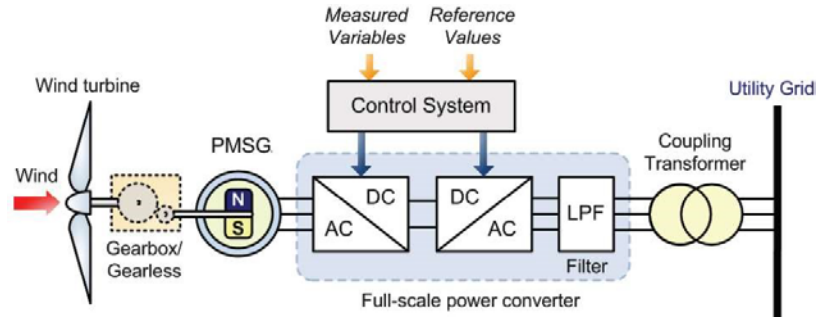


Figure 2.5. A wind turbine driven PMSG connected to a grid [83]

The back-to-back converters can control the reactive power, which is locally generated, and smooth grid connection from cut-in to cut-out wind speeds [84]. Some multi-pole wind turbine driven PMSGs do not have gearboxes, resulting in direct-driven PMSGs and hence reducing maintenance costs and efforts. This also makes the wind turbines more efficient [28].

The major advantages of wind turbine direct-driven PMSGs over the other types are [28, 84—86]:

- As the power converters decouple the wind turbine from the grid, grid codes, such as fault ride through, are easier to be accomplished.
- A wind turbine direct-driven PMSG is more efficient as there are less losses.
- A wind turbine direct-driven PMSG is robust and cost effective. Besides, it has less weight, reduced noise and improved voltage stability and power quality. Additionally, it requires less maintenance.
- There is no DC excitation system in a wind turbine direct-driven PMSG.
- It offers full controllability of the system for maximum wind power extraction and grid interface.

Furthermore, currently, as wind power penetration increases, these wind turbines are receiving more attention than DFIG-based wind turbines because of intensified grid code requirements among TSOs [84, 86].

Wind turbine direct-driven PMSGs can employ two types of power converters, which are characterized as grid-commutated and self-commutated power electronic converters. The formers usually use thyristors because of their cost and reliability. However, thyristors consume reactive power. Self-commutated converters can use GTOs, thyristors or power

transistors [28]. On the other hand, self-commutated converters can be either voltage or current source converters.

## 2.6 General Overview

The swing equation of a synchronous machine is a second order nonlinear equation of the rotor angle which shows oscillatory behaviour [14]. Since small power system disturbances in rotor speed hardly lead to any change in the rotor angle, they are not likely to influence the electrical torque developed in the synchronous generator [28]. Thus, the damping of rotor speed oscillations should come from damper windings, exciters and the rest of the power system. However, large disturbances affect the rotor speed, and protection systems should engage themselves into isolating the system from the sources of the disturbances.

Poorly damped or undamped oscillations are mainly the results of weak links and high concentration of synchronous generators [14]. When a generator is weakly coupled with a grid, the contribution of the rest of the grid to the damping torque decreases and hence the damping of oscillation deteriorates. Unfortunately, damper windings are not effective for oscillations with frequencies less than 1 Hz [28].

Unlike synchronous generators, wind turbine generators are not connected to a power system synchronously. Consequently, they do not directly participate in electromechanical oscillations [16, 30, 87]. Furthermore, a low-level penetration of wind power does not significantly affect the dynamic stability of a power system [28]. However, as the level of penetration increases, the authors of [16, 17, 30, 87] claim that the dynamic stability of the power system is affected for the following reasons:

- replacing synchronous generators, and thus reducing the total inertia of the system
- changing power flow, and hence affecting synchronizing torques □  
displacing synchronous generators with power system stabilizers
- wind power controllers bring their own dynamic stability problems

Squirrel-cage induction generators hardly engage themselves in electromechanical oscillations as their electromagnetic torques depend on rotor slips rather than speed differences between rotor and stator fluxes. Thus, unlike that of a synchronous generator, the mechanical part of a squirrel-cage induction generator is of the first order and does not show

oscillatory behaviour. Although oscillations are observed while including rotor transients in the model, which increases the model order, these oscillations are small and well damped. In principle, SCIGs are better damped than synchronous generators [28]. Hence, SCIG-based wind turbines have insignificant direct effects on the dynamic performances of a power system.

Several researchers investigated the impact of large-scale penetration of fixed-speed wind turbines on the dynamic stability of power systems. An agreement has been reached that high penetration of fixed-speed wind farm improves the damping performances of power systems [18, 30, 87—89] where conventional synchronous generators are replaced by equivalent SCIG-based wind farms.

Conversely, there is no consensus among researchers about the impacts of high penetration of variable-speed wind power on dynamic stability [30]. For instance, R.D. Fernandez et al. [88] have demonstrated that large-scale integration of DFIG-based wind farms into a power system significantly increases dynamic stability. Moreover, works in [89—91] have shown positive impacts of wind power integration.

On the other hand, L. José et al. [19] have shown that large-scale integration of DFIGbased wind farms may have both detrimental and beneficial impacts based on the status of controllers and a power system. References [16—26] also conclude high DFIG-based wind power penetration has both negative and positive impacts. In these efforts, factors such as level of wind power penetration, location of wind farms, level of loading, frequency of system oscillation, operating point of wind farm, generator technology, grid configuration, unit commitment of conventional units, amount of conventional generation replaced by wind power, stress level of the power system, and contingency were taken into consideration.

A. Mendonca and J. P. Lopes [27] illustrate changes in the operational structures of power systems with high wind power penetration may lead to considerable reduction of the damping capability of a power system. Similarly, damping can be reduced when wind power penetration increases and contributes to congest weak interconnection. And the authors conclude that interarea modes are more sensitive to high wind power penetration.

Reference [87] asserts that the damping performances of the New Zealand System are degraded to an unacceptable extent due to the introduction of wind farms. Thus, there would be a need for improving the damping performances of the system by fitting well-tuned power

system stabilizers to appropriate synchronous generators in the future. Further, a negative impact of high wind power penetration is also reported in [92].

Considering previously done investigations, variable-speed wind farms have both negative and positive influences on the dynamic performances of a power system depending on the status quo of the system. Factors that resulted in these various results are types of electromechanical oscillations, locations, manners and levels of wind power penetration, the load level of the power system, and different control modes of the wind turbines [30]. It is a bare fact that a further research on the impacts of high penetration of variable-speed wind farms on the dynamic stability of power systems is timely and crucial. Especially, the influences of stochastic wind disturbances are hardly investigated in the existing literature. Moreover, further investigations on control mechanisms that enhance damping performances are required.

## 2.7 Impacts of Wind Turbine Direct-Driven PMSGs: Review

As back-to-back converters decouple the PMSG from a power system, oscillation problems arising from a wind turbine direct-driven PMSG cannot directly affect the dynamic performances of the power system [28, 29]. However, the dynamic performances of the power system are indirectly influenced by replacing conventional generators, change in power flow, displacement of synchronous generators with a power system stabilizer (PSS) and wind power controllers [30]. The wind turbine has its own dynamic stability issues into the bargain. For the last six and seven years, research efforts have been devoted to analysing the impacts of large-scale PMSG wind power penetration on the dynamic stability of a power system. Due to the various dynamic characteristics of the wind turbine and the power system taken into consideration during the investigations, views vary. Generally, the views could be seen from two aspects—dynamic stability of the wind turbine direct-driven PMSG itself and systemwide dynamic stability.

### 2.7.1 Dynamic Stability of Wind Turbine Direct-Driven PMSG

Dynamic oscillations arise from the interaction of various rotating parts within a wind turbine direct-driven PMSG. Though the oscillations do not directly instigate instabilities in the rest of the power system by themselves, as the wind turbine and the power system are decoupled, they may result in local dynamic instabilities [28], which lead to the

disconnection of the PMSG from the power system. The disconnection, in turn, affects the power system in its own way, which may be a cause for load shedding or a total collapse of the system, depending on the degree of wind power penetration and available spinning reserve. In a wind turbine direct-driven PMSG, the drive train and converters are the main sources of oscillations [29, 93]. As the number of pole pairs of the PMSG increases, the drive-train shaft becomes soft and vulnerable to oscillations. Consequently, the torsional twist of the shaft may significantly affect the operation of the wind turbine. Therefore, drive-train oscillations should be cautiously handled [94].

Wind power controllers have the upper hand on the dynamic performances of a wind turbine direct-driven PMSG. The interaction between dynamic oscillations and wind power controllers could be analysed using the model shown in Figure 2.6 [93]. For example, a voltage control loop results in a poorly damped and sustained drive train oscillations unless parameters are appropriately selected [29, 95].

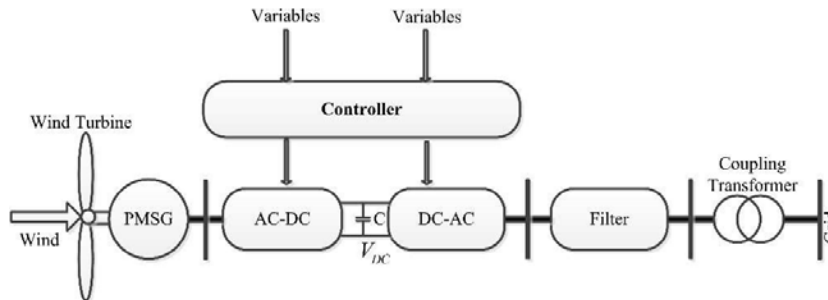


Figure 2.6. A wind turbine direct-drive PMSG connected to an infinite bus

On the other hand, it has been observed that inappropriate selection of parameters of wind power controllers leads to dynamic instabilities in a wind turbine direct-driven PMSG [96]. Indeed, proportional-integral (PI) controllers are widely used in wind power controllers, and appropriate tuning is essential. Otherwise, dynamic oscillations may lead the PMSG to instability [44, 93]. Furthermore, it will be very helpful indeed if advanced controllers that enhance the dynamic performances of such a PMSG are investigated.

### 2.7.2 System-Wide Dynamic Stability

The response of a power system to a disturbance depends on the magnitude of the disturbance. Naturally, a power system is nonlinear, and its response to small disturbances, where the disturbances are sufficiently small for linearization, depends on the operating point



[14, 15]. In fact, the distribution of the eigenvalues of the whole power system depends on this operating point; anything that alters the operating point unquestionably affects the eigenvalues [28]. In principle, as the level of penetration of the wind power increases, the power flow changes; and thus, the operating point. Consequently, the dynamic stability, which depends on the eigenvalues, will be affected. Thus, level of wind power penetration is a major factor that affects the dynamic stability of a power system. The eigenvalue approach is not adopted in the current work as stochastic wind speed disturbances span from small to large disturbances.

The IEEE 3-generator 9-bus test system, shown in Figure 2.7, is widely used in the investigation of the influences of large-scale PMSG-based wind power penetration on dynamic stability of a power system [97]. It is shown that increasing wind power penetration has positive impacts on system-wide dynamic stability of a power system depending on the operating point of the system before the occurrence of a disturbance [13, 29, 56, 93, 98].

Conversely, high PMSG-based wind farm penetration reduces the stability limits of a power system when a power factor controller is employed [9]. Power factor and voltage controls in a wind turbine have negative impacts on system-wide dynamic stability of a power system [8, 99]. In another research, it is observed that wind farm contributes little to the oscillatory modes of a test system [57].

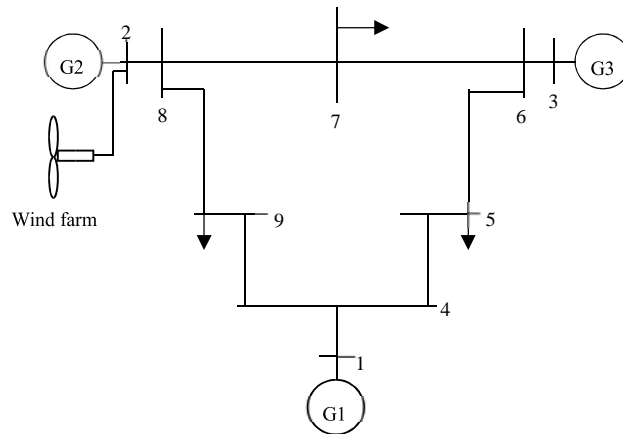


Figure 2.7. IEEE 3-generator 9-bus test system with a wind farm

System-wide dynamic stability also depends on the location and connection point of a PMSG-based wind farm in a power system [98]. Therefore, high PMSG-based wind power

penetration has both negative and positive impacts, depending on the way of grid-connection and type of connection point [100].

Other factors that affect the dynamic stability of a power system with high PMSG-based wind power penetration are friction coefficients of wind turbines and power factor control. Friction coefficients have a linear relationship with stability margin, whereas power factor control reduces the contribution of grid current in an oscillatory mode [57]. On the other hand, the wake effect has a negative impact on dynamic stability. Besides, wake effect changes the strong correlation between generators with oscillation [97].

Weak coupling between a PMSG-based wind farm and a power system affects the dynamic stability of the system. Such a scenario is investigated in [101, 102], and it is illustrated that grid coupling strength significantly affects the dynamic performances of a power system. Wind generation uncertainty and volatility have also their own impacts on electromagnetic oscillatory modes [7]. Wind shear and tower shadow are other factors which affect the dynamic stability of a power system with large-scale PMSG-based wind power integration. Time-domain simulations have shown that power system oscillations due to wind shear and tower shadow influences are pronounced in medium wind speeds [103]. The other point is that wind power controller parameters affect the dynamic stability of a power system [98, 104]. Wind farm capacity changes and type of transmission line between a wind farm and a common connection point can affect the dynamic stability of a power system [105]. Moreover, using cables in place of overhead transmission lines for power transfer can improve dynamic stability [105].

In general, considering research works reviewed in this section, the impacts of largescale PMSG-based wind power penetration on the system-wide dynamic stability of a power system are divergent. Different factors are considered under the investigations leading to four categories of results: beneficial, detrimental, indifferent, and both beneficial and detrimental impacts. Indeed, factors considered in one investigation may not necessarily be considered in another, i.e. the factors and scenarios considered have influenced the outcomes of the investigations. In contrast, the influence of stochastic wind speed series, which is the pillar of this work, has not been considered in any of the investigations. Contingency is not also addressed. Moreover, in most of the works, disturbances are assumed to be sufficiently small so that linearization of mathematical models is allowed, and disturbances affecting

rotor speeds of synchronous machines are not sufficiently addressed. Strikingly, this area requires a further research.

## 2.8 Review of Mitigation Techniques for Dynamic Performances

As reviewed in the previous section, a high penetration of PMSG-based wind power has negative effects on the dynamic performances of a power system though it may also have positive impacts. Consequently, for negative impacts, mitigation techniques that enhance the dynamic performances of not only the wind farm but also the concerned power system are required. As a progressing research area, unlike that of DFIG-based wind power, few authors have considered mitigation techniques to enhance the dynamic performances of a wind turbine direct-driven PMSG and its impacts on a power system. In the existing literature, generally, three mitigation and control approaches are observed— real power control, reactive power control, and FACTS-based approaches [30, 106, 107]. However, compared to that of DFIG-based wind turbines, the three approaches are not sufficiently investigated for wind turbine direct-driven PMSGs.

### 2.8.1 Active Power Control

In wind turbine direct-driven PMSGs, real and reactive powers are controlled separately, the basis for real power and reactive power based mitigation approaches [40]. And the control system is realized using classical vector control. The dynamic performances of a wind turbine direct-driven PMSG can be enhanced using this approach. Elimination of the gear results in torsional oscillations, which may lead to dynamic stability problems. However, active power control using mechanical methods such as springs and dampers can be used to overcome such problems [41]. Otherwise, the dynamic oscillations can be damped through pitch angle or speed controllers. Nevertheless, in all these cases, the responses achieved are slow [29]. In [49], a PID pitch angle controller is used for an SCIG-based wind turbine to enhance its stability as shown in Figure 2.8, where  $\omega_{ref}$  is reference rotor speed,  $\omega$  actual rotor speed,  $1/R$  droop,  $P_{ref}$  reference power,  $P$  measured output power of the generator, and  $\theta$  pitch angle. This approach can easily be adapted for a wind turbine direct-driven PMSG.

Alternatively, the PID controller in Figure 2.8 can be replaced by a fuzzy logic controller to achieve a better damping performance in a wind turbine direct-driven PMSG [42]. This implies that, though they haven't been yet tested, advanced controllers can also be

applied to pitch angle controllers for wind turbine direct-driven PMSGs. In Figure 2.8,  $\Delta P$  is error power due to governor speed characteristics.

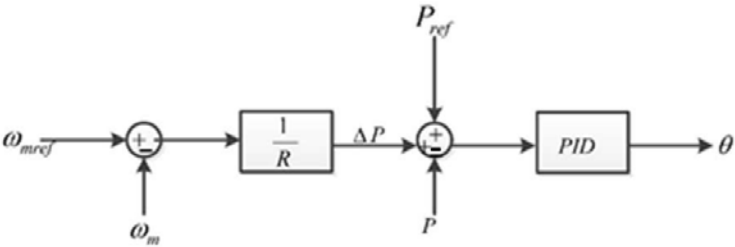


Figure 2.8. Pitch angle control

The other alternative of active power control is achieved through the back-to-back converters. The response of this approach is fast, and hence it is advantageous. Different alternatives are being investigated. For example, in [43], an active-damping strategy based on DC-link current estimation to damp torsional oscillations is proposed as shown in Figure 2.9, where PI is a proportional-integral controller, compensating torque, \* reference torque, generator torque, first order transfer function, rotor torque and wind turbine model. In addition, this controller reduces speed oscillations.

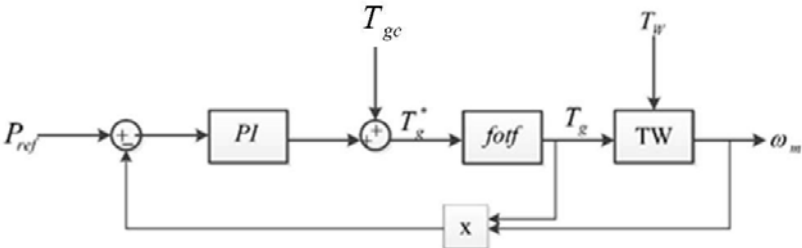


Figure 2.9. Active power damping scheme

An active power control approach based on torque compensation to improve the dynamic stability of a wind turbine direct-driven PMSG is proposed in [44]. The strategy contains a feed-forward loop based on DC current injected into a DC-link. Oscillatory modes are effectively suppressed and the stability of the PMSG is improved. Effective control of a wind turbine direct-driven PMSG can support the dynamic frequency of a power system. In this case, a supplementary loop added in the active power control loop modifies the controller to achieve effective network inertia response and can significantly improve dynamic stability [45] as shown in Figure 2.10. In this figure, \* is reference AC voltage, AC voltage of the

PMSG,  $I_d^*$  reference d-axis current,  $I_d$  d-axis current,  $V_d^*$  d-axis reference voltage,  $V_d$  d-axis voltage,  $\omega$  electrical speed of the PMSG,  $L_q$  q-axis inductance and  $I_q$  q-axis current.

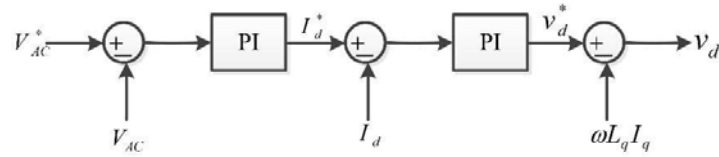


Figure 2.10. Active power supplementary loop

Finally, a conventional PSS can also be adapted to improve the dynamic performances of a wind turbine direct-driven PMSG [96]. Though active power control improves the dynamic stability of a wind turbine, it has its own drawbacks. One of the drawbacks is it may negatively affect drive train oscillations [108].

### 2.8.2 Reactive Power Control

Few authors explored the effectiveness of reactive power control in enhancing wind turbine dynamic performances. In [45], a supplementary reactive power controller is used to improve the damping performances of a power system as shown in Figure 2.11, where  $V_{gq}^*$  is grid-quadrature axis voltage,  $V_{gq}$  grid q-axis reference voltage,  $I_{gq}^*$  grid q-axis current,  $I_{gq}$  grid q-axis reference current,  $Q$  reactive power,  $Q^*$  reference reactive power,  $\omega_g$  grid angular frequency,  $L_g$  grid inductance and  $I_{gd}$  grid d-axis current. In this study, the results illustrate that the dynamic stability problem is mitigated.

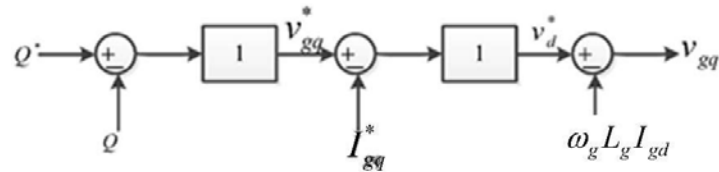


Figure 2.11. Reactive power supplementary loop

Moreover, Silvio Rodrigues et al., in [46], use multi-objective genetic algorithm to tune a PI controller that enhances the dynamic stability of a wind turbine direct-driven PMSG. Modulation of reactive power at the point of connection of the wind farm and a power system contributes to low-frequency oscillation damping [47]. A reactive power-damping

controller can be used to damp power system oscillations at steady state, and thus, the system damping performance is further improved [48]. Usually, reactive power control is implemented in the grid-side converter. It is also shown that in DFIG-based wind turbines, this approach does not affect drive train oscillations as the controller acts like an SVC and is on the grid-side of the back-to-back converters [109, 110]. Therefore, more research in this approach for wind turbine direct-driven PMSGs is crucial.

### 2.8.3 FACTS Devices

The two approaches discussed earlier are widely used to damp inner oscillations of a wind turbine direct-drive PMSG or PMSG-based wind farm. System-wide dynamic oscillations can be damped using FACTS devices. For instance, in [106, 107], a static compensator (STATCOM) is used to improve the stability of four parallel-operated PMSG-based offshore wind turbine generators feeding a power system. The proposed STATCOM joined with the designed damping controller effectively improves the dynamic stability of the power system under various disturbance conditions. The other FACTS devices such as static var compensators, thyristor controlled series capacitors (TCSC), series compensators (SSSC) and unified power flow controllers (UPFC) have not yet widely been investigated for wind turbine direct-driven PMSGs. Thus, a further research in this area is also important. Generally, compared to that of DFIG-based wind power penetration, mitigation of the dynamic stability of a power system with high PMSG-based wind power penetration is not sufficiently investigated. As the recent trend of the wind industry is tilted towards wind turbine direct-driven PMSGs [46], a further research in this sector is decisive.

### 2.8.4 Virtual Control

The dynamic performances of a wind turbine direct-driven PMSG and a power system containing it can be enhanced by employing virtual controls which emulate conventional approaches. Currently, the widely-used virtual control is virtual inertia control, applied to wind farms to support dynamic frequency control in a power system [111, 112]. Different schemes are used to realize virtual inertia control. The Conventional method is based on frequency deviation in a power system and is implemented as an appropriate supplementary frequency control loop in the generator-side converter controller [113, 114]. The other approach is based on optimal power tracking [115]. The third approach uses advanced control algorithm where self-tuning capacity and robustness are considered [116]. The fourth and

last approach uses the concept of emulating conventional synchronous machines and is named virtual synchronous machine approach [117]. The concept of virtual control is a new research area and can be extended to emulating other parameters of conventional power system components.

Therefore, in summary, the primary objective of this research is to investigate the impacts of stochastic wind speed disturbances on the dynamic performances of a wind turbine direct-driven PMSG, and influencing the dynamics of a power system containing a PMSG-based wind farm. In the light of the existence of negative effects, this thesis extends the concept of virtual control to emulating resistors, compensators and damper windings, in deriving virtual control mechanisms, to enhance the dynamic performances of PMSG-based wind farms, and thus the dynamic stability of a power system. Moreover, the thesis investigates the use of a virtual control alongside FACTS devices to improve the dynamic performances of a power system further.

## 2.9 Conclusion

This chapter has presented the review of power system dynamics, power system disturbances, wind speed modelling, and influences of wind power integration on power system dynamics. The impacts of large-scale PMSG-based wind power penetration on the dynamic stability of a power system have also been reviewed. Depending on factors taken into consideration during investigations, divergent results varying from positive to negative impacts are observed in the prevailing research works.

Several mitigation techniques to improve the dynamic performances of a wind turbine direct-driven PMSG and the power system containing it under different power system disturbances are proposed. The techniques are based on real power control, reactive power control and FACTS devices. In most studies, factors considered are divergent and the authors employ proportional-integral controllers. A new research area called virtual control has appeared, particularly, related to inertia control in wind farms. This thesis extends the concept of virtual control to enhance the dynamic performances of a wind turbine direct-driven PMSG by emulating resistors, compensators and damper windings.

The review has also depicted that wind speed disturbances are neglected in the investigations of the dynamic performances of a power system having wind power plants. As the penetration level grows further, the impacts of the stochastic wind speed disturbances on

the power system dynamics become significant. Chapter 3 presents characterization of wind speed time series for dynamic simulation of wind turbines using raw wind speed data obtained from Durban. The results will be used in Chapters 4, 5 and 6.

## CHAPTER 3

### MODELLING AND ANALYSIS OF WIND SPEED SERIES

#### 3.1 Introduction

Modelling, analysis, and simulation of the dynamic behaviour of a wind turbine directdriven PMSG require an appropriate wind speed model; hence, the wind speed series of a specific site where the wind turbine is planned to be erected should be appropriately modelled and analysed to attain comprehensive results. One of the main advantages of having the wind speed model compared to measured wind speed series is that the user can freely generate the required wind speed series for dynamic simulations. For that reason, this chapter deals with modelling and analysis of wind speed series, which are inputs to the models of the wind turbine direct-driven PMSGs in the next chapters of this thesis.

There are various types of wind speed models in the existing literature. Different methods have been employed for time series characterization of wind processes. Traditionally, Weibull distribution is used to represent wind speed series at a given site [33—35]. Normal, Gamma, Lognormal or combination of these distributions with Weibull distribution [31, 70—72] can also be used to model wind speed series. Kernel density method is used in [72]. A typical distribution may not necessarily represent the cumulative wind behaviour of all locations in a region [31]. Thus, the wind speed series for a particular location needs to be modelled. The above distributions cannot be used when chronology is vital [33]. In reality, the current wind speed depends on the previous one indicating chronology should be considered in the modelling. Evolutionary algorithms such as genetic algorithm and local search techniques are also used in wind speed modelling [74]. However, these algorithms are time consuming [33]. A Markov chain wind speed model which retains chronology and consumes less computing time can also be employed. In this work, this model along with Weibull and Gaussian distributions is used to generate synthetic wind speed data for dynamic simulations of wind turbines and validation of proposed dynamic performance mitigation



methods. Composite and Fourier Series models can also be used in the investigation of the dynamic performances of the PMSG.

## 3.2 Markov Chain Wind Speed Model

### 3.2.1 Introduction

Wind is a random stochastic process whose dynamic behaviour can be represented by a stochastic model [53]. Naturally, wind depends on pressure gradient, waves, jet streams, and local weather conditions [69]. The stochastic modelling of wind is a complicated task because of its strong variability in time and land terrains. Over a year, wind speed is periodic, showing seasonal variations; however, hourly average wind speed is a stochastic process with a Weibull probability density function; whereas within minutes, it follows a Gaussian random process [36].

Therefore, the Markov chain model, which retains chronology and consumes less computing time, could be employed to synthesize wind speed time series [36—39] for dynamic simulation and wind power forecasting. The accuracy of a Markov model increases with its order [37]. The first-order model is often adopted for its simplicity and less computing time [39]. A modified Markov model [75] illustrates better performances than the corresponding normal model in preserving the properties of wind speed series. Particularly, the second order semi-Markov process is more suitable for processes having states with time varying durations [36].

Few efforts have been done to characterize wind speeds and power for generation of electricity in South Africa using computer algorithms and frequency distribution methods [76—78]; however, the Markov model has never been used, particularly, in Durban, South Africa. As wind speed models strongly depend on location, an investigation into the wind speed series in the site is crucial. Therefore, in this work, a Markov chain model is employed to characterize the wind speed series in Durban. The model is also compared with Weibull distribution. The comparison shows the Markov Model is more effective than the Weibull distribution. Finally, Weibull and Gaussian probability density functions, along with the Markov model, are employed to produce synthetic wind speed series over minute and second intervals respectively. Generation of artificial wind speed series is crucial for dynamic simulation of wind turbines.

### 3.2.2 Data Analysis and Markov Chain Model (MCM)

#### 3.2.2.1 Wind Speed Data

The data used in this work have been obtained from South African Weather Services (SAWS). Hourly wind speed measurements were taken at Durban South Merebank (DSM) (29.9560°S, 30.9730°E) from January 2014 to December 2015. At the station, the anemometers were installed at 8 m hub height.

#### 3.2.2.2 Data Analysis

Wind speed directions are not considered in this thesis as wind energy density mainly depends on the speed. The wind speed data from the weather station at DSM were measured at a hub height of 8 m. However, the height of the tower of a wind turbine is far longer than 8 m. Thus, these wind speed data are converted to the corresponding higher hub height data by the power law wind speed profile [118] defined as:

$$v_2 = v_1 \left( \frac{h_2}{h_1} \right)^\alpha \tag{3.1}$$

- where  $v_2$  - wind speed at hub height 2
- $v_1$  - wind speed at hub height 1  $h_1$  - hub height 1  $h_2$  - hub height 2
- $\alpha$  - Hellman Exponent

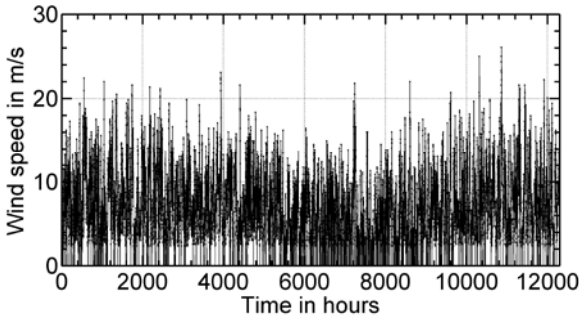


Figure 3.1. Observed wind speed series at DSM

Figure 3.1 shows the two years’ distribution of wind speed series at DSM. These hourly wind speed data are statistically analysed to generate monthly hourly mean wind speed data.

The resulting data are used to sketch the wind speed contour maps for Durban. Figures 3.2 and 3.3 show the wind speed contour maps for 8 and 70 metre hub heights at DSM weather station respectively. The hourly wind speed values shown in Table 3.1 are obtained at a hub height of 70 m and range from 0 to 23 m/s. However, monthly hourly mean wind speeds at the same hub height range from 1.5 to 12 m/s.

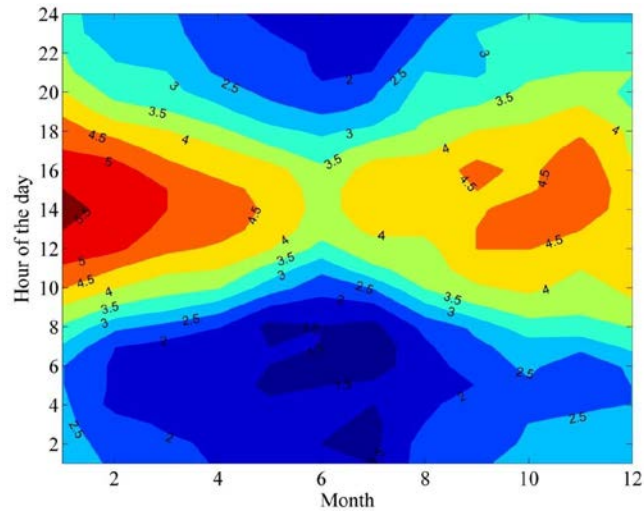


Figure 3.2. Monthly hourly mean wind speeds at DSM at 8 m hub height

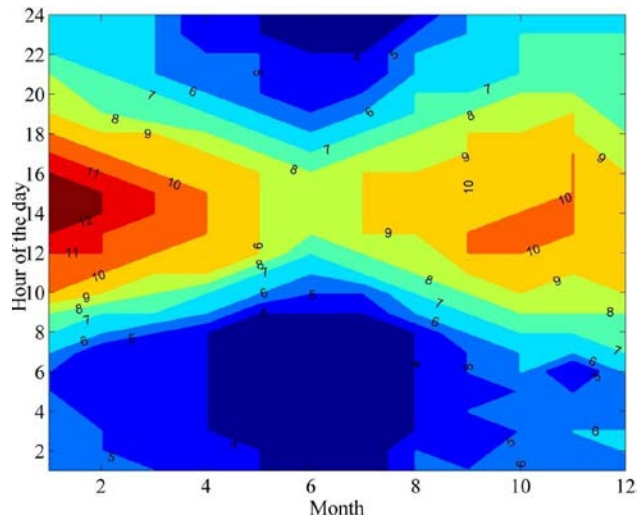


Figure 3.3. Monthly hourly mean wind speeds at DSM at 70 m hub height

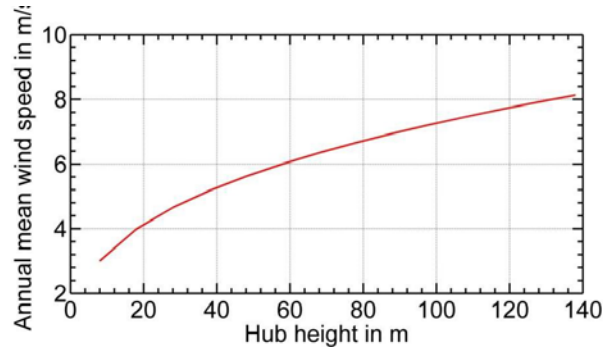


Figure 3.4. Annual mean wind speeds at different hub heights

Figure 3.4 shows the relationship between annual mean wind speed and hub height in Durban. As expressed in (3.1), the mean wind speed value increases with the increase in hub height. Figure 3.4 is plotted using (3.1). The Hellman exponent ranges from 0.27 to 0.33 [118].

### 3.2.3 Developing MCM

Markov chain is a stochastic process, satisfying the Markov property and characterized by memorylessness [119]. Indeed, the chain is a series of transitions between states (or values) of the process where the future state relies on the current state and not on how the process arrives at this particular state [36]. This model primarily takes into account the state, time index and statistical dependency of the random process [36, 119]. Moreover, the states may be finite or infinite. Thus, in this work, a finite number of states is considered.

Furthermore, the dimension of the state space considered has a significant effect on the accuracy of the MCM [120]. The accuracy of the model increases with the dimension of the state space and the statistical characteristics of the wind speed series are satisfactorily preserved.

In this section, the relationship between the stochastic properties of wind speed processes and the MCM are investigated. Initially, hourly wind speed measurements from DSM (29.9560°S, 30.9730°E) are classified into sixteen distinct states with 1 m/s intervals as shown in Table 3.1. Subsequently, a transition probability matrix (TPM) describing these states is determined using the Markov chain approach. Based on this matrix, an attempt is made to develop an algorithm which is implemented in MATLAB® to generate wind speeds

from the principal elements of the model. The wind speed series generated from the proposed model are then compared with the actual measurements via statistical tools and error analysis.

The probability density functions of the observed, generated and the Weibull distribution, whose scale shape parameters are obtained from observed data in section 3.2.5, are compared.

### 3.2.3.1 TPM and Limiting Probabilities

TPM is the base for any MCM. In developing this model, first, the states of the model should be decided. Hence, the wind speed states are classified in the interval of 1 m/s as shown in Table 3.1, except the first state which ranges from 0 to 2 m/s.

Table 3.1. Wind speed states and corresponding frequencies at 70 m hub height

State	Wind speed boundaries (m/s)	Observed Frequency	Expected Frequency
1	0—2	1848	1847.488
2	2—3	966	966.1512
3	3—4	1139	1138.239
4	4—5	1249	1248.867
5	5—6	1044	1043.591
6	6—7	843	842.002
7	7—8	932	931.7336
8	8—9	890	888.7116
9	9—10	638	637.9548
10	10—11	718	717.8528
11	11—12	561	560.5152
12	12—13	387	387.198
13	13—14	340	340.4884
14	14—15	266	265.5072
15	15—16	141	141.358
16	>16	328	328.1964
Total	16	12290	12290

The elements of the TPM shown in (3.2) are calculated as follows: for N states at each time step, there may be N moves between two consecutive time steps. Thus, the transition probability from state i at time t to another state j at time t+1, denoted by  $p_{ij}$ , is calculated from measured wind speeds at DSM.

The elements of the TPM are bounded within  $0 \leq p_{ij} \leq 1$  such that,  $\forall i, j \in 1, \dots, N$ . The element  $p_{ij}$  denotes the probability of switching from state  $i$  to state  $j$  or remain in the same state. All elements of the matrix are greater than or equal to zero. The general state TPM is given by:

$$P = \begin{bmatrix} p_{11} & p_{12} & \dots & p_{1N} \\ p_{21} & p_{22} & \dots & p_{2N} \\ \vdots & \vdots & \ddots & \vdots \\ p_{N1} & p_{N2} & \dots & p_{NN} \end{bmatrix} \quad (3.2)$$

As sixteen states are considered in the state space, the size of the transition matrix will become  $16 \times 16$ , where  $N$  is 16. The state TPM should fulfil the constraints given in (3.3) and (3.4).

$$0 < p_{ij} < 1 \quad (3.3) \quad \sum_{j=1}^N p_{ij} = 1 \quad (3.4)$$

The elements of  $P$  in (3.2) are calculated as:

$$p_{ij} = \frac{N_{ij}}{\sum_{j=1}^N N_{ij}} \quad (3.5)$$

where  $N_{ij}$  is the number of jumps from state  $i$  to state  $j$ . The elements of matrix  $P$  represent the frequency of the observed wind speed states, which come to the  $j^{\text{th}}$  state from the  $i^{\text{th}}$  state at the previous time step.

The data shown in Figure 3.1 are modelled using the Markov model. The elements of the matrix in (3.2) are calculated using (3.5), and Table 3.2 shows the elements of the TPM obtained.

In the MCM, another important factor is the limiting probability matrix (or steady state vector),  $\pi$ , which shows the total percentage occurrence of a state in a chain. This vector is equivalent to the  $m^{\text{th}}$  power of  $P$  i.e.,  $\pi = \lim_{m \rightarrow \infty} P^m$ . The steady-state behaviour of a Markov chain is given as [121]:

$$\pi [ \dots ] = [ \dots ] P \quad (3.6)$$

where  $\pi_i$  is the steady state probability for the  $i^{\text{th}}$  state.

Table 3.2. TPM

	1	2	3	4	5	6	7	8	9	10	11	12	13	14	15	16
1	0.73377	0.14881	0.07143	0.02273	0.0119	0	0	0	0	0	0	0.00054	0.00162	0	0	0
2	0.30745	0.30021	0.22774	0.09938	0.0352	0.01346	0	0	0	0.00207	0.00311	0	0	0.00104	0	0
3	0.10975	0.21071	0.32924	0.19315	0.08692	0.03336	0.01932	0	0	0.00439	0.00176	0.00176	0.00176	0	0.00088	0
4	0.04484	0.08006	0.21137	0.34988	0.16813	0.07526	0.03122	0.01922	0	0.004	0.0032	0	0.0016	0	0.0016	0.0008
5	0.01245	0.03736	0.0795	0.23659	0.2682	0.1705	0.11303	0.03831	0.02011	0.01149	0.00287	0.00287	0.00287	0.00192	0	0.00192
6	0	0	0.04508	0.13998	0.22657	0.21352	0.19336	0.09371	0.03559	0.01779	0.00356	0.00474	0.00356	0.00356	0	0.00474
7	0.00107	0	0.01931	0.05365	0.13841	0.21567	0.25966	0.16845	0.07296	0.04077	0.0118	0.00215	0.00215	0.00322	0	0.00215
8	0	0	0	0.03034	0.05843	0.08764	0.20899	0.2764	0.13933	0.10787	0.05618	0.01573	0.00899	0	0.00337	0.00225
9	0	0	0	0	0.02669	0.04867	0.12559	0.24176	0.21978	0.18838	0.07849	0.02983	0.01256	0.00314	0.00314	0.00628
10	0	0	0	0	0	0.02228	0.06267	0.15877	0.17688	0.27994	0.16156	0.06825	0.03203	0.01253	0.00418	0.00836
11	0	0	0	0	0	0	0.0303	0.06952	0.11765	0.22282	0.26025	0.16221	0.06595	0.03387	0.01426	0.00357
12	0	0	0	0	0	0	0	0	0.05685	0.13953	0.24289	0.19897	0.17829	0.08527	0.03618	0.02326
13	0	0	0	0	0	0	0	0	0.03824	0.07647	0.12941	0.20882	0.23235	0.16765	0.03824	0.05882
14	0	0	0	0	0	0	0	0	0.02256	0.04887	0.07895	0.12782	0.18421	0.2406	0.15789	0.12406
15	0	0	0	0	0	0.00709	0	0	0.02128	0.01418	0.03546	0.08511	0.20567	0.2766	0.14184	0.20567
16	0	0.00305	0	0	0	0	0	0	0.00305	0.0122	0.02744	0.02439	0.07012	0.10366	0.10061	0.65244

The sum of the elements within the limiting probability vector at steady state is given by:

$$= 1 \quad (3.7)$$

Table 3.3 shows the limiting vector, which is expressed as the fraction of the time the system in a state, is given by the 82<sup>nd</sup> (m = 82) power of the transition probability matrix, P. Moreover, the expected frequency column in Table 3.1 is obtained using this limiting vector. For example, if there are T hours in a given time interval, 0.0927\*T of the intervals will have wind speeds in the range 3 to 4 m/s, and 0.0456\*T will have wind speeds between 11 and 12 m/s. The limiting vector of the Markov chain model is close to the real wind speed series, as depicted in Table 3.1.

Table 3.3. The limiting vector

States	1	2	3	4	5	6	7	8
	0.1504	0.0786	0.0927	0.1016	0.0849	0.0686	0.0758	0.0723
States	9	10	11	12	13	14	15	16
	0.0519	0.0584	0.0456	0.0315	0.0276	0.0216	0.0115	0.0267

### 3.2.3.2 Generation of Wind Speed Series Using MCM

At this point in this work, the TPM representing wind speed series, limiting state probabilities and expected frequencies have been determined from wind speed measurements at DSM. Reasonably, the application of the Markov chain concept to wind speed series could assist in the synthesis of the random behaviour of wind speed series. Consequently, in this section, wind speed series are generated in MATLAB®. Finally, the accuracy of the proposed MCM is compared with the measurements from the DSM weather station.

The generation of synthetic wind speeds is based on the elements of the TPM, which lie between 0 and 1, in Table 3.2. In fact, the cumulative TPM (CTPM) whose elements are obtained from the TPM as shown in (3.8) is the basis for wind speed series generation using the MCM.

$$= \quad (3.8)$$



$P_{ik}$  is the transition probability in row  $i$  at state  $k$ . Table 3.4 shows the corresponding CTPM obtained from Table 3.2.

In the synthesis of the wind speed time series, MATLAB® random number generators are used to generate numbers based on the arranged states in Table 3.1. Subsequently, the randomly generated numbers are distributed among the different wind speed states according to the CTPM. Generally, the following algorithm is adopted in the synthesis of the wind speed data:

1. An initial state is taken randomly.
2. A set of uniformly distributed random numbers between 0 and 1 are generated.
3. A new wind speed state is determined when the upper boundary of the interval in which the random value generated in step 2 is greater than the element of the CTPM of the previous state and less than or equal to the element of the CTPM of the next state.
4. The intermediate wind speed values are obtained from a random number generator based on Weibull and Gaussian distributions for minute and second wise time intervals using the data obtained in step 3.

Therefore, this algorithm can be used to generate any desired number of wind speeds. A sample generated wind speed time series which are generated using this algorithm are shown in Figure 3.5.

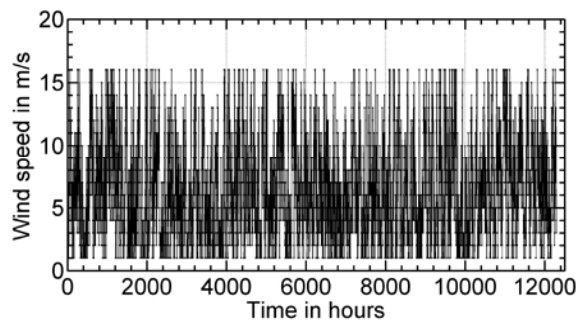


Figure 3.5. Synthetic wind speed data

Table 3.4. CTPM

States	1	2	3	4	5	6	7	8	9	10	11	12	13	14	15	16
1	0.733766	0.882576	0.954004	0.976732	0.988636	0.994046	0.996206	0.997286	0.997827	0.997827	0.997827	0.998368	0.999992	0.999992	0.999992	0.999992
2	0.307453	0.60766	0.835404	0.934783	0.969979	0.983437	0.988617	0.992757	0.993797	0.995867	0.998973	0.998973	0.998973	1.000008	1.000008	1.000008
3	0.109745	0.320457	0.649693	0.842845	0.929763	0.963126	0.982441	0.985951	0.989461	0.993851	0.995606	0.997362	0.999118	0.999118	0.999996	0.999996
4	0.044836	0.1249	0.336269	0.686149	0.854283	0.929544	0.960769	0.979984	0.988794	0.992797	0.996	0.996	0.997601	0.997601	0.999202	1.000003
5	0.012452	0.049808	0.12931	0.3659	0.6341	0.804598	0.917625	0.955939	0.976054	0.987548	0.990421	0.993295	0.996169	0.998084	0.998084	1
6	0	0.0142	0.059277	0.199253	0.425825	0.639348	0.832705	0.926418	0.962005	0.979799	0.983358	0.988103	0.991661	0.99522	0.99522	0.999965
7	0.001073	0.009653	0.028966	0.082614	0.221026	0.436692	0.696348	0.864803	0.937765	0.978537	0.99034	0.992486	0.994632	0.99785	0.99785	0.999996
8	0	0.00112	0.00449	0.034827	0.093254	0.180894	0.389883	0.666288	0.805614	0.913479	0.969659	0.985389	0.994378	0.994378	0.997748	0.999996
9	0	0	0.00471	0.01571	0.042398	0.091063	0.216652	0.45841	0.67819	0.866573	0.945066	0.974894	0.987453	0.990592	0.993732	1.000011
10	0	0	0.00139	0.00696	0.01253	0.034814	0.097488	0.256263	0.433143	0.713087	0.874647	0.942892	0.974926	0.98746	0.991639	0.999995
11	0	0	0.00357	0.00535	0.01426	0.01961	0.049913	0.119432	0.237079	0.459895	0.720145	0.882355	0.948309	0.982177	0.996437	1.000002
12	0	0	0	0	0.00258	0.00258	0.01288	0.03868	0.095528	0.235062	0.477956	0.676923	0.855217	0.940489	0.976664	0.99992
13	0	0	0	0	0	0	0.0206	0.05	0.088235	0.164706	0.294118	0.502941	0.735294	0.902941	0.941176	1
14	0	0	0	0	0	0	0	0.015	0.037556	0.086429	0.165376	0.293195	0.477406	0.718008	0.875902	0.999962
15	0	0	0	0	0	0.007092	0.007092	0.014182	0.035459	0.049643	0.085104	0.170211	0.375884	0.65248	0.794324	0.999998
16	0	0.003049	0.003049	0.003049	0.003049	0.003049	0.003049	0.006099	0.009148	0.021343	0.048782	0.073172	0.143294	0.246952	0.347562	1.000001

### 3.2.4 Validation of the Markov Model

To validate the MCM, the statistical characteristics of the synthetic wind speed series are compared with that of the measured ones as shown in Table 3.5.

Table 3.5. Comparison of measured and generated wind speeds

	Measured wind speeds	Synthetic wind speeds	Error (%)
Median	5.9800	5.8357	2.4
Mean	6.46	6.42	0.62
Standard deviation	4.48	4.41	1.56

Another metric used to validate the MCM is probability density function (PDF). The PDF of any stochastic model provides adequate information rooted in the data by assessing the frequency distribution and general statistical parameters such as mean and standard deviation. Accordingly, the PDF of the wind speed series measured at DSM for a period of two years (at 1 hour time interval) is compared with that of synthetic wind speeds, generated by the developed MCM for model validation.

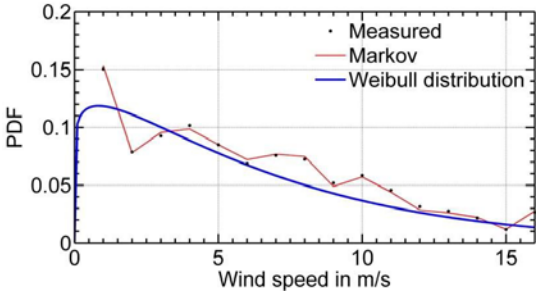


Figure 3.6. PDFs of measured, generated wind speeds and Weibull distribution

The Root-Mean-Square Error (RMSE) given by (3.9) can also be used to evaluate the performance of the MCM. This statistical tool measures the average distance between the observed and generated data in Figure 3.6.

$$RMSE = \sqrt{\frac{1}{T} \sum_{i=1}^N (E_i - F_i)^2} \tag{3.9}$$

$E_i$  is the dataset from measurement and  $F_i$  is the proposed model dataset for the number of sample size,  $T$ .  $N$  is the size of the data set and  $i$  is a counter in (3.9).

The RMSE value of the PDF distributions for the measured and the MCM generated wind speed series is 0.0021, and that of the PDF distributions for the measured and the Weibull is 0.0160.

### 3.2.5 Weibull Distribution

Currently, the Weibull distribution is widely employed in modelling wind speed series in dynamic simulations of wind turbines. Its PDF is given as [122]:

$$f(x) = \frac{b}{a} \left(\frac{x}{a}\right)^{b-1} e^{-\left(\frac{x}{a}\right)^b} \quad x \geq 0, \quad a, b > 0 \quad (3.10)$$

where  $a$ ,  $b$  and  $x$  represent the wind speed, the scale and shape parameters of the Weibull distribution respectively.  $a$  and  $b$  are calculated using the maximum likelihood estimation method [123] from the observed wind speed data and are found to be 6.75 and 1.11 respectively. Figure 3.6 shows the plot of the Weibull distribution PDF.

### 3.2.6 Intermediate Wind Speeds

Although the MCM generates hourly mean wind speed series, it is not capable of generating wind speed series in between hours and minutes because the wind speed series obtained from DSM were hourly mean wind speeds. This is one limitation of this work. For this reason, Weibull and Gaussian (3.11) [122] distributions are employed to predict wind speeds between successive hours and minutes using parameters obtained from the Markov model.

$$f(x) = \frac{1}{\sigma\sqrt{2\pi}} e^{-\frac{(x-\mu)^2}{2\sigma^2}} \quad (3.11)$$

where  $x$  and  $\mu$  represent the wind speed and the mean of the wind speeds, and  $\sigma$  is the corresponding standard deviation.

Thus, the codes for the Weibull and Gaussian distributions are incorporated in the main MATLAB® code. The mean and the standard deviation of the Gaussian distribution are 6.24 and 4.36 respectively. Figures 3.7 and 3.8 show the intermediate wind speed series where

linear interpolation is adopted to obtain continuous wind speed. Flat interval wind speeds in between minutes and seconds can also be employed.

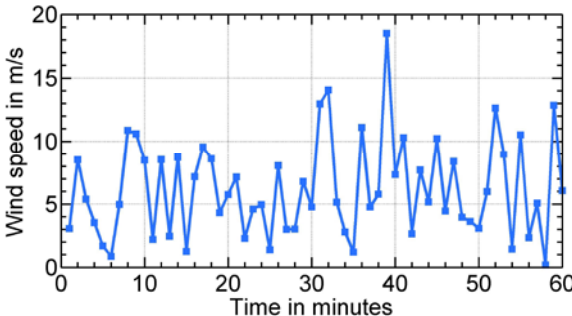


Figure 3.7. Wind speeds generated using a Weibull distribution based on MCM data

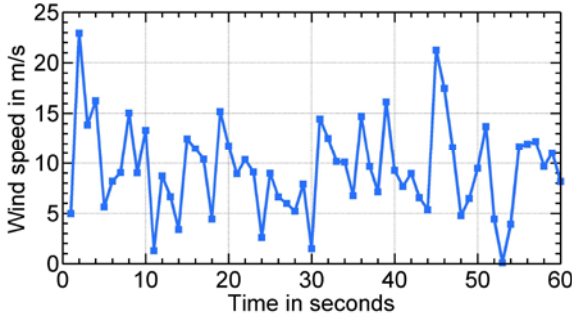


Figure 3.8. Wind speeds generated using Gaussian distribution

### 3.2.7 Wind Power Density (WPD) Distribution

The WPD distribution indicates the wind power available at different wind speeds. Generally, it is given as [124]:

$$P = \frac{1}{2} \rho v^3 f(v) \quad (3.12)$$

where  $f(v)$  is the frequency of wind speeds and  $\rho$  is air density which is  $1.225 \text{ kgm}^{-3}$  for standard conditions. The cumulative density probability of wind speeds and power in Durban is shown in Figure 3.9.

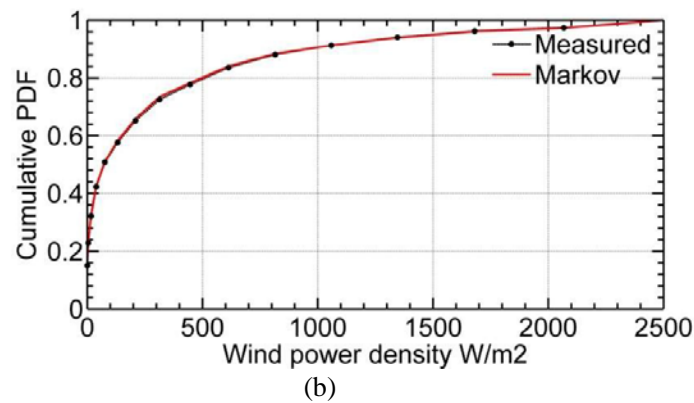
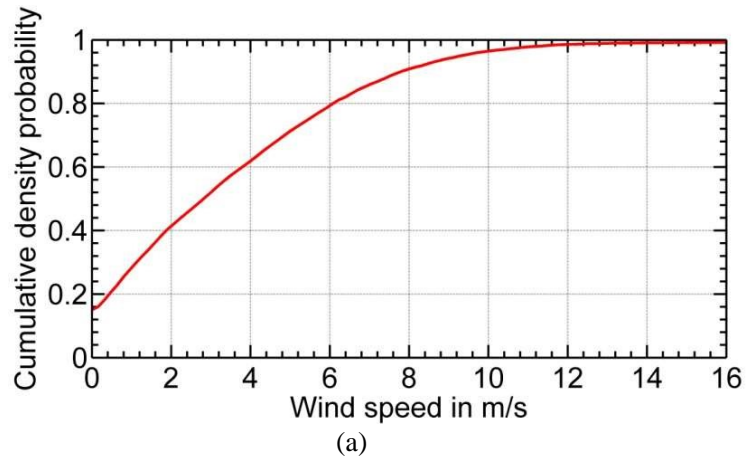


Figure 3.9. Cumulative density probability for (a) wind speeds (b) wind power density in Durban

### 3.2.8 Results and Discussion

#### 3.2.8.1 Wind Speed Analysis

Figure 3.1 showed the hourly mean wind speed series from January 2014 to December 2015 in Durban. These data were obtained from SAWS. The wind speed, which is very stochastic, highly depends on temperature variations as shown in Figure 3.2, contour map for hourly monthly wind speeds. Wind speed increases with solar radiation. In fact, wind is created by differential heating of the earth's surface by the sun. The daily maximum wind speed is observed from 13h00 to 16h00 where maximum temperature is also observed, whereas the minimum speed occurs after midnight. Wind speed density is high during working hours, which is crucial for wind turbine operators. Furthermore, Figure 3.2 showed the dependence of wind speed series on seasonal variations. From December to March,

relatively hot months, the wind speeds are relatively high (2.5 – 5.5 m/s monthly average wind speed). On the other hand, from April to August, corresponding to the dry season, usually, low wind speeds (1.5 – 3 m/s monthly average wind speed) are expected. September, October and November see monthly average wind speeds ranging from 2 to 4.5 m/s. Wind speed also increases with hub height as shown in Figures 3.3 and 3.4.

### 3.2.8.2 MCM and Weibull Wind Speed Distributions

The MCM was developed. The main component of this model is the TPM, shown in Table 3.2. Observing this matrix, the highest probabilities are around the main diagonal of the matrix. This indicates that if the current state is given, there will be a high probability that the next wind speed will remain in the same state. For instance, if the present wind speed is in the range 5 to 6 m/s, there will be a probability of 0.27 that the subsequent wind speed will stay the same. This shows wind speed retains chronology.

Another characteristic of the transition matrix is that the transition probability of a state to a higher state is less than the probability of transition to a corresponding lower state. For example, if the current state is state 5 (5–6 m/s), the probability of transition from state 5 to state 6 (6–7 m/s) is 0.17 whereas the transition probability from state 5 to state 4 (4–5 m/s) is 0.24. In general, the transition probability matrix shows that the probability of transition from a state to a far higher or lower state is less probable. For instance, if the current state is 2 (2–3 m/s), the probability of switching to state 15 (15–16 m/s) is 0. Similarly, the probability of switching from state 14 (14–15 m/s) to state 3 (3–4 m/s) is 0.

Table 3.5 gave the statistical comparison between the measured and synthetic wind speeds, shown in Figure 3.5, generated by the MCM. The medians are close to each other (5.98 m/s vs. 5.84 m/s respectively). Similarly, the difference between the means (6.46 m/s vs. 6.42 m/s respectively) is insignificant. Moreover, there is no pronounced difference between the standard deviations (4.48 m/s vs. 4.41 m/s respectively). Hence, statistically, the three statistical tools of the synthetic wind speeds are very close to that of the measured ones, showing the suitability of the MCM for modelling wind speed series in Durban.

The traditional way of representing wind speed series is using the Weibull distribution, discussed in section 3.2.5. The PDFs of the measured, the MCM wind speed series and the Weibull distribution were compared in Figure 3.6. The Markov model has a better goodness-of-fit than the Weibull distribution as it takes chronology into consideration. This

validates the accuracy of the MCM, which gives a fair representation of the wind speed measurements.

Figure 3.6 showed PDFs of the measured wind speeds, generated wind speeds and Weibull distributions. The RMSE value of the PDF distributions of the measured data and the Markov model is 0.0021, but the RMSE value of the PDFs of the measured data and the Weibull distribution is 0.0160. The RMSE of the MCM is within the acceptable range ( $\leq 0.05$ ) and by far better than that of the Weibull distribution. Therefore, the Markov model gives an excellent representation of the measured wind speed series at the DSM weather station.

### 3.2.8.3 Intermediate Wind Speed Series

Figure 3.7 showed the wind speed series generated using the Weibull distribution. In this distribution, the minimum and maximum wind speeds are 0.1795 and 18.5 m/s. In Figure 3.8, the Gaussian wind speed distribution was shown and the corresponding minimum and maximum wind speeds are 0.0754 and 22.9 m/s respectively. These wind speeds are close to the ones observed in the measurement.

### 3.2.8.4 Power Density Distribution

Figure 3.9 showed the wind speed and wind power density distributions in Durban. Large wind turbines require a cut-in wind speed of 3.5 m/s [125]. From the figure, it can be observed that there is a 50% probability of obtaining wind speeds greater than this threshold at 70 m hub height. In fact, increasing the hub height increases the chance of obtaining wind speeds greater than the cut-in speed as shown in Figure 3.4, but this action also increases the initial capital cost of the wind turbine. For a good performance of a wind turbine, the mean wind speed at this height should be about 10 m/s [126]. Figure 3.3 showed that the monthly mean wind speeds in December, January, February and March were suitable for wind farms. On the other hand, Figure 3.10 showed the power density distribution over a year for twentyfour hours for 70 m hub height. For effective operation of a large wind turbine, potential sites are considered to have wind power densities ranging from 300 to 550  $\text{Wm}^{-2}$  at 70 m hub height [127]. It can be observed, according to this requirement, all months except May and June were in the domain of suitable months for wind farms. This domain can be further extended by taking higher hub heights as in Figure 3.11. The optimum hub height in



Durban is expected to be around 85 m as shown in Figure 3.12. Therefore, compared to other windy areas, wind power installation in Durban might be more expensive.

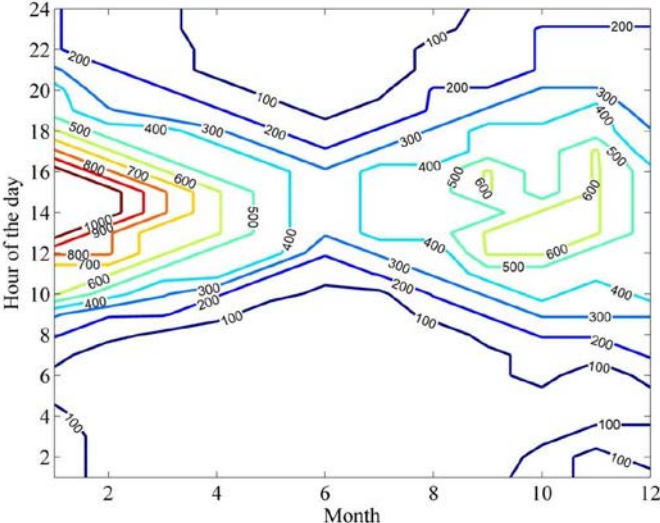


Figure 3.10. Wind power density over a year at 70 m hub height

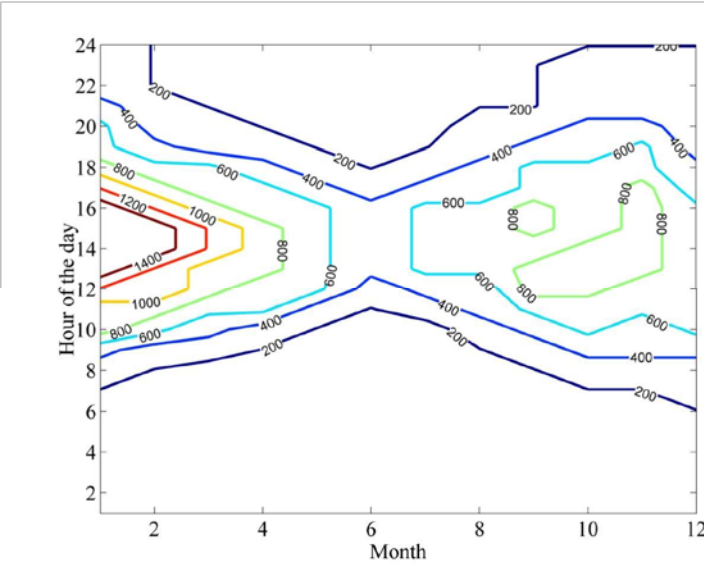


Figure 3.11. Wind power density at 100 m hub height

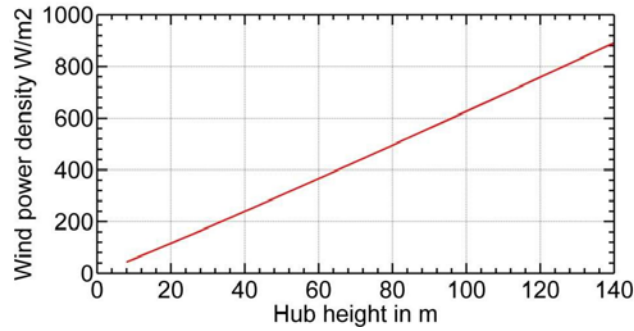


Figure 3.12. Mean wind power density at different hub heights

### 3.3 Composite Wind Speed Model

Wind speed components such as the spatial effect of wind behaviour, gust, ramp changes and background noise affect the dynamic performances of a wind turbine direct-driven PMSG. Hence, one of the wind speed models employed in the existing literature takes these components into consideration [6]. Thus, the model is given as:

$$v(t) = v_b + v_r + v_g + v_n \quad (3.13)$$

where  $v_b$ ,  $v_r$ ,  $v_g$ , and  $v_n$  are the base, ramp, gust and noise components respectively.

The base wind speed is a constant, generally taken as the average of the wind speeds over a certain period.

$$v_b = \frac{1}{T} \int_0^T v(t) dt \quad (3.14)$$

is a constant.

Gust represents the sudden change in wind speed. In the simulation of the dynamic performances of a wind turbine direct-driven PMSG, it can be used for the investigation of the system performances under large disturbances in the wind speed. It is given as [128]:

$$v_g(t) = \begin{cases} 0 & \text{for } t \leq t_{g1} \\ \frac{V_{gm}}{2} \left( 1 - \cos \left( 2\pi \left( \frac{t - t_{g1}}{t_{g2}} \right) \right) \right) & \text{for } t_{g1} < t < t_{g2} \\ 0 & \text{for } t \geq t_{g2} \end{cases} \quad (3.15)$$

where  $V_{gm}$  represents the maximum gust.  $t_{g1}$  and  $t_{g2}$  are starting and end time of the gust wind.

The ramp component depicts the gradual change in the character of the wind speed and is given by:

$$= \frac{0}{0} \left( \begin{matrix} \leq \\ - \\ < \\ \geq \end{matrix} \right) \leq \quad (3.16)$$

where represents the maximum ramp wind. and are starting and end time of the ramp wind.

The noise component can be assumed to be Gaussian noise, having a probability density function given in (3.11); however, in the noise case, the mean and standard deviations are the average and standard deviations of the noise component of the wind speed. A typical composite wind speed is shown in Figure 3.13. In the figure, large wind speed disturbances are observed around the 20<sup>th</sup>, 30<sup>th</sup> and 58<sup>th</sup> seconds while small wind speed disturbances are observed throughout the simulation time.

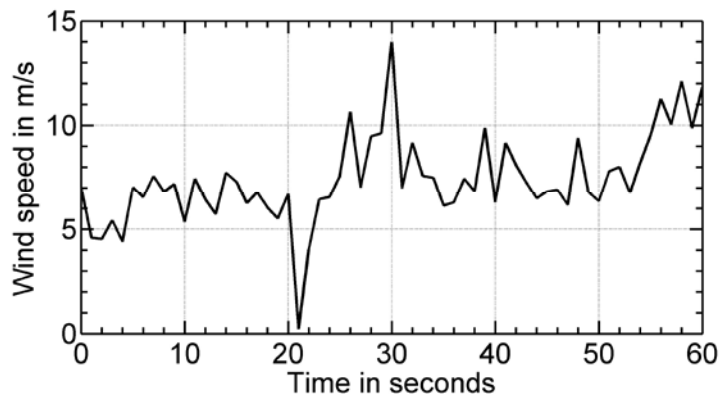


Figure 3.13. Typical composite wind speed series

### 3.4 Fourier Series Wind Speed Model

Wind speed is a random variable and relies on the climate and geographic location of the wind farm. The instantaneous value of the wind can be modelled by superimposing a constant term, deterministic shape functions of time representing gusts and other wind events, and a noise with an adequate spectrum, the latter representing turbulence. For control

purposes, a Fourier series [6] can approximate such behaviour of the wind. Consequently, (3.17) represents a simple wind speed model.

$$v(t) = v_{hub} + \sum_{n=1}^N [a_n \sin(\omega_n t) + b_n \cos(\omega_n t)] \quad (3.17)$$

$v_{hub}$  is the hub wind speed,  $v_{hub}$  refers to the base component of the wind speed,  $a_n$  and  $b_n$  are sine and cosine coefficients respectively,  $\omega_n$  is the angular frequency of the harmonics, and  $N$  is the number of harmonics. Appropriate selection of the harmonics can approximate the gust, ramp and background noise components of the wind speed. The harmonics are important to study the dynamic performances of the wind turbine direct-driven PMSG in relation to wind speed disturbances. A typical wind speed represented by Fourier series method is shown in Figure 3.14. There is a step jump at the seventh second, which will be used in Chapter 4 for dynamic performance analysis of a wind turbine direct-driven PMSG.

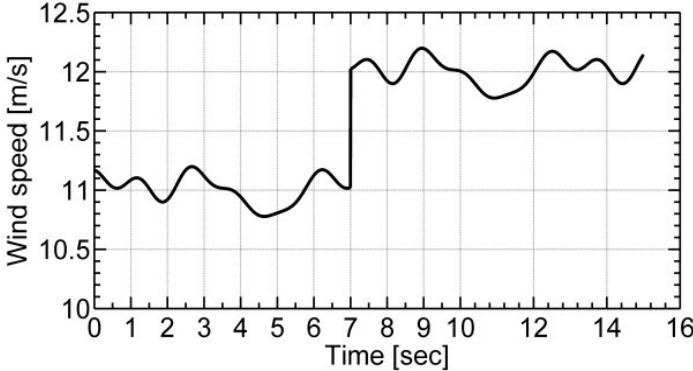


Figure 3.14. Wind speed series represented by a Fourier series method

### 3.5 Conclusion

This chapter presented the modelling and analysis of wind speed series for power system dynamic simulations. Mainly, three types of wind speed models based on stochastic and conventional approaches, namely Markov chain, composite and Fourier series models, had been taken into consideration. The results would be used in Chapters 4, 5 and 6 for validation of proposed mitigation models for enhancing the dynamic performances of a wind turbine direct-driven PMSG and analysis of the impacts of PMSG-based wind farm penetration in a power system. In section 3.2, wind speed measurements from DSM were categorized into sixteen states and used in developing a MCM to generate synthetic wind

speed time series. Metrics like median, mean, standard deviation and probability density function had shown that the developed model represented the measured wind speed series reasonably. Intermediate wind speeds between hours and minutes were generated using Weibull and Gaussian distributions, respectively based on the synthetic, wind speed time series generated by the Markov model. Secondly, in section 3.3, a composite wind speed model consisting of base, gust, ramp and noise components was presented and discussed. Finally, in section 3.4, a wind speed model employing a Fourier series method was discussed and the results from this model will be used in Chapter 4 for analysis and mitigation of the dynamic performances of a wind turbine direct-driven PMSG. Chapter 4 will present the modelling and analysis of a wind turbine direct-driven PMSG for dynamic simulations.

## CHAPTER 4

### MODELLING A WIND TURBINE DIRECT-DRIVEN PMSG FOR DYNAMIC SIMULATIONS

#### 4.1 Introduction

A wind turbine direct-driven PMSG, which is one of the major renewable energy sources in modern power systems, is a complex system. Investigating the dynamic models and mitigation methods for enhancing the dynamic performances of this PMSG is, therefore, crucial in power systems consisting of PMSG-based wind farms. The common disturbances in a wind power plant are wind speed variations, disconnection from the grid, and short circuits on the transmission line connecting the wind turbine to the grid. These disturbances, if not properly controlled, may lead to the instability of the PMSG, which in turn may be the cause of instability of the grid itself. Since wind variations are the prevalent phenomena, this work focuses on the effects of stochastic wind disturbances. The stochastic nature of wind, indeed, severely affects the dynamic performances of the PMSG. For that reason, taking the wind speed models presented in Chapter 3 into account, this chapter models and analyses a wind turbine direct-driven PMSG.

The chapter begins by modelling the different components of the wind turbine direct-driven PMSG and a power grid considered as infinite bus. Subsequently, a novel mitigation method based on compensators is proposed to enhance the dynamic performances of the PMSG. Indeed, this method employing virtual control has not been addressed in the

existing literature. After that, the system is simulated using MATLAB/Simulink. Simulations and analysis of the dynamic responses of the PMSG to different scales of wind speed disturbances are presented.

### 4.2 Wind Turbine Direct-Driven PMSG

Figure 4.1 shows the configuration of a wind turbine direct-driven PMSG connected to a power grid through back-to-back converters, a filter, and a transformer. The converters convert the low frequency (10 – 15 Hz) voltage of the generator into a 50 or 60 Hz voltage, while the filter filters harmonics created by the converters out. The transformer steps up the output voltage of the filter to the grid voltage level [28, 66, 93, 129]. The next sub-sections discuss the dynamic models of the major components of this system.

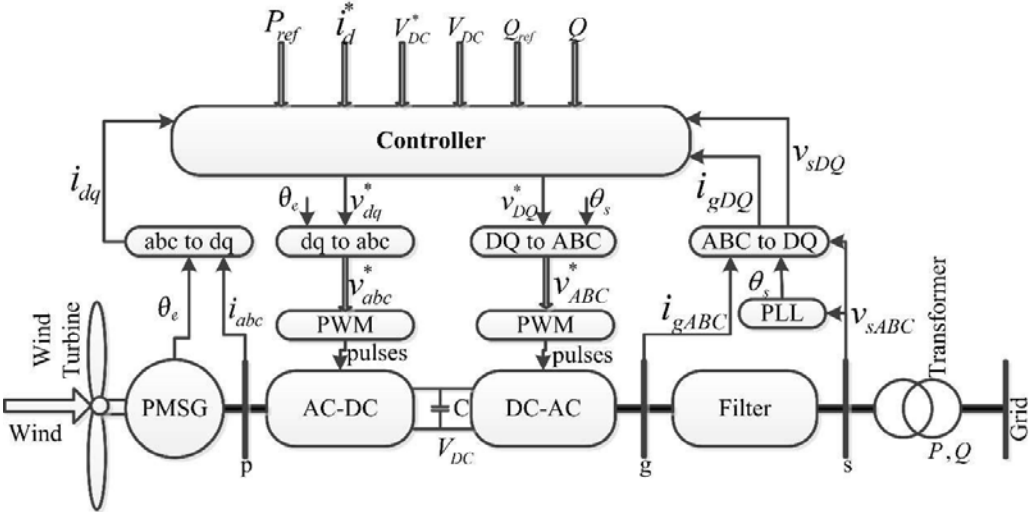


Figure 4.1. A wind turbine direct-driven PMSG connected to a grid

#### 4.2.1 Drive Train

In Figure 4.1, the power electronic converters decouple the wind turbine direct-driven PMSG from the power grid. Thus, disturbances occurring beyond the back-to-back converters have no direct influences on the dynamic performances of the PMSG [93]. Consequently, a one-mass model shown in (4.1) gives the model of the drive train.

$$\frac{1}{s} = - \left( \begin{matrix} - & \end{matrix} \right) \tag{4.1}$$

$$= + \tag{4.2}$$

In (4.1) and (4.2),  $J$  and  $J_r$  are the moments of inertia of the whole drive train, the wind turbine, and the PMSG respectively.  $\omega_r$  is the rotor speed, and  $T_m$  and  $T_e$  refer to the mechanical and electromagnetic torques respectively.  $T_e$  is given as in (4.3).

$$= \frac{1}{2} \rho A v^3 C_p \tag{4.3}$$

The density of air,  $\rho$ , tip to wind speed ratio,  $\lambda$ , blade pitch angle,  $\beta$ , area swept by the blades of the wind turbine,  $A$ , and the wind speed ( $v$ ) determine the mechanical power,  $P_m$ , of the wind turbine. It is given as:

$$P_m = \frac{1}{2} \rho A v^3 C_p(\lambda, \beta) \tag{4.4}$$

where  $C_p$  is the power coefficient of the turbine depending on  $\lambda$  and  $\beta$  as given in (4.5) and (4.6) [28].

$$C_p = 0.5 \left( \frac{116}{\lambda} - 0.4 \right) - 5 \left( \frac{\beta}{\lambda} \right) \tag{4.5}$$

Where

$$C_p = \left[ \frac{1}{\lambda + 0.08} - \frac{0.035}{\lambda} \right] + 1 \tag{4.6}$$

#### 4.2.2 Pitch Angle and Speed Controllers

The pitch angle controller tries to keep the PMSG at its rated power for wind speeds exceeding the nominal value. Various pitch angle controllers have been tested and implemented in wind turbines [130, 131]. In this thesis, a proportional controller, as shown in (4.7), is employed. For the wind turbine used in this work, (4.5) and (4.6) give the maximum power coefficient. Figure 4.2 shows the  $C_p$ -TSR-pitch curves of this turbine at the rated wind speed. In this figure, the minimum and maximum pitch angles are approximately 0 and 25 degrees respectively. In (4.7),  $K_p$  is a proportional constant, and  $\omega_r^*$  is a reference rotor

speed. The rotor reference speed is the rotor speed at the rated wind speed. For wind speed values which are less than the rated value, is assumed to be zero.

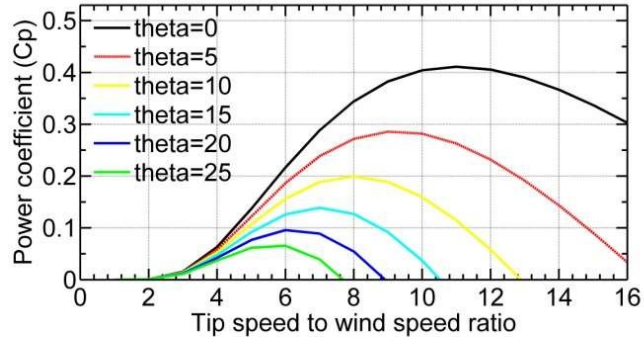


Figure 4.2.  $C_p$ -TSR-pitch curves of the wind turbine at 11 m/s wind speed

$$= ( - ) \tag{4.7}$$

The wind turbine power depends on the wind speed and the pitch angle as shown in (4.5) and (4.6). For a particular wind speed and pitch angle, there is an optimum rotor speed at which the output power is also optimum. The controller tries to keep the generator at this optimum power. Equation (4.8) governs the speed regulator [132]. Reference [130] gives a more explanation and a good analysis of the problem of regulation trajectory design.

$$= \begin{cases} > , \\ \leq , \end{cases} \tag{4.8a}$$

is the reference wind turbine power, whereas is the rated power. refers to the power constant of the corresponding wind turbine and depends on the optimum tipspeed ratio ( ) and maximum power coefficient of the wind turbine. is given as:

$$= \frac{1}{2} , ( ) \tag{4.8b}$$

where R is the length of the blade of the wind turbine.

### 4.2.3 DC-Link Model

In Figure 4.1, as the active power flow through the back-to-back converters and the DClink is balanced, the net power is nil as shown in (4.9).



$$+ + = 0 \quad (4.9)$$

In (4.9), , and are the output power of the PMSG, the DC-link power and the real power supplied to the grid respectively. Expressions for these powers are given in (4.10), (4.11) and (4.12). Inflow power is assumed to be positive.

$$= = - \quad (4.10)$$

$$= + \quad (4.11)$$

$$= + \quad (4.12)$$

is the voltage across the capacitor, is the current through the capacitor, and refer to the D- and Q-axis voltages at the grid side converter terminal. As the wind turbine direct-driven PMSG and the grid are decoupled, they may operate at different frequencies and the d- and q- axes are not necessarily the same as the D- and Q- axes. and are grid currents. Finally, the model of the DC-link is given as:

$$= + + + \quad (4.13)$$

#### 4.2.4 Grid Side Converter Controller

In Figure 4.1, the D- and Q-axis voltages at the terminal of the grid side converter are expressed as in (4.14) and (4.15) respectively [132]. The speed voltages are the results of Park's transformation.

$$= + + \quad (4.14)$$

$$= + + \quad (4.15)$$

and refer to the D- and Q-axis voltages at the right end of the filter. , , and are resistance, inductance and frequency of the filter shown in Figure 4.1.

In Figure 4.3, the grid side controller has four PI controllers, which control the DC voltage, the D- and Q-axis currents, and the reactive power [132]. All quantities with the superscript \* are reference inputs.  $i_{Dg}^*$  is reactive power.  $K_{p4}$ ,  $K_{i4}$ ,  $K_{p5}$ ,  $K_{i5}$  and  $K_{p6}$ ,  $K_{i6}$  are the gains of the controllers. For unity power factor, the reference reactive power is kept at zero.

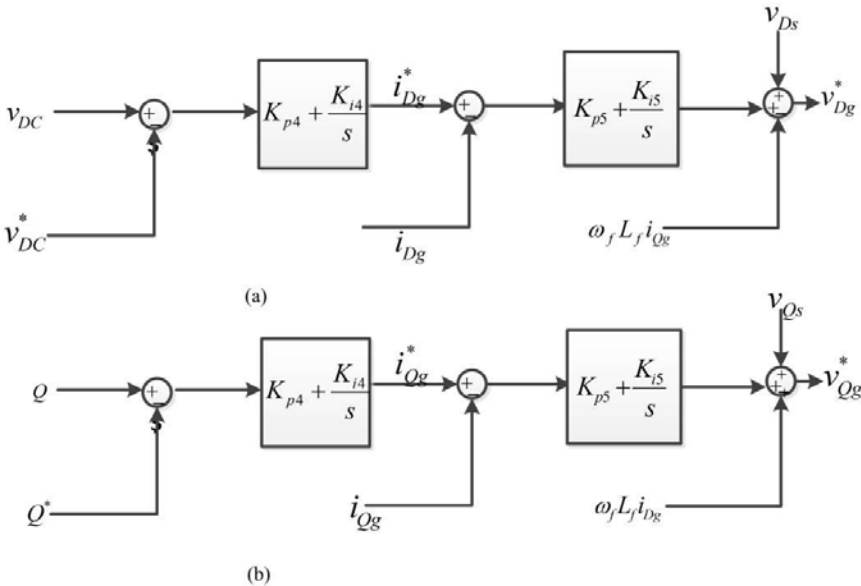


Figure 4.3. Grid-side controller structure

4.3 Power Grid Model

Part of the configuration in Figure 4.1 is shown again in Figure 4.4 in the form of a oneline diagram. In the diagram,  $X_T$  and  $X_L$  refer to the transformer and transmission line impedances respectively, where the respective resistances are neglected, and  $V_{DQs}$  is the grid voltage, which leads the terminal voltage of the filter,  $V_{DQi}$ , by  $\delta$ . The grid is considered as an infinite bus whose voltage magnitude and phase angle are constants.

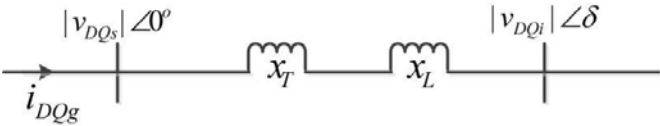


Figure 4.4. One-line diagram of the grid, transmission line and transformer

The current,  $i_{DQg}$ , which flows from the wind turbine to the grid, in Figure 4.4, is given as:

$$\angle 0 - \angle \delta \tag{4.16a}$$

$$= \frac{\quad}{( \quad + \quad )}$$

where  $j$  is a complex operator. Simplifying (4.16a) gives:

$$= \frac{0 - | \quad |}{+} - j \frac{0 + | \quad |}{+} + \quad (4.16b)$$

For unity power factor, as  $i$  is in phase with  $v$ , its real and imaginary parts can be expressed as:

$$= \frac{-| \quad |}{+} \quad (4.17)$$

$$= \frac{- \quad + | \quad |}{+} \quad (4.18)$$

In Figure 4.4, the net real power flows in the same direction as the grid current from the wind turbine direct-driven PMSG to the power grid.

#### 4.4 Proposed Mitigation Method (Using Compensators)

##### 4.4.1 PMSG Model with Compensators

In filters, oscillations and harmonics are damped using active damping techniques, which employ lead, lag or lead-lag compensators [129]. In this work, the same trend is adopted to enhance the dynamic performances of a wind turbine direct-driven PMSG.

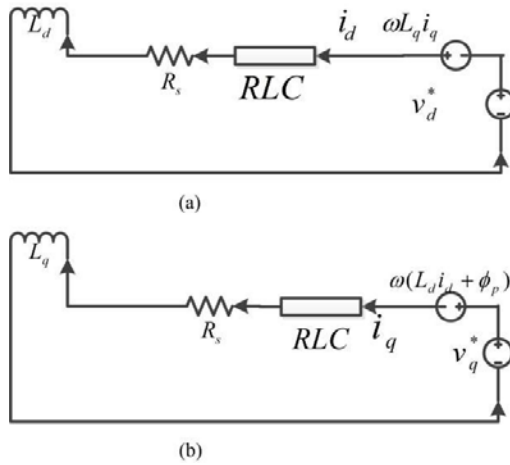


Figure 4.5. (a) d-axis and (b) q-axis equivalent circuits of a PMSG with proposed compensator

The proposed virtual resistive-inductive-capacitive (RLC) circuit, shown in Figures 4.5 (a) and (b), acts as a compensator and supports the stator resistance in damping local oscillations. In practice, this compensator can be realized in the generator side converter controller.

Applying Kirchhoff's voltage law to the equivalent circuits, shown in Figures 4.5(a) and (b), the corresponding new d- and q-axis voltages, which will be considered as references in the controller, are given as in (4.19) and (4.20).

$$v_d^* = v_{d0} + R_s i_d + v_{RLC_d} + \omega L_d i_q \tag{4.19}$$

$$v_q^* = v_{q0} + R_s i_q + v_{RLC_q} + \omega(L_q i_q + \phi_p) \tag{4.20}$$

$v_{d0}$  and  $v_{q0}$  are the voltage drops across the respective virtual RLC circuits.  $L_d$  and  $L_q$  refer to the d- and q-axis inductances,  $\omega$  is the rotor speed in electrical radians,  $i_d$  and  $i_q$  are the d- and q-axis currents, and  $\phi_p$  is the permanent magnet flux.

Analysing (4.19) and (4.20) gives the block diagrams in Figures 4.6(a) and (b) respectively, which are used to model the dynamic behaviour of the PMSG. In both diagrams, the inner loops represent the generator, whereas the outer feedback loops are components appearing due to the virtual compensators. The voltage compensator  $H(s)$  can be a lead, lag

or lead-lag compensator depending on the values of the elements of the virtual RLC circuit as given in (4.21a).

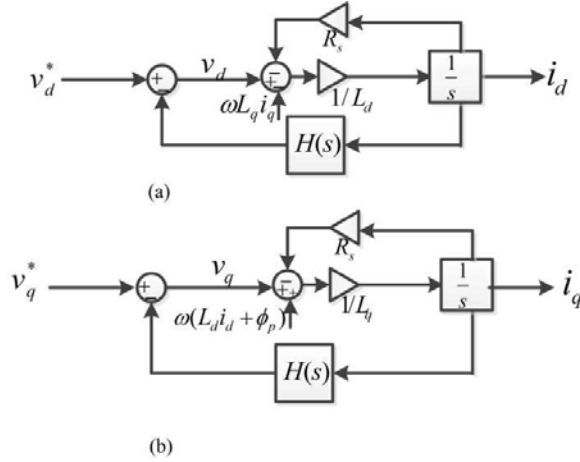


Figure 4.6. Block diagram of the PMSG (a) d-axis and (b) q-axis equivalent circuits with

$$\begin{aligned}
 H(s) &= \frac{s+z}{s+p} \text{ for lag or lead} \\
 &= \frac{(s+z_1)(s+z_2)}{(s+p_1)(s+p_2)} \text{ for lead-lag}
 \end{aligned}
 \tag{4.21a}$$

and are gains; , and are the zeroes, whereas , and are the poles of the compensator H(s).

The virtual RLC circuits only appear as compensators in the generator-side controller, and the gains, zeroes and poles of the compensators can be obtained using Simulink Compensator Design tool (root locus method) or any controller design method. The values of the resistors and inductors can be calculated from the parameters of the compensators depending on the configuration of the R, L and C elements. For example, for two virtual lead or lag RL circuits, with impedances in s-domain  $Z_1(s) = R_1+sL_1$  and  $Z_2(s) = R_2+sL_2$ , connected in parallel, where the capacitive element is zero, H(s) becomes:

$$H(s) = \frac{(sL_1 + R_1)(sL_2 + R_2)}{s(L_1 + L_2) + (R_1 + R_2)}
 \tag{4.21b}$$

In (4.21b), one of the inductances can be assumed to be zero, for example  $L_1 = 0$ . This turns H(s) into a lead or lag compensator depending on the values of  $R_1$ ,  $R_2$  and  $L_2$ . The R

and L components of the virtual circuit are related to the zero, pole and gain of the compensator as:

$$\begin{aligned}
 &= \frac{R_2}{L_2} \\
 &= \frac{R_1 + R_2}{L_2} \\
 &= \dots
 \end{aligned}
 \tag{4.21c}$$

where  $R_1$  and  $R_2$  are resistances and  $L_1$  and  $L_2$  are inductances.

The electromagnetic torque developed in the PMSG is given as [6]:

$$T_e = \frac{3}{4} ( \dots )
 \tag{4.22}$$

where  $p$  is the number of poles of the PMSG.

#### 4.4.2 Modified Generator Side Converter Controller (MGSCC)

This controller controls the real power of the PMSG through the q-axis voltage,  $v_q$ , aiming at minimizing power loss. The d-axis current is maintained at zero to decrease the nonlinearity of (4.22) and minimize current coupling. The d-axis voltage is obtained through controlling the d-axis current and compensating the output of the current controller by  $H(s)$ , as shown in Figure 4.7(a).

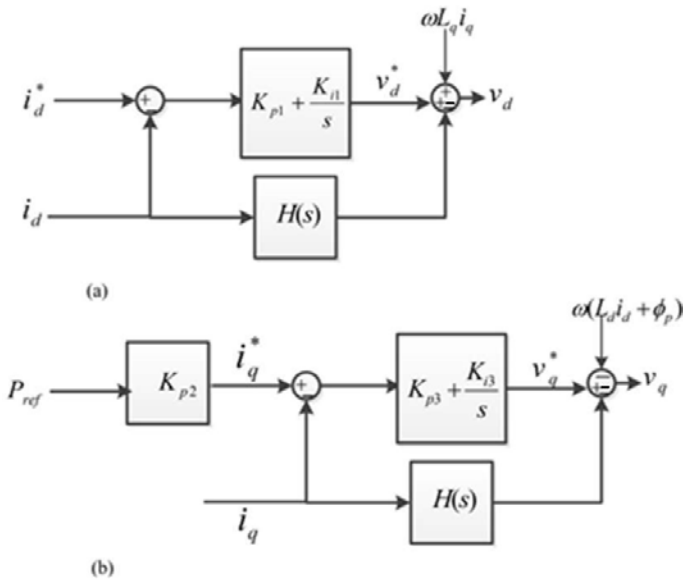


Figure 4.7. Generator side controller with virtual compensators (a)  $i_d$  controller (b)  $i_q$  controller

The dynamic processes of the converters can be ignored because of the fact that they are by far faster than the electromagnetic and mechanical dynamic processes, and it can be assumed that  $v_{d1}$  and  $v_{q1}$  in Figure 4.7 are the same as the d- and q-axis voltages of the generator side converter.

In this control structure, a proportional and two proportional-integral (PI) controllers are used, as shown in Figure 4.7.  $K_p$ ,  $K_{i1}$ , and  $K_{i2}$  are the corresponding gains, and the superscript \* shows that the variable is a reference. The PI controllers in Figures 4.7(a) and 4.7(b) control  $i_d^*$  and  $i_q^*$  respectively.

The negative forward loops, with the transfer function shown in (4.21a), are the results of the proposed virtual compensators. In general, the controller can be interfaced with the generator side converter through a dq-abc axis transformer and a PWM generator as shown in Figure 4.1.

#### 4.5 Simulation Results and Discussion

In this section, the validity of the proposed method is verified by implementing the models in MATLAB/Simulink. The dynamic performances of the wind turbine direct-driven PMSG depend on the system characteristics, the stochastic nature of the wind and local load disturbances in the wind turbine. Particularly, the nature of wind makes the evaluation of these performances challenging, and in this thesis, load and stochastic wind speed disturbances are considered.

The disturbances that may occur in the wind turbine direct-driven PMSG are wind speed variations, disconnection from the grid and short circuits on the line connecting the wind turbine with the power grid. Since wind speed variations are the most frequent disturbances, this work focuses on wind speed disturbances.

The thesis aims to illustrate the effectiveness of virtual compensators in enhancing the dynamic performances (both transient and small-signal stabilities) of a wind turbine directdriven PMSG under stochastic wind speed disturbances. Focusing on this, standard PI

controllers are employed as they are simpler in construction, easier to implement, widely used and provide satisfactory performances under various operating conditions of a system.

This work tested standard methods such as Ziegler-Nichols' method and Simulink Compensator Design tool using root locus method to tune various PI controllers used, and it has been observed that the best performances of the system is obtained when the gains for the PI controllers, obtained from Simulink Compensator Design tool, were used. For instance, Table 4.1 compares the performances of the rotor speed when the PI controllers are tuned with the standard and Simulink methods. In the test, a constant wind speed of magnitude 12 m/s was applied to the wind turbine and the rotor was initially running at 1.0 per unit speed and the PMSG was supplying no load. Thus, in this thesis, the systematic selection of controller parameters was done using Simulink Compensator Design tool which employed the root locus method [133].

In general, the performance indices employed are rise time for assessing the speed of response, settling time for measuring the stability and speed of response, and maximum percent overshoot for determining the relative stability of the wind turbine. The procedures in [133, 134] are used in calculating maximum percent overshoot and damping ratio. The damping ratio shows the damping capability of the PMSG.

Table 4.1. Dynamic performances of rotor speed response

Metrics	ZN method	Simulink design tool
Overshoot	-63%	-56%
Settling Time	10.5 s	8.0 s
Rising Time	3.8 s	2.0 s
Damping Ratio	0.14	0.18

Sections 4.5.1, 4.5.2, and 4.5.4 present the time-domain simulation results when the PMSG is subjected to large load changes, wind speed disturbances and stochastic wind speed disturbances respectively. The simulations were carried out based on the data in Table A1, Table A2 and Figure 4.2, the  $C_p$ -TSR pitch curves of the wind turbine, analytically represented in (4.5) and (4.6).

4.5.1 Large Load Changes

In this section, a constant wind speed having 12 m/s was applied to the wind turbine direct-driven PMSG. Thereafter, the effects of virtual lag, lead and lead-lag compensators on



the dynamic performances of the wind turbine direct-driven PMSG were observed under different operating conditions.

#### 4.5.1.1 Effect of a Lag Compensator

Figure 4.8 shows the speed response of the wind turbine direct-driven PMSG when a virtual lag compensator is employed in the generator side controller. Initially, the rotor was running at 1.0 per unit speed and there was no load. However, the PMSG started supplying power to the grid (or infinite bus) at time equals zero. The electrical power drawn has a braking effect on the PMSG and its rotor speed decreases as shown in Figure 4.8. When the lag compensator is not employed, it is clearly seen that there are speed oscillations and the pitch angle, speed and PI controllers bring the generator back to the nominal speed at about time equals 8 seconds by regulating the mechanical power and reference voltages. The results in Figure 4.8 show that the virtual lag compensator has successfully damped speed oscillations. The maximum percent undershoot is significantly reduced, illustrating the system being more stable and fast with the lag compensator.

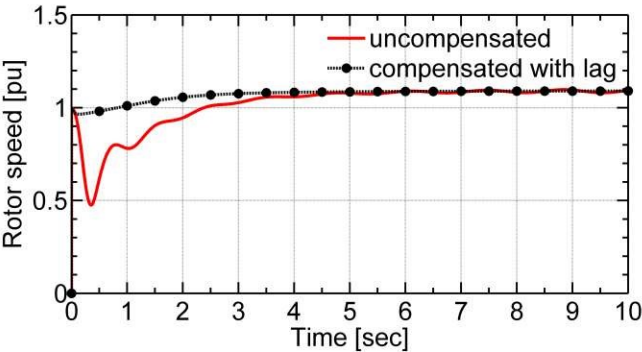


Figure 4.8. Effect of a lag compensator on rotor speed

In the same way, the rise time of the rotor speed is reduced from 2.0 to 0.0 seconds, and the settling time is reduced from 8.0 to 2.0 seconds, as shown in Table 4.2. Thus, the lag compensator is effective in damping rotor speed oscillations for large load changes and has significantly enhanced the speed response.

Figure 4.9 shows the real and reactive power responses of the PMSG where oscillations are damped by the inclusion of the virtual lag compensator. In Table 4.2, the rise and settling times of the real power response are reduced from 5.0 to 3.0 seconds and 8.0 to 3.0 seconds

respectively while the settling time of the reactive power response is reduced from 1.4 seconds to 0. The damping ratio of the real power response is also increased from 0.13 to 1.0. Consequently, the stability and the damping performances of the PMSG related to real and reactive power are enhanced by including the virtual lag compensators.

Table 4.2. Dynamic performances of PMSG with and without a lag compensator

		P	Q	Te	Tm	V <sub>DC</sub>	
Overshoot (%)	WOL	-56	-95.8		163.04	-26.5	47.83
	WL	0.0	0.0		0.0	6.67	49.57
Settling Time (s)	WOL	8.0	8	1.4	6	8.4	2.0
	WL	2.0	3.0	1.0	2.0	5.0	0.02
Rise Time (s)	WOL	2.0	5	0.0	0.12	0.02	0.001
	WL	0.0	3.0	0.0	0.74	0.01	0.001
Damping Ratio	WOL	0.18	0.13		0.15	0.39	0.23
	WL	1.0	1.0		1.0	0.65	0.22

WL- with lag compensator; WOL- without lag compensator; - undefined ( -rotor speed in pu, P- active power in pu, Q- reactive power in pu Te- electromagnetic torque in pu, Tm-mechanical torque in pu and V<sub>dc</sub>- DC voltage in Volts, V<sub>base</sub> = 575 V and S<sub>base</sub> = 1.5(10<sup>6</sup>) MVA, f<sub>base</sub> = 60 Hz)

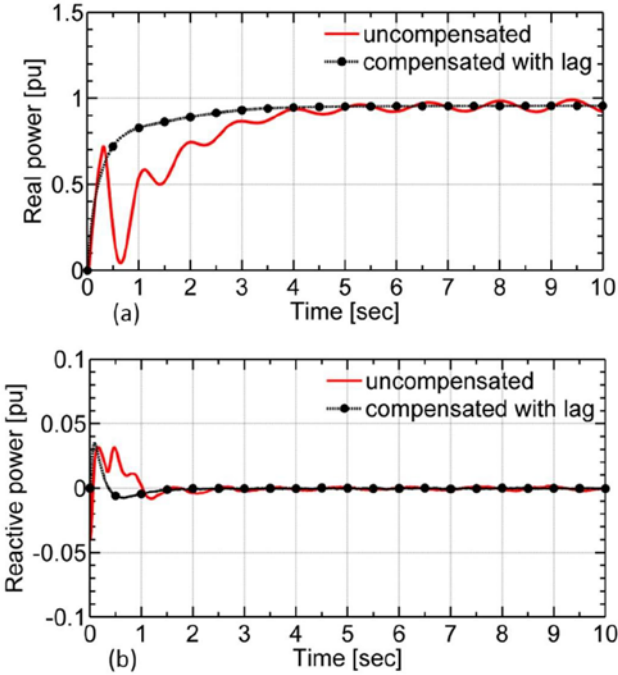


Figure 4.9. Effect of a lag compensator on (a) real power (b) reactive power responses

Figure 4.10 shows the torque responses of the PMSG. The oscillations in the electromagnetic torque response are suppressed by the virtual lag compensator. In Table 4.2, the settling time of the electromagnetic torque is reduced from 6.0 to 2.0 seconds while the corresponding damping ratio is increased from 0.15 to 1.0. Therefore, the virtual lag compensators are able to improve the stability and dynamic performances of the electromagnetic torque of the wind turbine direct-driven PMSG.

The simulation results in Figure 4.11 show that the oscillations in DC-link and terminal voltages are also effectively damped. In Table 4.2, the settling time of the DC-link voltage is reduced from 2.0 to 0.02 seconds illustrating the improvement in the stability of the DC-link voltage.

Therefore, in general, for large load changes, the dynamic performances of the wind turbine direct-driven PMSG can be enhanced by employing virtual lag compensators for the d- and q-axis terminal voltages of the generator.

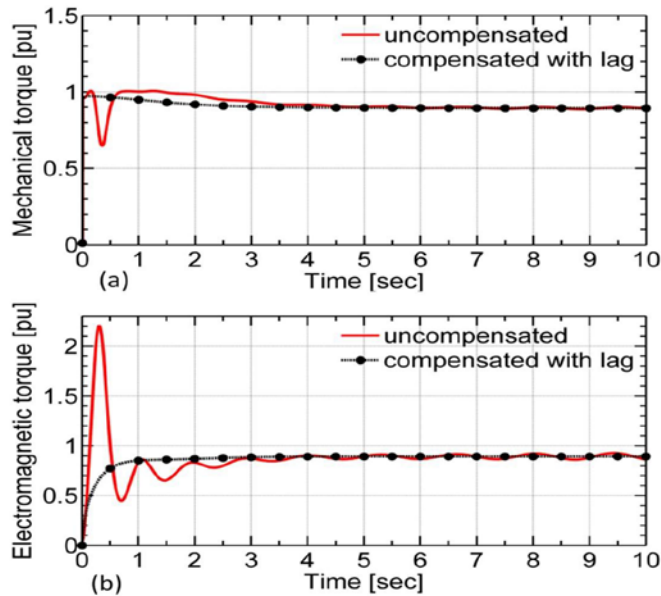


Figure 4.10. (a) Mechanical torque response (b) Electromagnetic torque response

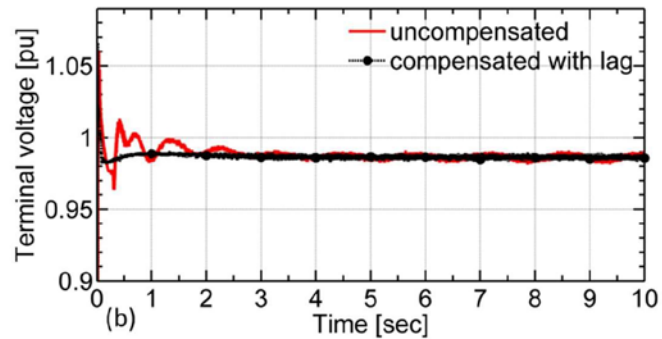
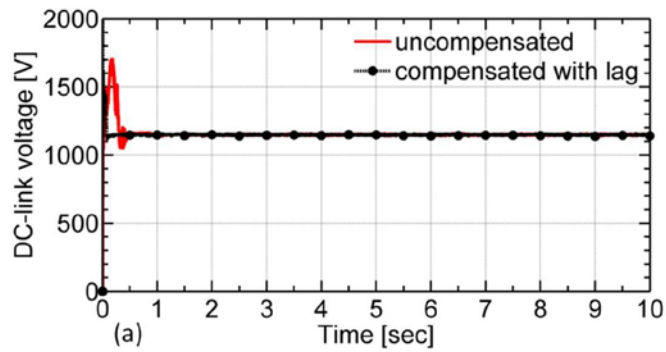


Figure 4.11. Effect of a lag compensator on (a) DC- link voltage (b) terminal voltage responses

#### 4.5.1.2 Effects of a Lead Compensator

In this case, the lag compensator in section 4.5.1.1 was replaced by a lead compensator to investigate the effects of a virtual lead compensator on the dynamic performances of a wind turbine direct-driven PMSG. The simulation results show that the effects of the lead compensator on the dynamic performances of the wind turbine direct-driven PMSG are positive, as shown in Figures 4.12 and 4.13.

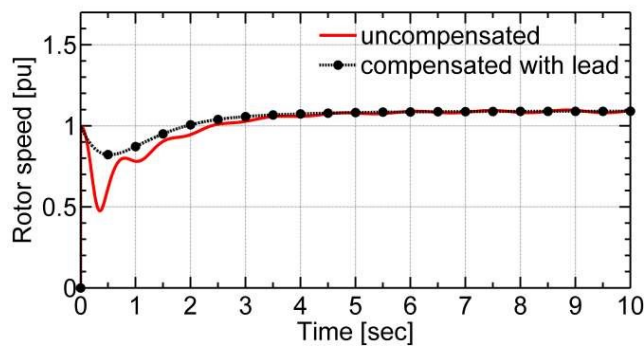


Figure 4.12. Effect of lead compensator on rotor speed

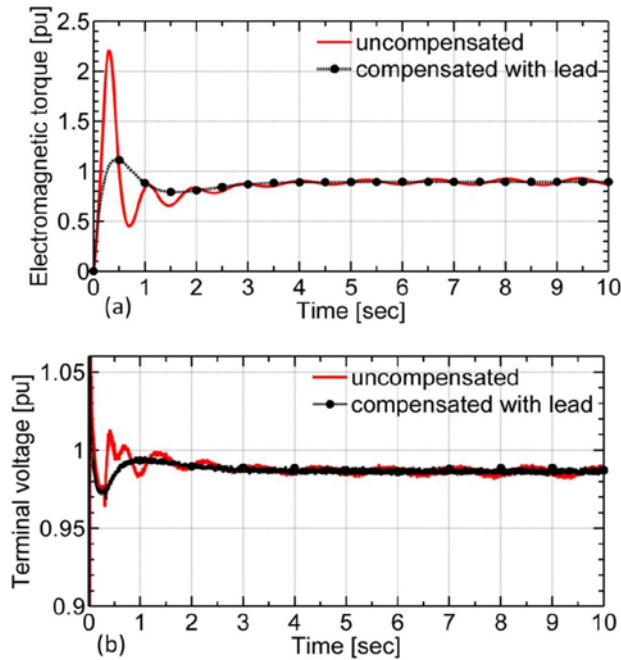


Figure 4.13. (a) electromagnetic torque (b) terminal voltage responses

In all the three figures, the rise and settling times are reduced and the damping ratios are increased illustrating the damping capability of the virtual lead compensator. Table 4.3 shows that when the zero comes close to the pole of the compensator, the damping ratio of the rotor

speed of the wind turbine increases, and thus, the PMSG becomes relatively more stable. Comparing Figure 4.8 with Figure 4.12 reveals that a virtual lag compensator is more effective than a virtual lead compensator.

Table 4.3. Effect of zero of a lead compensator on the damping ratio of rotor speed

Test No.	Lead zero	Lead pole	Damping ratio
1	-24	-25	0.189745
2	-23	-25	0.185946
3	-15	-25	0.160293
4	-5	-25	0.12269

#### 4.5.1.3 Effect of a Lead-Lag Compensator

In this section, the effectiveness of a virtual lead-lag compensator in enhancing the dynamic performances of a wind turbine direct-driven PMSG is investigated. Simulation results have shown that a lead-lag compensator effectively enhances the damping performances of a wind turbine direct-driven PMSG by reducing rise and settling times and

increasing the damping ratios of the PMSG responses. Overshoots/undershoots are also reduced. For instance, Figure 4.14 shows the effectiveness of such a compensator. In fact, comparing the plot in Figure 4.14 with the one in Figure 4.10(b) illustrates that the lead-lag compensator is totally dominated by the lag component. The performances of the lead-lag and lag only compensators are nearly the same. In general, the virtual compensators damp the local oscillations of the PMSG by emulating real RLC compensators.

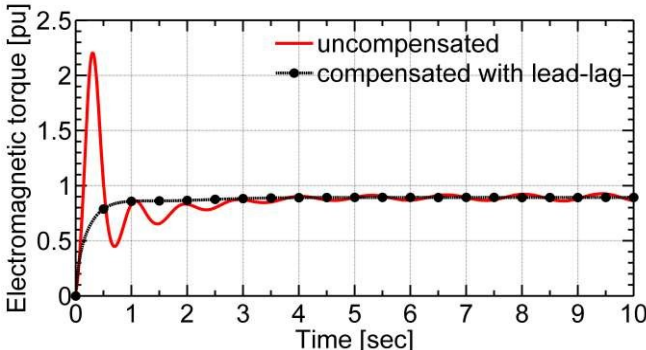


Figure 4.14. Effect of a lead-lag compensator on electromagnetic torque response

#### 4.5.2 Wind Speed Disturbances

This thesis has considered harmonics and a sudden rise in the wind speed as shown in Figure 3.14 to investigate the response of the wind turbine direct-driven PMSG to wind disturbances. At the seventh second, the base wind speed suddenly rises from 11 to 12 m/s. All the three virtual compensators were considered in this section.

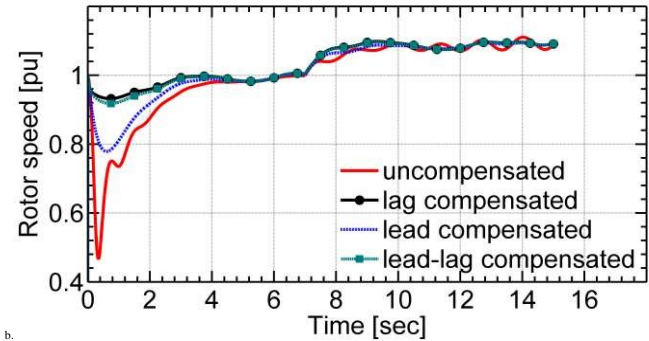


Figure 4.15. Rotor speed response for small disturbances

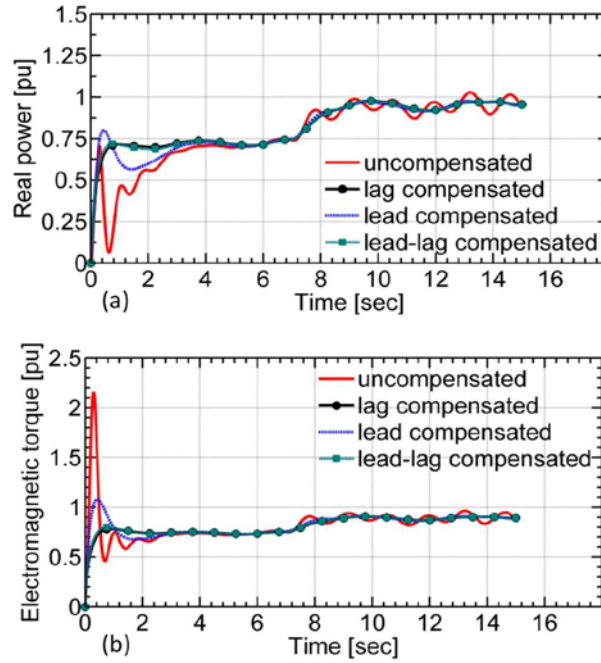


Figure 4.16. (a) Real power (b) electromagnetic torque responses for wind speed disturbances

The results of time-domain simulation in Figure 4.15 show that rotor speed oscillations are well damped during wind perturbations when a lag compensator is employed. For the disturbance at the seventh second, the response of the wind turbine is fast and more stable with the lag compensator. The effect of the lead-lag compensator is mainly dominated by the lag component, and it is nearly as effective as the lag one. In addition, the lead compensator successfully damps local oscillations, but it is less effective than the other two. From Figure 4.16, it can be observed that the compensators are effective in suppressing real power and electromagnetic torque oscillations.

Predominantly, the lag compensator damps the electromagnetic torque oscillations caused by the disturbance in the seventh second, as shown in Figure 4.16(b). This is due to the fact that the virtual compensators increase the damping ratio and reduce rise and settling times of the PMSG responses. The electromagnetic torque oscillation will slowly increase, illustrating dynamic instability in the generator, if a compensator is not employed. Moreover, the compensators have the capacity of filtering harmonics.

The local oscillations, which can be caused by wind gusts, create more stress in the drive-train of the wind turbine direct-driven PMSG. They can also cause over currents and over voltages which endanger the PMSG, DC-link capacitor and the power converters. In this regard, the virtual compensators are crucial in tackling these problems associated with wind gusts.

### 4.5.3 Effectiveness of Compensators over Range of Wind Speeds

The control dynamics of wind turbines are highly dependent on the operational region of the machine. Thus, the behaviour of the virtual compensators should be assessed over a range of wind speed disturbances, from the cut-in to cut-out wind speeds which are assumed to be 7 and 25 m/s respectively in this section. This test was done and the results are presented in Figures 4.17 and 4.18.

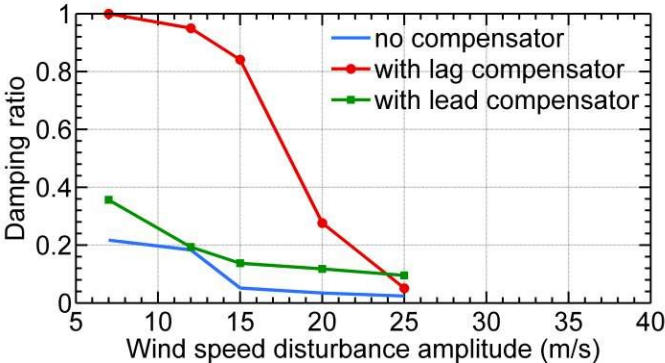


Figure 4.17. Effects of lag and lead compensators on the damping ratio of rotor speed

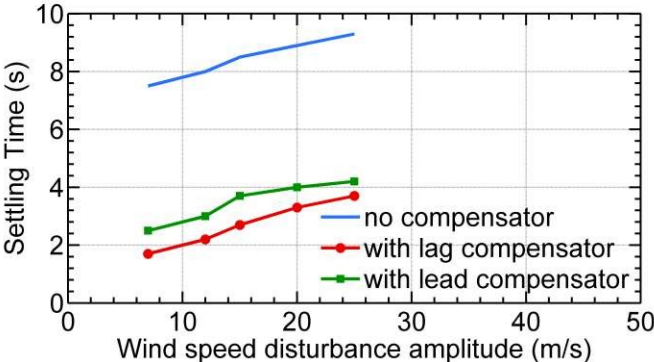


Figure 4.18. Effects of lag and lead compensators on the settling time of rotor speed



Figure 4.17 shows the effect of lag and lead compensators on the damping ratio of the rotor speed for different amplitudes of wind speed disturbances at the corresponding optimum, tip speed ratios (TSR). Both types of compensators enhance the damping ratio. It can also be observed that as the amplitude of wind disturbance increases, the compensators become less efficient. Similarly, in Figure 4.18, the compensators reduce the settling time of the rotor speed for different wind speed disturbances.

In general, implementing virtual compensators in the generator side converter controller significantly enhances the dynamic performances of a wind turbine direct-driven PMSG under different operating conditions. The results show that virtual lag compensators outperform virtual lead compensators.

#### 4.5.4 Response to Stochastic Wind Speed Series

So far, this chapter has investigated the performances of different types of compensators in enhancing the damping performances of a wind turbine direct-driven PMSG for constant wind speeds with large load changes and small variations in the wind speed, and the compensators have significantly improved the dynamic performances of the generator. However, wind is a stochastic process and its behaviour is far from a constant signal. Usually, large disturbances are observed in wind speed series. Therefore, in this section, the effectiveness of the compensators is verified using wind speed time series generated by the MCM developed in Chapter 3, shown in Figure 3.8. Accordingly, only the lag compensator is considered in the validation process to avoid redundancy.

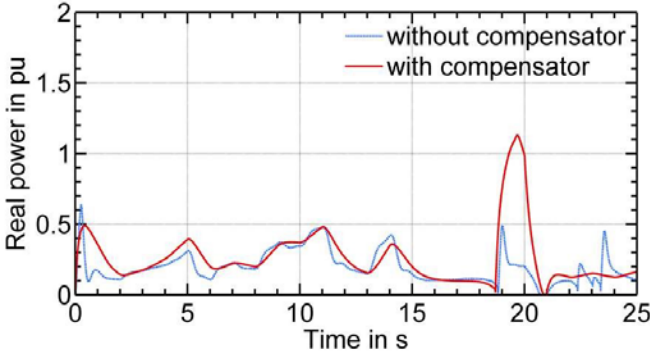


Figure 4.19. Electromagnetic torque response for stochastic wind speed series

Figures 4.19 and 4.20 illustrate the electromagnetic torque and power responses of the PMSG with wind speed series from the Markov model. It can be observed that the virtual compensator improves the dynamic performances of the electromagnetic torque of the PMSG. Particularly, it is important for suppressing oscillations in the electromagnetic torque created by rapid changes in the wind speed (19 to 25 seconds). The lag compensator has also reduced the overshoots and oscillations of the output power of the PMSG as in Figure 4.20. Therefore, this shows that the lag compensator significantly enhances the damping performances of the PMSG in highly fluctuating wind environments.

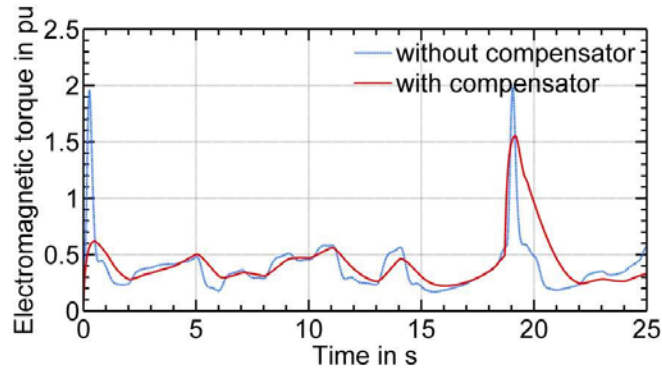


Figure 4.20. Real power response for stochastic wind speed series

In general, the results show that virtual compensators efficiently enhance the dynamic performances of the wind turbine direct-driven PMSG by damping local oscillations. Speed, power, and torque oscillations, caused by wind disturbances, are well damped. Moreover, they significantly improve the DC-link and the terminal voltage responses by reducing rise and settling times, overshoots and increasing damping ratio. Lag compensators are more effective than lead compensators. However, the performances of lead-lag compensators are mainly dominated by the lag components, and they are nearly as effective as lag compensators.

The technique proposed in this work is applicable in smoothing the rotor speed and the output power of a wind turbine direct-driven PMSG. In addition to enhancing the dynamic stability of the PMSG, the virtual compensators reduce stresses in the drive-train, DC-link capacitor and power converters under stochastic wind disturbances. They also reduce voltage harmonics induced in to the power grid.

## 4.6 Conclusion

This chapter has dealt with the modelling and analysis of the different components of a wind turbine direct-driven PMSG such as the drive train, generator, DC-link, generator and grid side controllers. It has also modelled a power grid for dynamic analysis. In Chapter 3, the stochastic nature of wind, which may constantly disturb the PMSG, had been discussed. In response to this disturbance, this chapter has proposed the model of virtual compensators for enhancing the dynamic performances of the PMSG.

In this scheme, virtual compensators adjusted the terminal d- and q-axis reference voltages in the generator side controller to enhance the dynamic performances of the PMSG. MATLAB/Simulink simulation results on a PMSG connected to an infinite bus have shown that virtual lag compensators are able to effectively damp local oscillations. In this case, the results showed that lag compensators successfully reduced the rise and settling times of the rotor speed, electromagnetic torque, active power and reactive power. They have also increased the corresponding damping ratios. Similarly, the results showed that lead compensators damped local oscillations; however, they were less efficient as compared to lag compensators. On the other hand, the lag components dominated the performances of lead-lag compensators. Hence, the use of virtual compensators can smooth the rotor speed and power of a wind turbine, which in turn results in reduced power fluctuations in a power grid.

Finally, simulation studies were conducted with wind speed series generated by a Markov model to investigate the impacts of stochastic wind speed series on the dynamic performances of the PMSG. The dynamic performances of the wind turbine direct-driven PMSG have been highly influenced by the stochastic wind speed series. However, the results show that the proposed scheme has added positive damping to the local oscillations caused by wind disturbances and is effective in enhancing the dynamic performances of the PMSG. Generally, the output power of the PMSG is effectively smoothed, which is helpful in improving the dynamic stability of the power grid. Chapter 5 will further continue exploring novel methods for enhancing the dynamic performances of the wind turbine direct-driven PMSG under stochastic wind disturbances.

## CHAPTER 5

### ENHANCING THE DYNAMIC PERFORMANCES OF A WIND TURBINE DIRECT-DRIVEN PMSG

#### 5.1 Introduction

Damping local oscillations and hence enhancing the dynamic performances of a wind turbine direct-driven PMSG is vital in its operation as well as integration into a power grid. A multi-pole PMSG, by its very nature, has no damper windings and, consequently, lacks intrinsic damping potential. For this reason, in a fluctuating wind environment, local

oscillations are amplified further. Unless the oscillations are contained, they may lead the generator to local instability. In such a case, the corresponding protection system will disconnect the PMSG from the power grid. In the worst scenario, the disconnection may disturb the grid at large and create cascaded instabilities as it affects the power balance in the system. Enhancing the dynamic performances of the PMSG is, therefore, indisputably crucial in steady state as well as transient operations of power systems having PMSG-based wind turbines.

In Chapter 4, virtual compensators were proposed to enhance the dynamic performances of a wind turbine direct-driven PMSG. They have been proven to be efficient in mitigating the dynamic problems associated with the PMSG. Following a similar trend, this chapter investigates three mitigation approaches, which are not addressed in the existing literature. Initially, virtual resistors (VRs) in series and parallel to stator windings are modelled in Section 5.2. Secondly, in Section 5.3, feedforward algorithms (FFAs), stemming from fictitious stator damper windings, are characterized. The fictitious damper windings are modelled and developed into FFAs. Furthermore, the use of supplementary damping controllers (SDCs), a third mitigation technique, is proposed in Section 5.4.3. The d-axis SDC relies on the rotor speed deviation, while the q-axis SDC depends on the DC-link voltage deviation. Finally, all the three mitigation techniques are implemented along with proportional integral controllers in the generator side converter control system, whose layout is given in Section 5.4.

In effect, time domain simulation results on the mitigation schemes proposed to enhance the dynamic performances of the wind turbine direct-driven PMSG connected to an infinite bus are presented in Section 5.5. Investigations are done for large load changes and wind speed disturbances.

## 5.2 Mitigation Using VRs

This section models and analyses the proposed VRs for the wind turbine direct-driven PMSG. The VRs do not incur power loss and can be connected either series or parallel to the stator windings of the generator. For that reason, in this thesis, both series and parallel connections are modelled, analysed and realized in the generator side converter controller. The effectiveness of each connection in suppressing local oscillations is presented in Section 5.5.

### 5.2.1 PMSG Model Including VRs

In filters, oscillations and harmonics are damped using different active damping techniques employing VRs such that they do not incur power losses [129]. In this thesis, a similar trend is followed to damp the local oscillations of the PMSG, hence improving its damping performances. The VRs are adopted to serve as supplementary algorithms, and in practice, they should be realized in the generator side converter controller. The winding resistance of the generator can slightly damp power and speed oscillations, and contributes little to the damping of local oscillations, and thus, the need for the VRs.

Figure 5.1 shows the d- and q-axis equivalent circuits of a PMSG with VRs, connected in series and parallel to stator windings. Though there are different ways of parallel connections, the ones shown in Figures 5.1(c) and (d) are chosen for not reducing the effective resistance of the circuit when seen from the voltage source terminals. Applying KVL to the circuits in Figures 5.1(a) and (b), the corresponding new d and q- a- axis voltages, considered as references in the control system, are given in (5.1) and (5.2).

$$v_d^* = \omega L_d i_d + R_s i_d + R_v i_d + v_d^* \quad (5.1)$$

$$v_q^* = \omega L_q i_q + R_s i_q + R_v i_{qv} + (\omega L_d i_d + \phi_p) \quad (5.2)$$

$R_s$  and  $R_v$  are armature and VR resistances respectively.  $L_d$  and  $L_q$  are d- and q-axis inductances,  $\omega$  is rotor speed in electrical radian, and  $i_d$  and  $i_q$  are d- and q-axis currents, and  $\phi_p$  is permanent magnet flux.

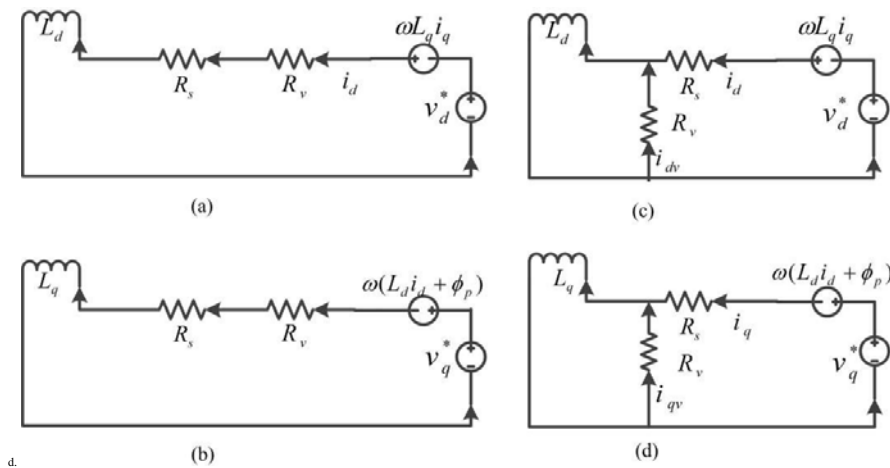


Figure 5.1. Equivalent circuits of a PMSG with VRs (a) d-axis circuit with series VR (b) q-axis circuit with series VR (c) d-axis circuit with parallel VR (d) q-axis circuit with parallel VR

Similarly applying the same method to Figures 5.1(c) and (d) gives,

$$v_d^* = v_d + \frac{R_s}{s} i_d + \frac{R_v}{s} i_d \quad (5.3)$$

$$v_q^* = v_q + \frac{R_s}{s} i_q + \frac{R_v}{s} i_q + \omega(L_d i_d + \phi_p) \quad (5.4)$$

where  $i_d$  and  $i_q$  are d- and q-axis virtual currents.

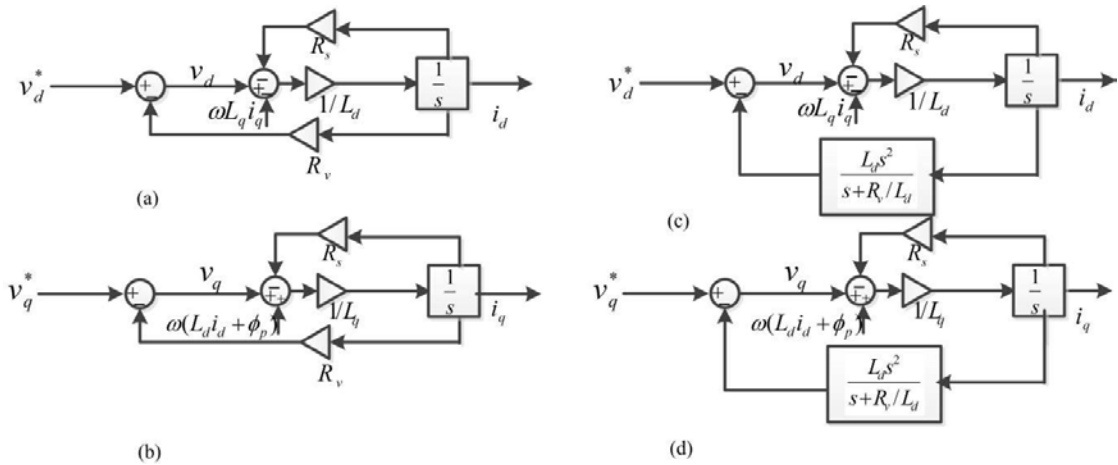


Figure 5.2. Block diagrams of the PMSG equivalent circuits (a) d-axis circuit with series VR (b) q-axis circuit with series VR (c) d-axis circuit with parallel VR (d) q-axis circuit with parallel VR

Analysing (5.1), (5.2), (5.3) and (5.4) gives the block diagrams in Figures 5.2(a), (b), (c) and (d) respectively, which are used to analyse the dynamic behaviour of the PMSG. In all the four diagrams, the inner loops represent the model of the generator itself, whereas the outer negative feedback loops are components that appear due to the VRs. The actual d- and q-axis voltages are modelled and obtained to be the differences between the reference voltages and the virtually existing VR voltages.

### 5.3 Mitigation Using FFAs

#### 5.3.1 PMSG Model with Fictitious Damper Windings

Figure 5.3 shows the alignment of stator windings (a, b, and c), field winding (f) and fictitious damper windings (e, g, and h) of the PMSG. Indeed, the concern of this thesis is the characterization and evaluation of the fictitious damper windings for enhancing the dynamic performances of the PMSG. In practice, these windings do not exist in the generator; as a result, they do not incur either power loss or extra cost. They do not also occupy space. Unlike the stator windings, the fictitious damper windings are approximately connected at their ends in the way that makes three-phase short-circuited windings. The two types of stator windings are deemed to function jointly as a virtual three-phase transformer.

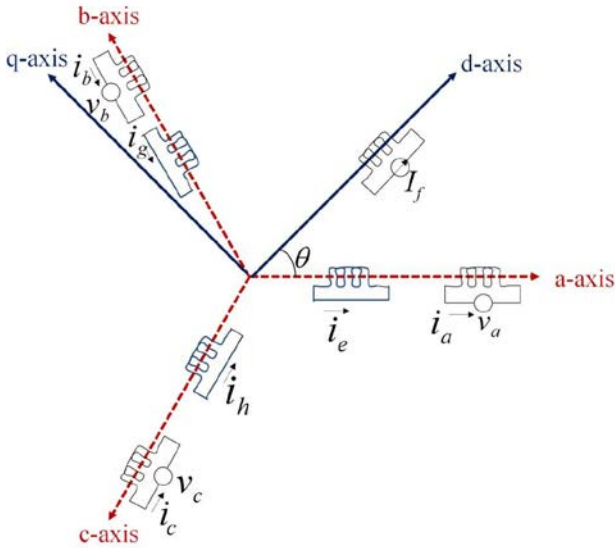


Figure 5.3. Windings of the PMSG and fictitious damper windings

The permanent magnet on the rotor of the PMSG is approximated by a constant current source,  $I_f$ , and a fictitious winding. Applying KVL around the three fictitious damper circuits gives (5.5), where the corresponding currents are  $i_e$ ,  $i_g$ , and  $i_h$ .

$$\begin{bmatrix}
 L_{ee} & L_{eg} & L_{eh} \\
 L_{ge} & L_{gg} & L_{gh} \\
 L_{he} & L_{hg} & L_{hh}
 \end{bmatrix}
 \begin{bmatrix}
 i_e \\
 i_g \\
 i_h
 \end{bmatrix}
 =
 \begin{bmatrix}
 0 \\
 0 \\
 0
 \end{bmatrix}
 \tag{5.5}$$



is the per phase resistance of the fictitious damper windings. Additionally, the corresponding flux linkages are given in (5.6).

$$\lambda = -R_d i_d + L_{d1} i_d + L_{d2} i_f \quad (5.6)$$

In short form, (5.6) can be rewritten as:

$$\lambda = -R_d i_d + L_{d1} i_d + L_{d2} i_f \quad (5.7)$$

where  $\lambda$  is the vector of the flux linkages of the fictitious damper windings. The diagonal elements of the inductance matrix are the self-inductances, whereas its offdiagonal elements are mutual inductances.  $L_{d1}$  denotes the mutual inductance matrix between the stator and fictitious damper windings, and  $L_{d2}$  is the mutual inductance between the damper and fictitious field windings.

Owing to the rotation of the rotor of the PMSG, the inductances of the fictitious damper windings are time-varying. Thus, a close analysis of the self-inductances [14] for the PMSG reveals that:

$$L_{d1} = L_{d1} + L_{d1} \cos(2\theta) \quad (5.8a)$$

$$L_{d2} = L_{d2} + L_{d2} \cos(2\theta + \alpha) \quad (5.8b)$$

$$L_{d3} = L_{d3} + L_{d3} \cos(2\theta - \alpha) \quad (5.8c)$$

where  $\theta$  is the electrical angle of the d-axis from the a- axis in the anti-clockwise direction. Equation (5.8) indicates that the self-inductances have fixed and time-dependent parts.  $L_{d1}$  is the average self-inductance and  $L_{d1}$  is the amplitude of the component of the self-inductance that oscillates with double frequency. Similarly, the mutual inductances between the damper windings are given in (5.9).

$$L_{d12} = -0.5 L_{d12} + L_{d12} \cos(2\theta - \alpha) \quad (5.9a)$$

$$L_{d13} = -0.5 L_{d13} + L_{d13} \cos(2\theta + \alpha) \quad (5.9b)$$

$$L_{d23} = -0.5 L_{d23} + L_{d23} \cos(2\theta) \quad (5.9c)$$

In the analysis of the mutual inductances between the fictitious damper and stator windings, the axes of the damper windings are aligned with the stator windings. Consequently, the mutual inductances are:

$$= \quad + \quad (2) \quad (5.10a)$$

$$= \quad + \quad (2 + \_ ) \quad (5.10b)$$

$$= \quad + \quad (2 - \_ ) \quad (5.10c)$$

$$= \quad = -0.5 \quad + \quad (2 - \_ ) \quad (5.10d)$$

$$= \quad = -0.5 \quad + \quad (2 + \_ ) \quad (5.10e)$$

$$= \quad = -0.5 \quad + \quad (2 - ) \quad (5.10f)$$

where is average mutual inductance and the amplitude of the component of the mutual inductance oscillating with double frequency.

On the other hand, (5.11) gives the inductances between the fictitious damper and field windings.

$$= \quad ( ) \quad (5.11a)$$

$$= \quad ( - - ) \quad (5.11b)$$

$$= \quad ( + - ) \quad (5.11c)$$

denotes the d-axis mutual inductance between the fictitious damper and field windings at equals 0.

Park's transformation is widely used to transform time variant balanced three-phase AC quantities, into time-invariant DC quantities. The transformation matrix is indicated in (5.12) [14].

$$\begin{pmatrix} \cos(\theta - \frac{2\pi}{3}) \\ \cos(\theta - \frac{2\pi}{3}) - \sin(\theta - \frac{2\pi}{3}) \\ 1 \end{pmatrix} = \begin{pmatrix} \cos(\theta - \frac{2\pi}{3}) & \sin(\theta - \frac{2\pi}{3}) \\ \sin(\theta - \frac{2\pi}{3}) & \cos(\theta - \frac{2\pi}{3}) \\ 1 & 1 \end{pmatrix} \begin{pmatrix} \cos(\theta + \frac{2\pi}{3}) \\ \cos(\theta + \frac{2\pi}{3}) - \sin(\theta + \frac{2\pi}{3}) \\ 1 \end{pmatrix} \quad (5.12)$$

Now, applying Park's transformation directly to (5.5) gives (5.13).

$$\begin{bmatrix} \lambda_{d'} \\ \lambda_{q'} \\ \lambda_{0'} \end{bmatrix} = \begin{bmatrix} 0 & 0 & 0 \\ 0 & 0 & 0 \\ 0 & 0 & 0 \end{bmatrix} \begin{bmatrix} i_{d'} \\ i_{q'} \\ i_{0'} \end{bmatrix} \quad (5.13)$$

$\lambda_{d'}$ ,  $\lambda_{q'}$  and  $\lambda_{0'}$  are the d-, q- and 0- axes fictitious damper winding flux linkages respectively, and  $i_{d'}$ ,  $i_{q'}$  and  $i_{0'}$  are the corresponding d-, q- and 0- axes fictitious damper currents. Simplifying (5.13) results in:

$$\begin{bmatrix} \lambda_{d'} \\ \lambda_{q'} \\ \lambda_{0'} \end{bmatrix} + \begin{bmatrix} 0 & - & 0 \\ 0 & 0 & 0 \\ 0 & 0 & 0 \end{bmatrix} \begin{bmatrix} i_{d'} \\ i_{q'} \\ i_{0'} \end{bmatrix} = \begin{bmatrix} 0 \\ 0 \\ 0 \end{bmatrix} \quad (5.14)$$

where  $\omega$  is the electrical speed of the PMSG. In (5.14), for a three-phase balanced operation, the 0- axis component vanishes. Thus, the d- and q-axis voltage equations of the fictitious damper windings become:

$$\lambda_{d'} - \omega \lambda_{q'} = 0 \quad (5.15a)$$

$$\lambda_{q'} + \omega \lambda_{d'} = 0 \quad (5.15b)$$

In the same way, applying Park's transformation to (5.6) yields (5.16).

$$\begin{bmatrix} \lambda_{d'} \\ \lambda_{q'} \\ \lambda_{0'} \end{bmatrix} = 1.5 \begin{bmatrix} L_{\sigma} & 0 & 0 \\ 0 & L_{\sigma} & 0 \\ 0 & 0 & L_{\sigma} \end{bmatrix} \begin{bmatrix} i_{d'} \\ i_{q'} \\ i_{0'} \end{bmatrix} + \begin{bmatrix} 0 & 0 & 0 \\ 0 & 0 & 0 \\ 0 & 0 & 0 \end{bmatrix} \begin{bmatrix} i_{d'} \\ i_{q'} \\ i_{0'} \end{bmatrix} \quad (5.16)$$

$i_{d'}$ ,  $i_{q'}$  and  $i_{0'}$  are the d-, q- and 0- axis stator currents.  $L_{\sigma}$  is the leakage inductance of the damper windings. In a balanced system operation, (5.16) can be reduced to (5.17).

$$\lambda_{d'} = L_{\sigma} i_{d'} \quad (5.17a)$$

$$\lambda_{q'} = L_{\sigma} i_{q'} \quad (5.17b)$$

is the constant magnetic flux of the PMSG reaching the damper windings. and are the d- and q-axis inductances of the damper windings, whereas and are the d- and q-axis mutual inductances between the stator and fictitious damper windings. Now, including (5.15) in the model of the ordinary PMSG [86] gives (5.18), which is a new apparent PMSG model. The sign difference observed between (5.1) and (5.18a) is because of the polarity of the d-axis voltage adopted.

$$u_d = \dot{\psi}_d + i_d R_s + \omega \psi_q \quad (5.18a)$$

$$u_q = \dot{\psi}_q - i_q R_s - \omega \psi_d \quad (5.18b)$$

$$\dot{\psi}_d = -\omega \psi_q + u_d^* \quad (5.18c)$$

$$\dot{\psi}_q = \omega \psi_d + u_q^* \quad (5.18d)$$

$u_d^*$  and  $u_q^*$  are the respective new d-axis and q-axis reference voltages in the generator side converter controller. The d-axis and q-axis stator flux linkages are given as:

$$\psi_d = \psi_{pm} + L_{sd} i_d + L_{sdq} i_q \quad (5.18e)$$

$$\psi_q = L_{sqd} i_d + L_{sq} i_q \quad (5.18f)$$

respectively, where  $\psi_{pm}$  is the constant magnetic flux linkage of the PMSG.

Substituting (5.18e and 5.18f) and (5.17a and 5.17b) in (5.18a and 5.18b) and (5.18c and 5.18d) respectively, and rewriting results in:

$$u_d = \dot{\psi}_{pm} + L_{sd} \dot{i}_d + L_{sdq} \dot{i}_q + \omega L_{sqd} i_d + \omega L_{sq} i_q + i_d R_s + \omega \psi_q \quad (5.19a)$$

$$u_q = L_{sqd} \dot{i}_d + L_{sq} \dot{i}_q - \omega L_{sd} i_d - \omega L_{sdq} i_q - i_q R_s - \omega \psi_d \quad (5.19b)$$

$$\dot{\psi}_d = -\omega \psi_q + u_d^* \quad (5.19c)$$

$$\dot{\psi}_q = \omega \psi_d + u_q^* \quad (5.19d)$$

and are the d-axis and q-axis equivalent inductances of the fictitious damper windings respectively. Similarly, substituting (5.19c and 5.19d) in (5.19a and 5.19b) gives:

$$u_d^* = -\omega L_{sd} \frac{d}{dt} i_d - \omega L_{sdq} \frac{d}{dt} i_q + \omega L_{sqd} i_d + \omega L_{sq} i_q + i_d R_s + \omega \psi_q \quad (5.20a)$$

$$\begin{aligned}
 * = & - \frac{L_{sd}}{L_D} \frac{di_{sd}}{dt} + \omega L_{sq} i_{sq} + \frac{L_{Qsd} R_d}{n L_D} - \left( \frac{\omega L_{Qsd} L_{Qsd}}{L_D} + \frac{\omega L_{Qsq}}{n} \right) i_{sq} \\
 & - \frac{\omega L_{Qsd}}{n} + \frac{\omega}{nL} + \frac{\omega}{nL_Q} + \frac{\omega}{nL_Q} L_{Qsq} \psi
 \end{aligned} \tag{5.20b}$$

Equation (5.20) can be further simplified to (5.21) if the stator and fictitious damper windings are assumed to form a virtual transformer having n turn's ratio.

$$* = \frac{L_{sd}}{L_D} \frac{di_{sd}}{dt} + \omega L_{sq} i_{sq} + \frac{L_{Qsd} R_d}{n L_D} - \left( \frac{\omega L_{Qsd} L_{Qsd}}{L_D} + \frac{\omega L_{Qsq}}{n} \right) i_{sq} \tag{5.21a}$$

$$* = L_{sq} \frac{di_{sq}}{dt} - \omega \frac{\omega L_{Qsd}}{n} + \frac{\omega}{nL} + \frac{\omega}{nL_Q} + \frac{\omega}{nL_Q} L_{Qsq} \psi \tag{5.21b}$$

The actual d- and q- axis voltages of the PMSG are expressed as:

$$= * - \tag{5.22a}$$

$$= * - \tag{5.22b}$$

where

$$= \frac{\omega L_{Qsd}}{n} - \left( \frac{\omega L_{Qsd} L_{Qsd}}{L_D} - \frac{\omega L_{Qsq}}{n} + \frac{\omega}{nL} \right) \tag{5.23a}$$

$$= \frac{\omega L_{Qsd}}{n} + \frac{\omega}{nL} + \frac{\omega}{nL_Q} + \frac{\omega}{nL_Q} L_{Qsq} \psi \tag{5.23b}$$

Analysing (5.21) to (5.23) gives the block diagrams of the PMSG in Figures 5.4(a) and (b). In both diagrams, the inner loops represent the model of the PMSG, while the outer modified feedback loops are components appearing due to the assumed fictitious damper windings. Unlike the existing models in the literature, the d- and q- axis block diagrams are not decoupled. For this reason, the generator side control structure based on fictitious damper windings for efficient dynamic performances are not also decoupled. The dependence of the

feedbacks on the d-axis current, q-axis current and permanent magnet flux makes the intended control structure versatile.

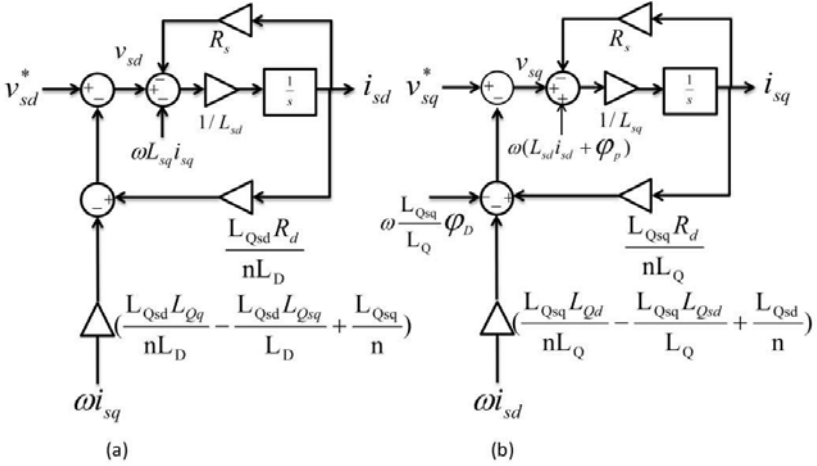


Figure 5.4. Block diagram of (a) d-axis and (b) q-axis of the PMSG with fictitious damper windings

It is noted that the fictitious stator damper windings do not incur any power loss and do not involve in modifying the electromagnetic torque at both transient and steady states like the main windings of the PMSG.

5.4 Modified Generator Side Converter Controllers (MGSCC)

5.4.1 MGSCC with VRs

Figure 5.5 shows the MGSCC with VRs employed in this section. It controls the active power of the generator through the quadrature axis voltage,  $v_{sq}$ , aiming to minimize the power loss [132]. On the other hand, it keeps the direct axis current at zero to decrease the nonlinearity of (4.22) and minimize current coupling and is achieved through the direct axis voltage,  $v_{sd}$ . In this control structure, a proportional and two proportional-integral (PI) controllers are employed. The PI controller in Figure 5.5(a) controls the d-axis current, whereas the one in Figure 5.5(b) controls the q-axis current.  $K_p$ ,  $K_i$ , and  $K_{i2}$  are the gains of the controllers. The superscript \* denotes a reference value. The negative forward loop, with a transfer function shown in (5.24), is the effect of the inclusion of the VRs.

$$\begin{aligned}
 & \text{for series virtual resistor} \\
 ( ) = & \frac{R_s + \frac{L_{Qsd}R_d}{nL_D}}{s + \frac{L_{Qsd}L_{Qq}}{nL_D} - \frac{L_{Qsd}L_{Qsq}}{L_D} + \frac{L_{Qsq}}{n}} \quad \text{for parallel virtual resistor} \tag{5.24}
 \end{aligned}$$

+ /

is d or q, depending on the equivalent circuit.

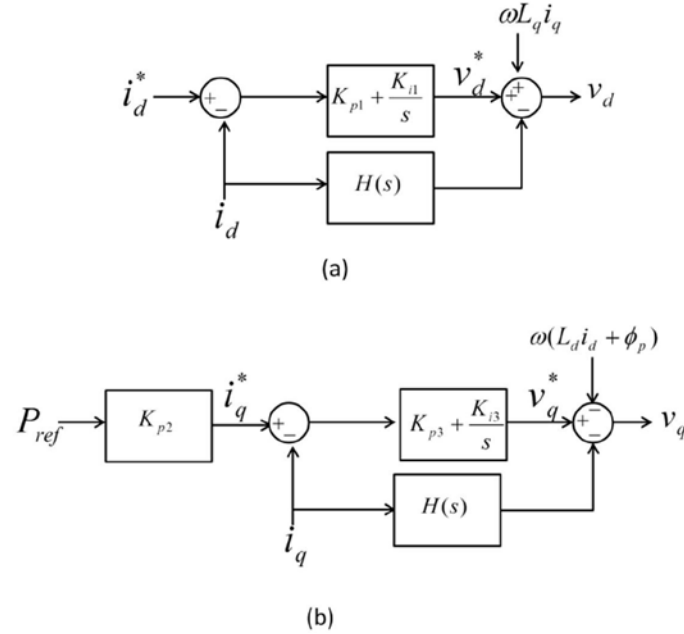


Figure 5.5. Proposed generator side controller (a)  $i_d$  controller (b)  $i_q$  controller with VR scheme

#### 5.4.2 MGSCC with FFA

The generator side control structure is primarily derived from Figure 5.4. This controller is dedicated to control the real power of the PMSG through the q- axis voltage, , by minimizing power loss as discussed in section 5.4.1. The d-axis current is maintained at zero to decrease the nonlinearity of (4.22) and minimize current coupling. The d-axis voltage is obtained through controlling the d-axis current and compensating it with the d-axis FFA (loop), which takes both d- and q-axis currents as its inputs, as shown in Figure 5.6(a). And the q- axis voltage is obtained by controlling the q- axis current and compensating it with the q- axis FFA, which takes the q-axis current, d-axis current and the permanent magnet flux as its inputs as shown in Figure 5.6(b). The negative FFAs are, indeed, the results of the proposed fictitious damper windings.

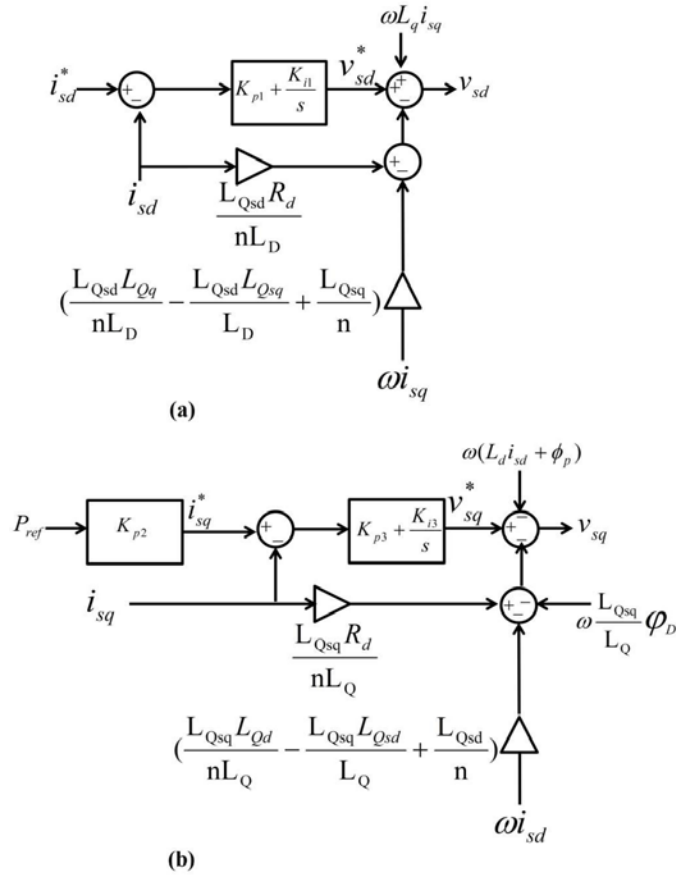


Figure 5.6. Proposed generator side controller (a)  $i_{sd}$  (b)  $i_{sq}$  controller with FFA

The dynamic processes of the converters are much faster than the electromagnetic and mechanical dynamic processes. Thus, in this control structure and other related controllers in this research, the corresponding models of the converters are neglected, and in Figure 5.6 are the same as the d- and q-axis voltages of the generator side converter.

In this control structure, the PMSG is modelled using a proportional and two proportional-integral (PI) controllers as in section 5.4.1. Generally, the controller can be interfaced with the generator side converter through a dq-abc axis transformer and a PWM generator as depicted in Figure 4.1.

### 5.4.3 MGSCC with SDCs

Figure 5.7 shows the MGSCC with the corresponding SDCs. As discussed in the previous sections, the objectives of this controller are controlling the real power of the PMSG through the q- axis voltage, , aiming at minimizing power loss, and maintaining the d-axis



current at zero to decrease the nonlinearity of (4.22) and to minimize current coupling. The d-axis current control is achieved through the d-axis voltage, [132].

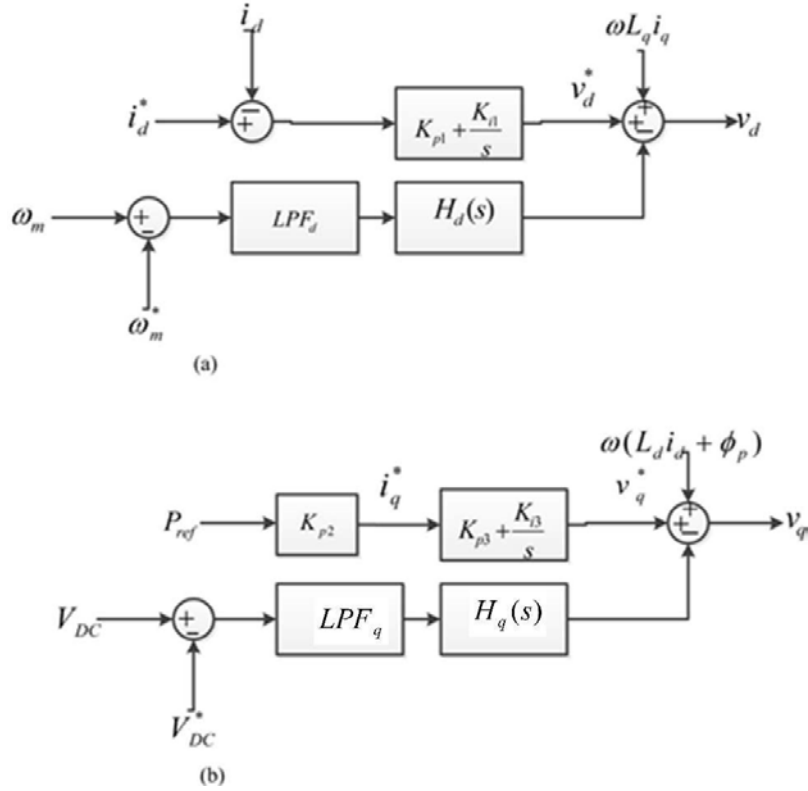


Figure 5.7. Proposed generator side controller with (a) d-axis SDC and (b) q-axis SDC

The proposed SDCs, the contribution of this work, are implemented in this controller.  $H_d(s)$  and  $H_q(s)$  are the corresponding d- and q- axis SDC transfer functions. The transfer functions may have different forms. However, for this work, proportional-integral controllers have performed well in enhancing the dynamic performances of the wind turbine. The controllers are tuned as discussed in Chapter 4. In the main control structure, a proportional and two proportional-integral (PI) controllers are used as shown in Figure 5.7. The main controllers in Figures 5.7(a) and (b) control  $i_d$  and  $i_q$  respectively. The inputs to the SDCs should pass through low pass filters,  $LPF_d$  and  $LPF_q$ , to suppress harmonics.

The d-axis SDC is added to the d-axis voltage control of the generator side controller to enhance the damping of local oscillations. The signal from d-axis SDC helps in increasing the damping torque by controlling the d-axis voltage vector of the PMSG with respect to the reference d-axis reference voltage. Similarly, the q-axis SDC is added to the q-axis voltage control of the generator side controller to enhance the damping of local oscillations. The

signal from q-axis SDC helps in increasing the damping torque by controlling the q-axis voltage vector of the PMSG with respect to the reference q-axis reference voltage.

From (5.1) it can be observed that as the d-axis current is maintained at zero, the d-axis reference voltage heavily depends on the q-axis current and the rotor speed. This voltage can be obtained by observing rotor speed and d-axis current deviations. Thus, the proposed d-axis SDC modifies the corresponding reference voltage by taking the rotor speed deviation as its input. The speed error passes through a low-pass filter to eliminate harmonics that affect the performance of the SDC. On the other hand, (4.13) shows there is a strong relationship between the q-axis current and the DC-link voltage. In fact, the q-axis reference voltage is directly affected by the q-axis current. Consequently, the q-axis SDC depends on the DC-link voltage deviation. Similarly, the voltage deviation passes through a low pass filter to eliminate higher order harmonics. In general, the damping controllers act as negative forward loops.

## 5.5 Simulation Results and Discussion

This section implements the models of all the components of the wind turbine directdriven PMSG and the power grid discussed in Chapter 4 in MATLAB/Simulink for time domain analysis, incorporating the models of the proposed mitigation methods developed in this chapter. Consequently, the influences of the VRs, FFAs and SDCs on the dynamic performances of the PMSG are investigated and compared. The objective is to illustrate how the VRs, FFAs and SDCs enhance the dynamic performances of the PMSG. In doing so, as discussed in the previous chapter, standard PI controllers along with the mitigation methods are employed as they are simpler in construction, easier to implement, widely used and provide satisfactory performances under various operating conditions of a system. The same PI controller gains used in Chapter 4 are employed.

As a rule, the performance indices employed in this chapter are rising time for assessing the speed of response, settling time for measuring the stability and speed of response, and maximum percent overshoot for determining the relative stability of the PMSG. The settling time is associated with steady state error. In this work, a 10% steady state error is considered. Maximum percent overshoot and damping ratio show damping capacity. The damping ratios are calculated based on the procedures given in [133, 134]. The time constant of a response shows stability and speed of response. Sections 5.5.1 and 5.5.2

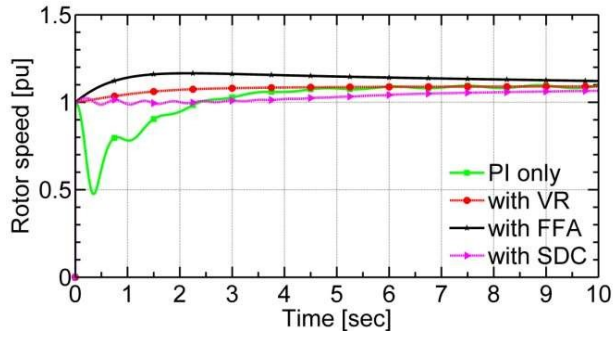
present the simulation results of the PMSG with and without the proposed schemes, when subjected to constant wind speed and stochastic wind disturbances respectively. The simulations were carried out based on the data in Tables A1, A2 and A3.

### 5.5.1 Response to Constant Wind Speed and Large Load Changes

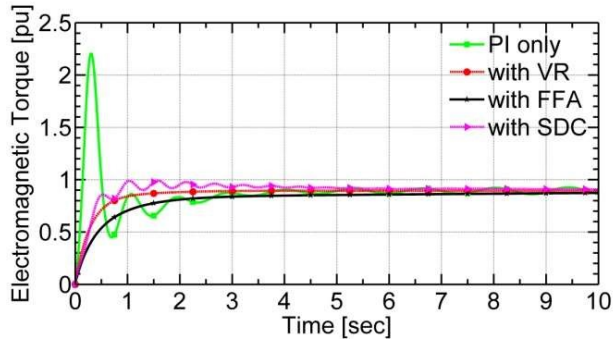
Figure 5.8 shows the speed and electromagnetic torque responses of the wind turbine direct-driven PMSG subjected to a 12 m/s constant wind speed. Initially, when the proposed schemes are not employed, the rotor was running at a speed of 1.0 and there was no load. The PMSG started supplying power at  $t = 0$ . The use of the series VRs, FFA and SDCs has significantly damped the rotor speed and electromagnetic oscillations by reducing rise and settling times and increasing damping ratio. As electromagnetic torque oscillations are responsible for drive-train stresses, they should be prevented from damaging the wind turbine direct-driven PMSG. The maximum percent overshoots (or undershoots) of the corresponding responses are significantly reduced, illustrating the system being more stable with the proposed damping mechanisms. Comparing to the PI only control structure, the significant increases in the damping ratios, as shown in Table 5.1, indicate that the system with all the three mitigation methods has become more stable.

All the three schemes are efficient in enhancing the dynamic performances of the PMSG as shown in Figures 5.8(a) and (b). From Table 5.1, it looks difficult to choose the best mitigation scheme. For instance, the VR scheme is the best method in eliminating the rotor speed undershoot, while the FFA is the best in reducing reactive power and DC-link voltage oscillations. The SDCs are the most efficient techniques in reducing the DC-link voltage overshoot. Therefore, the choice of the mitigation method depends on the metrics required in planning and operation of the system. However, overall, the results show that the FFA outperforms in most of the metrics. Therefore, it will be advisable to implement FFAs in the control system of a wind turbine direct-driven PMSG.

In Table 5.1 with the presence of the FFAs, the rising time of the rotor speed declines from 2.0 to 0.0 seconds, while that of the electromagnetic torque increases from 0.1 to 1.16 seconds as oscillations are reduced. The corresponding 10% settling times are significantly reduced from 2.4 to 0.001 seconds and from 3.0 to 1.2 seconds respectively, indicating the FFAs have made the system faster. A similar trend is observed for wind turbine system employing VRs and SDCs.



(a)



(b)

Figure 5.8. (a) Rotor speed (b) electromagnetic torque for step wind speed

The simulation results in Figures 5.9, 5.10 and Table 5.1 additionally show that the oscillations in real power, reactive power, electromagnetic torque, DC-link and terminal voltages are effectively damped by the application of the proposed mitigation methods. Figure 5.9(a) confirms that oscillations on the real power output of the generator are positively damped and this is important in standalone as well as grid integrated operations of the PMSG. Particularly, it can be observed that in Figure 5.9(b) that the FFAs assist the reactive power control of the generator successfully to maintain the reactive power of the generator to zero. However, the performance of the SDCs is poor in smoothing the real power of the PMSG out, particularly, during the first 3 to 4 seconds. Generally, with respect to real and reactive power control, the SDCs are less efficient than the other two.

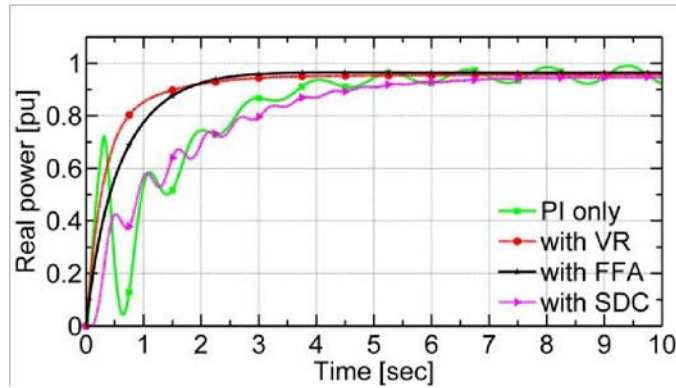
Table 5.1. Dynamic performance of the wind turbine direct-driven PMSG

Metrics		P	Q	Te	Vdc	
PI Only	Overshoot (%)	-56	-95.8	200	145.55	47.83
	Settling Time (s)	2.4	5.0	1.0	3.0	1.0
	Rise Time (s)	2.0	3.44	0.02	0.1	0.001
	Damping Ratio	0.0355	0.0033	0.175	0.15	0.055
	Time constant (s)	0.0035	0.26	0.01	0.11	0.002

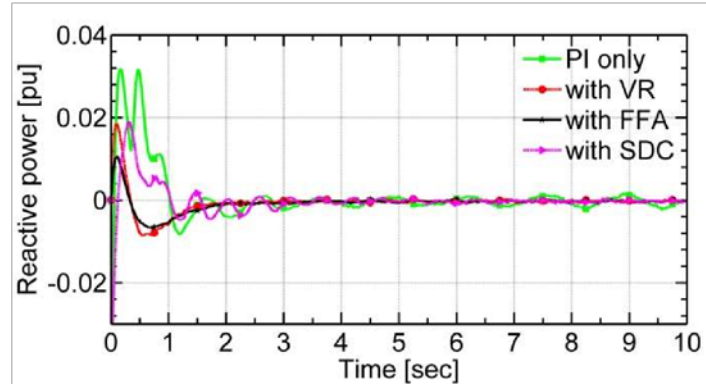
With VRs	Overshoot (%)	0.0	0.0	100	0.0	47.83
	Settling Time (s)	2.0	2.0	1.0	1.0	0.01
	Rise Time (s)	0.0	1.8	0.01	0.75	0.007
	Damping Ratio	>1.0	>1.0	0.59	>1.0	0.52
	Time constant (s)	0.001	0.36	0.12	0.4	0.0003
With FFA	Overshoot (%)	1.36	0.0	45	0.0	39.1
	Settling Time (s)	0.001	1.5	0.25	1.2	0.01
	Rise Time (s)	0.0	1.48	0.01	1.16	0.0001
	Damping Ratio	0.4	>1.0	0.17	>1.0	0.99
	Time constant (s)	0.0036	0.5	0.02	0.5	0.001
With SDCs	Overshoot (%)	2	-	100	4.47	30.43
	Settling Time (s)	1.8	5.0	0.8	2.0	0.05
	Rise Time (s)	0.0	4.65	0.01	1.18	0.008
	Damping Ratio	0.0032	-	0.59	0.23	0.47
	Time constant (s)	0.003	1.5	0.12	0.31	0.0003

-rotor speed in pu, P- active power in pu, Q- reactive power in pu Te- electromagnetic torque in pu, and Vdc- DC voltage in Volts,  
 $V_{base} = 575 \text{ V}$  and  $S_{base} = 1.5(10^6) \text{ MVA}$ ,  $f_{base} = 60 \text{ Hz}$ )

During wind gusts, the DC-link voltage may go beyond its allowable limit, endangering the solid-state switches of the converters and the DC-link capacitor. The results in Figure 5.8(b) and Figure 5.10(a) show that the overshoots in electromagnetic torque and DC-link voltage are reduced and the corresponding oscillations are also damped by FFAs. Hence, FFAs can effectively reduce overshoots and add positive damping to the oscillations of the wind turbine direct-driven PMSG to protect the corresponding components. On the other hand, the terminal voltage is also effectively controlled, avoiding the need for extra reactive power compensators need in the wind turbine. Therefore, for constant wind speeds, the dynamic performances of the wind turbine can be enhanced by employing FFAs or the other mitigation methods, which adjust the d- and q-axis reference voltages.



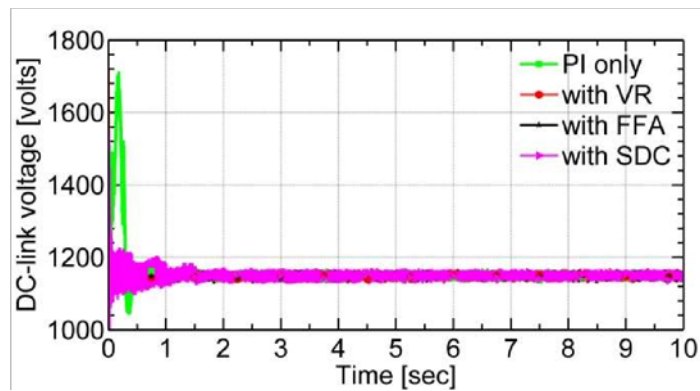
(a)



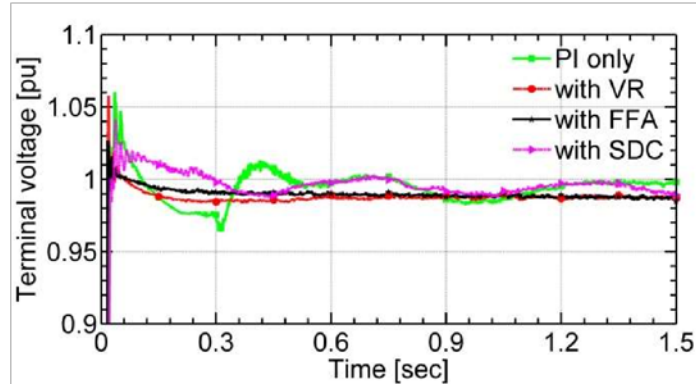
(b)

Figure 5.9. (a) Real (b) reactive power responses to a step wind speed

Simulation results, depicted in Figure 5.11, have shown that the parallel connection of VRs with stator windings as shown in Figure 5.1(c) and 5.1(d) destabilizes the wind turbine direct-driven PMSG. This is because parallel connections ultimately reduce effective impedances. Therefore, the results indicate that parallel VRs, which result in unrealisable transfer function, are not considered for enhancing the stability of a PMSG.



(a)



(b)

Figure 5.10. (a) DC-link (b) terminal voltage responses to a step wind speed

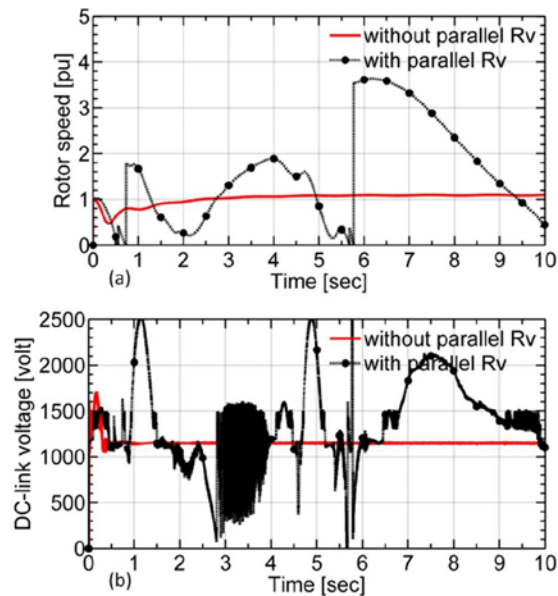


Figure 5.11. Effect of parallel VRs on (a) rotor speed (b) DC- link voltage

Overall, the simulation results have demonstrated that the wind turbine direct-driven PMSG has become more stable and faster when the proposed mitigation schemes are employed. Therefore, it can be inferred that the three mitigation methods more successfully enhance the dynamic performances of a wind turbine direct-driven PMSG for the case of constant wind. In case of high wind fluctuations, the performance of SDCs was found to be poor, whereas the series VRs and FFAs remain efficient. Thus, the next subsection investigates the performances of only VRs and FFAs during stochastic winds.

### 5.5.2 Response to Stochastic Wind Speed Series

Naturally, one hardly finds constant wind speeds. Wind speeds are stochastic processes. This section, therefore, analyses and discusses the performances of the VR and FFA mitigation methods during stochastic wind speed series. A Markov model characterized in Chapter 3 generates the stochastic wind speed series as shown in Figure 5.12. Time domain simulations were carried out to study the effects of the two algorithms on the dynamic performances of a wind turbine direct-driven PMSG connected to a grid, considering the stochastic wind speed series.

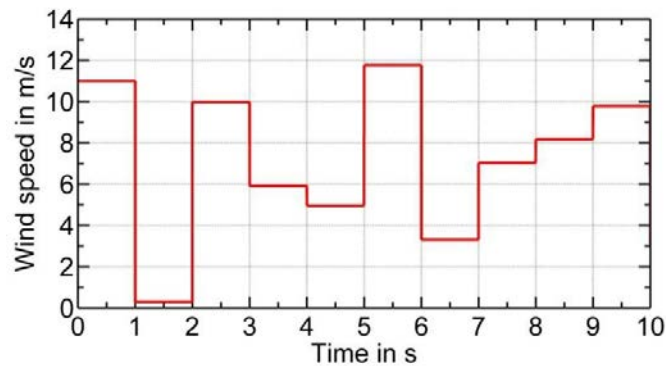
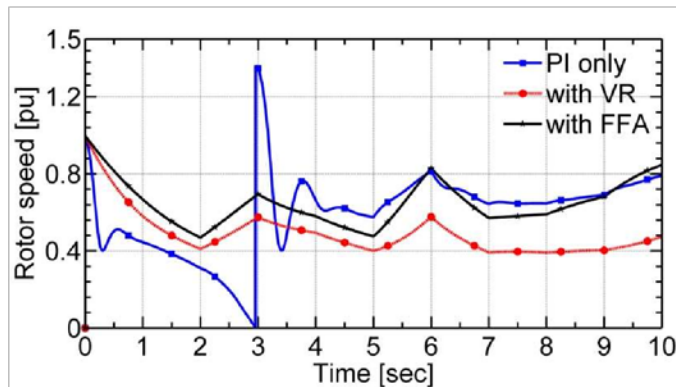
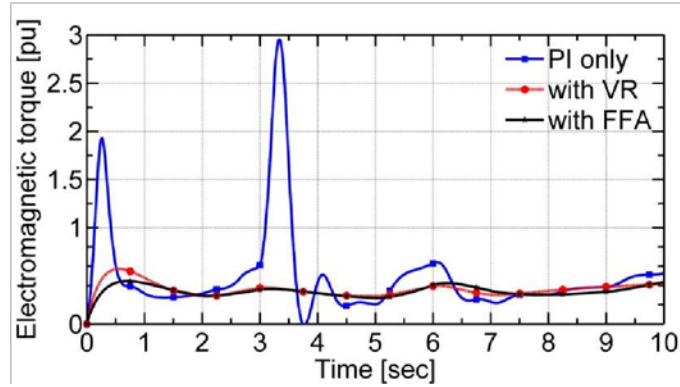


Figure 5.12. Stochastic wind speed series



(a)

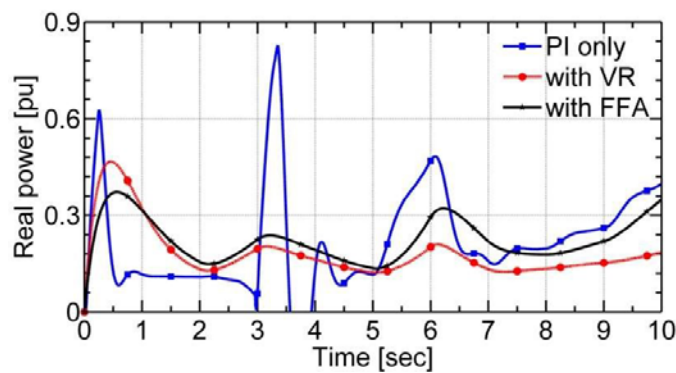




(b)

Figure 5.13. (a) Rotor speed (b) electromagnetic torque responses for stochastic wind speed series

The responses of the PMSG over 10 seconds are observed. Figures 5.13 (a) and (b) illustrate the rotor speed and electromagnetic torque responses of the PMSG for the stochastic wind speed series. The standard deviation of the wind speed series is 3.5 m/s, and from the results shown in Figure 5.13 it can be observed that both the VRs and FFAs provide positive damping to oscillations in the rotor speed and the electromagnetic torque. However, the response with the FFAs shows more damping being added as compared with the VRs. When there are wide speed variations, the algorithms become more effective in damping electromagnetic oscillations as shown in Figure 5.13(b). At the 3<sup>rd</sup> second, the rotor speed without the algorithms shoots to 1.40 p.u. which is then well compensated by the VRs and FFAs. Concisely, the results have shown that the algorithms have significantly reduced the overshoots and oscillations of the electromagnetic torque of the PMSG caused by wind speed spikes.



(a)

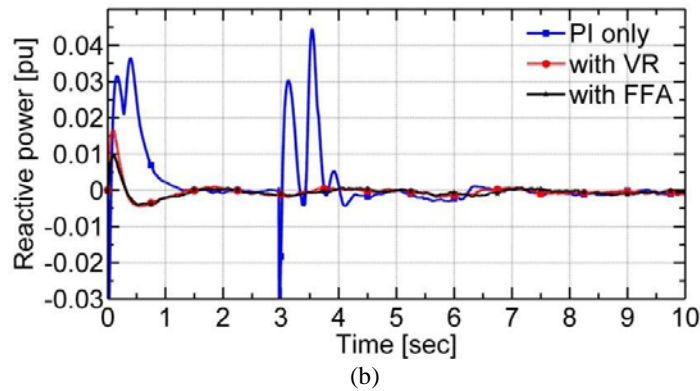


Figure 5.14. (a) Real (b) reactive power responses for stochastic wind speed series

Similarly, the results in Figure 5.14 have shown that the VRs and FFAs have reduced real and reactive power oscillations caused by rapid wind speed variations, resulting in less power fluctuations. The decline in real power fluctuations is imperative among transmission system operators. Overshoots and undershoots caused by wind spikes and troughs are reduced and nearly average real power is obtained. The control system is expected to maintain the reactive power at zero for unity power factor, but it is severely affected by the stochastic wind. However, the results have shown that the VRs and FFAs provide significant support to the control system in eliminating the reactive power errors as shown in Figure 5.14(b), increasing its performance. The VRs and FFAs, therefore, reduce real and reactive power disturbances caused by wind turbine direct-driven PMSGs in power systems.

Figure 5.15(a) shows the comparison between DC-link voltage responses with and without the mitigation methods. The results have shown that the VRs and FFAs have reduced the fluctuations, decreasing chances of damages due to wind gusts on the solid-state switches and the DC-link capacitor. The terminal voltage responses shown in Figure 5.15(b) are nearly levelled by the VRs and FFAs. Generally, the VR and FFA algorithms reduce the fluctuations in DC-link and terminal voltages. Voltage spikes are also suppressed. A close observation reveals that the FFAs are superior to the VRs. Furthermore, comparing the results in Table 4.2 with Table 5.1 shows that the FFAs outperform virtual compensators in most of the dynamic performance indices.

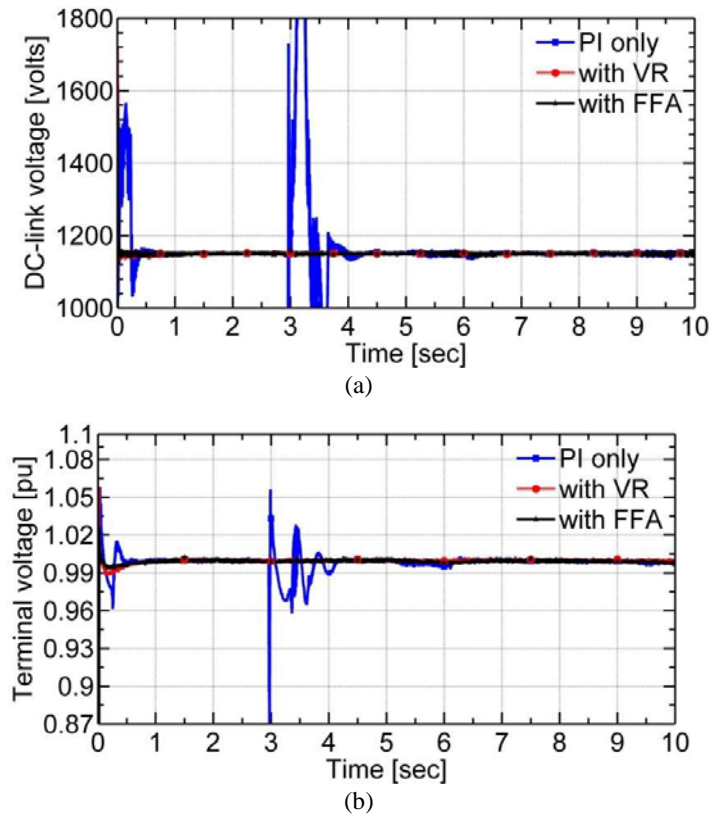


Figure 5.15. (a) DC-link (b) terminal voltage responses for stochastic wind speed series

Transmission system operators have grid codes which newly commissioned power plants should meet. Damping ratios, time constant and settling times of dominant electromechanical modes are three frequently used as performance indices in the grid codes. The VRs and FFAs are found to be efficient in improving these parameters for a PMSG. It can, therefore, be inferred that the use of VRs and FFAs in the control system of wind turbine direct-driven PMSGs is crucial.

## 5.6 Conclusion

The previous two chapters presented the characterization and modelling of wind speeds and a wind turbine direct-driven PMSG for dynamic simulations. In taking the characterization, modelling and analysis further, in response to wind disturbances, this chapter has investigated different mitigation methods to enhance the dynamic performances of the PMSG. Three approaches, namely VRs, FFAs and SDCs have been adopted for enhancing the dynamic performances of the PMSG during wind speed fluctuations.

In the first scheme, the inclusion of the VRs in the control structure has resulted in enhancing the dynamic performances of the PMSG. Simulation results demonstrated that the inclusion of VRs, connected in series to stator windings, supported the damping of local oscillations. They significantly reduced the rise and settling times of the rotor speed, electromagnetic torque, active power and reactive power. Moreover, the corresponding damping ratios were increased. In contrast, parallel connection of VRS to stator windings, has shown to have a negative impact on the damping of local oscillations.

The other scheme proposed to enhance the dynamic performances of the PMSG is the use of SDCs, along with proportional-integral controllers. In the proposed scheme, the d-axis damping controller is a supplementary controller based on the rotor speed deviation, whereas the q- axis controller is a supplementary controller based on the DC-link voltage deviation. Both SDCs were implemented in the generator side controller and their influences on the dynamic performances of the PMSG were investigated. Simulation results showed their effectiveness in damping local oscillations. In the presence of the SDCs, the rise and settling times of the rotor speed, electromagnetic torque, active power and reactive power were further reduced and the corresponding damping ratios were increased. However, SDCs are not effective in smoothing the rotor speed and power of the PMSG during rapid wind speed variations.

The third scheme was the use of FFAs in areas having rapid wind speed fluctuations. Simulation results have shown that stochastic wind speeds have a negative impact on oscillations in the rotor speed, power and electromagnetic torque of the PMSG. The corresponding settling times are also negatively affected. It is shown that the FFAs efficiently enhance the dynamic characteristics of the PMSG by damping local oscillations. As a result, speed, power, and torque oscillations, caused by wind speed disturbances, are well damped. The FFAs also significantly improve the DC-link and the terminal voltage responses; they are superior to VRs, SDCs and virtual compensators. In general, the techniques proposed in this work are applicable in smoothing the rotor speed and the output power of a wind turbine directdriven PMSG.

In Chapter 6, the FFAs will be employed while investigating the impacts of integration of PMSG-based wind farms in power systems.

## CHAPTER 6

# IMPACTS OF A PMSG-BASED WIND FARM ON POWER SYSTEM DYNAMICS

## 6.1 Introduction

A power system has different components such as generators, passive elements and controllers. The passive elements like transformers, transmission lines and passive loads hardly affect the dynamics of the system. In fact, the types and the interactions of generators and controllers determine the overall dynamic performances of the system. The behaviours of conventional generators and controllers and their effects on system dynamics are well investigated and established [14]. Conversely, the dynamic characteristics of PMSG-based wind farms, which are different from that of conventional generators and affect the system dynamics differently, are not sufficiently investigated especially considering stochastic wind speed series. In Chapters 4 and 5, a wind turbine direct-driven PMSG has been modelled, and the corresponding dynamic performances have been studied. Mitigation methods have also been proposed to improve the dynamic performances of the PMSG. In this chapter, the influences of a PMSG-based wind farm on power system dynamics are investigated. As the PMSGs are decoupled from the power system by the back-to-back converters, they will not directly affect system dynamics. However, the wind power integration brings intermittent power, structural changes and reduces the number of conventional generators, and hence indirectly affecting the dynamic behaviour of the system. The intermittent nature of the wind power is challenging for the system dynamics control.

For ensuring the safety, security, and proper integration of a newly commissioned PMSG-based wind farm into a national grid, it should meet the technical specifications stipulated in the grid code of a national power system. Generally, the code is set by a responsible authority. Some of the requirements with regard to power system dynamics are the damping ratio, time constant and settling time of a dominant electromechanical mode in the system. The deviations of these technical specifications caused by the wind power should be within acceptable ranges. The stochastic nature of wind affects the dynamics of the PMSGs and hence the whole system dynamics. Especially, as the penetration of wind power rises, the corresponding influences on the dynamic behaviour of the system become plausible. The impacts, therefore, should be investigated, and proper mitigation methods are applied to deter negative impacts.

Therefore, in this chapter, a modified IEEE 14-bus test system is employed to investigate the influences of a large-scale PMSG-based wind power penetration on the dynamic performances of a power system. Thus, the impacts of dynamic characteristics of PMSG-based wind farm, back-to-back converters and stochastic wind speed series are thoroughly investigated. Furthermore, mitigation techniques for negative effects employing FACTS devices along with virtual control are proposed.

## 6.2 The Test System

In this thesis, the IEEE 14-bus test system is used as the base for the investigation of the impacts of PMSG-based wind power integration on the dynamic performances of a power system. This test system, representing an approximation of the American Electric Power System and having 14 buses, 5 machines and 11 loads [135], is commonly employed in dynamic performance investigations [136, 137].

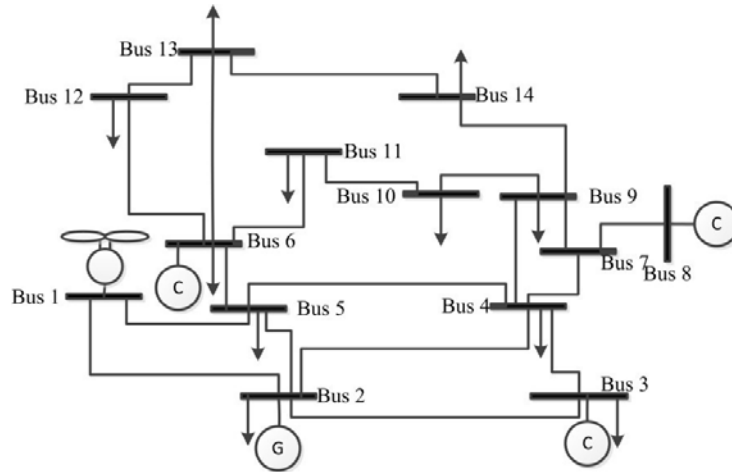


Figure 6.1. Modified IEEE 14-bus test system

Figure 6.1 shows the single-line diagram of the modified IEEE 14-bus test system. The test system accommodates the PMSG-based wind farm at bus 1. It contains a synchronous generator at bus 2 and three synchronous condensers at buses 3, 6 and 8. The 11 loads add up to 259 MW real and 81.3 MVAR reactive powers. Tables B1 and B2 in appendix B give the line and bus data of the IEEE 14-bus test system respectively [137].

The reasons for adopting the IEEE 14-bus test system are:

- The IEEE 14-bus test system fairly represents a moderate power system which takes less time during simulation in MATLAB/Simulink than, for instance, the IEEE 39-bus test system. The simulation time of the software significantly increases with the increase in the number of buses.
- The models and parameters of the test system are available in the existing literature. However, if practical systems are considered, it will be difficult to access the corresponding models and parameters as they may not be documented or the practical data may be confidential.
- The models of this test system are less complicated than the practical models which are large and make the time domain simulation cumbersome.
- The results obtained from the test system are more general than the ones which may be obtained using the models of a practical system.
- Simulation results can be easily compared with other investigations done using the same test system.

In this research, the conventional generator at bus 1 in the IEEE 14-bus test system is fully replaced by a PMSG-based wind farm. Excess loads which initially supplied by synchronous generator 1 are now taken over by the conventional generator at bus 2. A 25% wind power penetration level is considered.

## 6.3 Modelling the Test System

### 6.3.1 PMSG-Based Wind Farm Model

In Chapters 4 and 5, an individual wind turbine direct-driven PMSG connected to an infinite bus was modelled and investigated. These days, the maximum power output of a single wind turbine of this type has reached 8 MW [58]. To achieve tens or hundreds of megawatts of wind power, several wind turbines should come together and be connected to the common coupling point (CCP), bus 1 of Figure 6.1, as shown in Figure 6.2. This parallel connection of wind turbines forms a wind farm. The size of wind turbines is growing with technology. However, as the number of wind turbines in a farm decreases, the aggregate power becomes more fluctuating and hence increasing influence on the power system dynamics. Moreover, the stochastic wind speed series aggravates the problem.



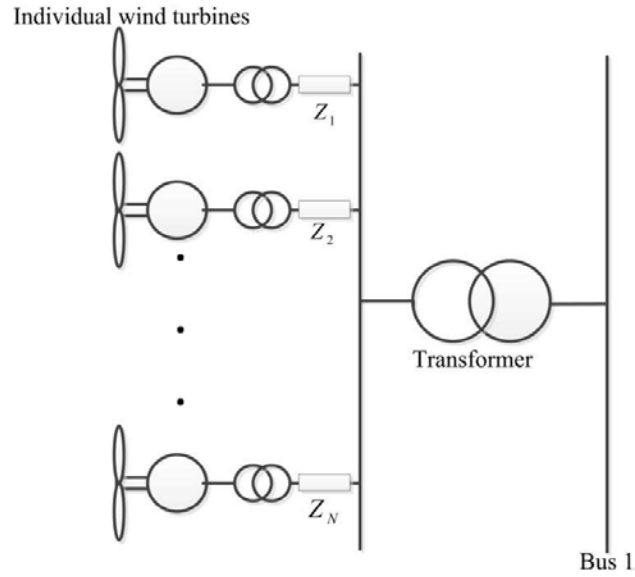


Figure 6.2. A typical PMSG-based wind farm

A wind farm spans over a wide geographical area and depending on the type of the generators used, it may be SCIG, DFIG, PMSG-based or mixed wind farm. One of the challenges in modelling the wind farm is that the wind speed varies over the geographical location of the farm. Consequently, though all the wind turbines are identical, the power output of each wind turbine varies with the corresponding wind speed. On the other hand, modelling all the individual wind turbines demands vast memory and is time-consuming, which is not affordable. Therefore, a simple aggregate model, which retains the dynamic characteristics of the wind turbine direct-driven PMSGs, is required.

In aggregate modelling of a PMSG-based wind farm, the rotor speed of the individual wind turbine should be tracked [32]. For the sake of simplification of the aggregate model, an aggregate wind speed model is adopted as in [138] that can fairly show the influence of the stochastic wind speed series in the test system dynamics. In general, the following assumptions are considered [139]:

- In this work, the wind profile is assumed to be uniform over the geographical location of the wind farm.
- Tower shadow and wake effects are neglected.
- The distribution network within the wind farm is also aggregated considering voltage drops and power losses.

Overall, the total MVA rating and real power of the wind farm are given as:

$$= \tag{6.1}$$

$$= \tag{6.2}$$

where is the MVA rating of the wind farm, is the real wind power and N is the number of wind turbine direct-driven PMSGs. The equivalent PMSG-based wind turbine of the N wind turbines is depicted in Figure 6.3.

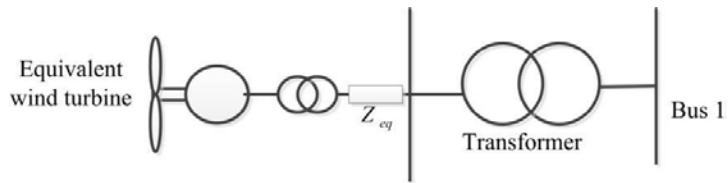


Figure 6.3. Equivalent wind turbine direct-driven PMSG

Considering identical wind turbine direct-driven PMSGs, voltage drops and power losses, and applying source transformation technique, the equivalent impedance in the aggregate system is given as:

$$= \frac{\sum_{i=1}^N Z_i}{N^2} \tag{6.3}$$

Similarly, the equivalent transformer reactance of the wind farm is:

$$= \frac{\sum_{i=1}^N x_i}{N^2} \tag{6.4}$$

where and are the equivalent and individual reactances of the wind turbine transformers respectively.

## 6.3.2 Synchronous Machine Model

### 6.3.2.1 The Swing Equation

The dynamic characteristics of the wind turbine direct-driven PMSG have influences on the dynamic performances of the IEEE 14-bus test system. Compared to the electromagnetic responses of conventional synchronous machines, the dynamic responses of the PMSG are slow (shown in Chapters 4 and 5) and will have no significant effects on the electromagnetic dynamics of the synchronous machines. For this reason, the classical model of a synchronous machine is sufficient to study the impacts of the PMSG-based wind farm on the dynamic performances of the test system. In the analysis of large disturbances, it is customary to use the classical model as it reduces the complexity of the system and computation time [14, 140].

Figure 6.4 shows the steady state circuit model of a cylindrical rotor type synchronous machine. In this model, only one of the three phases is shown.  $E_a$ ,  $V_t$ ,  $I_a$ ,  $r_a$  and  $x_d$  are induced voltage, terminal voltage, armature current, armature resistance, and direct-axis reactance of the synchronous machine respectively.

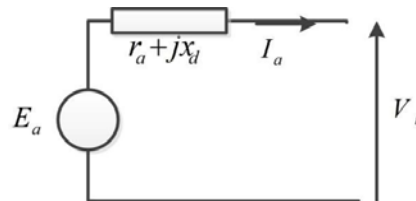


Figure 6.4. A steady state circuit model of a synchronous machine

According to the fundamental theorem of flux linkages, during a disturbance, the flux linkage of any closed circuit having finite resistance and reactance cannot change instantaneously [141]. Thus, as field flux cannot change instantly, one can show that the induced transient voltage is given as in (6.5) [14].

$$e' = E_a + (r_a + jx_d) I_a \quad (6.5)$$

$e'$  and  $x_d'$  are induced transient voltage and transient direct-axis reactance of the synchronous machine respectively. The synchronous generator is represented by a constant voltage source behind transient impedance. This model is valid only when cylindrical rotor type and constant rotor flux linkages are assumed.

The total complex power transfer (in p.u.) between Generator 2 and bus 2 in Figure 6.1 can be given as:

$$S = [V_2 + j(X_{T2} + X_{T2})]^* \quad (6.6)$$

where  $V_2$  is the voltage at bus 2 and  $X_{T2}$  is the total reactance between the generator and bus 2. Neglecting the armature resistance and simplifying (6.6) gives the real power transfer to bus 2 as shown in (6.7).

$$P = \frac{|V_1| |V_2| \sin(\delta)}{X_{T2}} \quad (6.7)$$

$\delta$  is the phase angle difference between  $V_1$  and  $V_2$ , and commonly known as the power angle, and  $\delta = \delta_1 - \delta_2$ . Equation (6.7) gives the real power transfer between any two voltage sources (or nodes).

The time plot of the power angle ( $\delta$ ) clearly shows the dynamics of the synchronous machine. An ever-increasing power angle means the system is unstable. The electromechanical motion of the rotor of each synchronous machine in the test system is governed by the swing equation given in (6.8) [14].

$$2H \frac{d^2\delta}{dt^2} = P_m - P_e \quad (6.8)$$

$P_m$  and  $P_e$  are the input mechanical and output electrical powers of the synchronous generator respectively.  $\omega_s$  is the synchronous speed of the generator.  $H$  is the normalized inertia constant of the synchronous generator given in seconds. Practically, the inertia constant of a synchronous machine is calculated as:

$$H = \frac{J \omega_s^2}{2P_r} \quad (6.9)$$

where  $J$  and  $S$  are the total moment of inertia and MVA rating of the synchronous machine respectively. The swing equation can also be given in terms of the rotor speed of the synchronous machine as shown in (6.10).

$$\frac{2}{H} \Delta = - \dots \quad (6.10)$$

$\Delta$  is the speed deviation from the synchronous speed, .

Generally, the rotor speed is given as:

$$= + \Delta \quad (6.11)$$

In practice, the winding resistances and the damper windings contribute to the damping of oscillations in the power angle and rotor speed. As a result, the model in (6.10) can be rewritten to accommodate the damping effect. Equation (6.12) shows the complete model of the dynamics of the rotor of the synchronous machine.

$$\frac{2}{H} \Delta + D \Delta = - [ \dots ] \quad (6.12)$$

$D$  is damping coefficient representing the effects of the damper windings.

### 6.3.2.2 Governor Model

A first order turbine and a simplified governor model are employed to regulate the mechanical power input to the synchronous generator. The governor model combined with the corresponding turbine in s-domain is given as [32]:

$$-\left(\frac{1}{1+sT_1}\right)\left(\frac{1+sT_2}{1+sT_3}\right) - \Delta ) - \Delta \quad (6.13)$$

where  $R$  is the droop characteristic,  $T_1$  is the time constant of the turbine,  $T_2$  and  $T_3$  are filter time constants. In (6.13), the turbine has upper and lower limits which should be included in the MATLAB/Simulink model.

### 6.3.2.3 Exciter Model

The terminal voltage and reactive power output of a synchronous machine rely on its excitation system. In order to regulate the terminal voltage and the reactive power, the excitation system should be properly regulated by an exciter model. This model contains the excitation system and its controller. There are different types of exciter models stipulated in

[32, 142]. For the sake of its simplicity and ease of implementation in MATLAB/Simulink, the one shown in (6.14) is adopted.

$$\frac{1 + \dots}{1 + \dots} \left( \frac{\dots}{1 + \dots} + \dots \right) \quad (6.14)$$

is the exciter voltage, and are the time constants of an amplifier which amplifies the error voltage, is the set point reference voltage, is the power system stabilizing signal and is the terminal voltage transducer output. In (6.14), both the amplifier and the exciter are subjected to windup limits.

### 6.3.3 Load Model

All the 11 loads in the IEEE 14-bus test system are assumed to be static three-phase loads. Consequently, they are precisely implemented as series RLC loads in the MATLAB/Simulink load network by entering the corresponding real and reactive powers. Moreover, the transmission lines in the test system are modelled as short lines and implemented as series RLC branches in the Simulink model.

## 6.4 Mitigation Techniques

In this section, the models of the different techniques improving the dynamic performances of the modified IEEE 14-bus test system are explored. First, the effects of enhancing the dynamic performances of the PMSG on the test system dynamics are viewed. Subsequently, the models of conventional methods such as capacitor banks and filters are discussed. Finally, the models of the proposed FACTS devices are presented.

### 6.4.1 Enhancing the Dynamic Performances of the PMSG

In Chapters 4 and 5, compensators, VRs, FFAs and SDCs have been proposed to enhance the local damping performances of the wind turbine direct-driven PMSG, which is the main component of the PMSG-based wind farm. The corresponding models and parameters were shown in those chapters. In this chapter, the investigation is extended to the power system dynamics. Thus, the investigation of the effects of these proposed techniques on the dynamic performances of the IEEE 14-bus test system is presented in section 6.5.

## 6.4.2 Conventional Methods

In Chapter 4, the reactive power of the wind turbine direct-driven PMSG is maintained at zero. This implies that the PMSG is not able to supply reactive power to the test system at bus 1 in Figure 6.1. As a result, there will be a voltage distortion and reactive power shortage at this bus unless corrected by the other generator, synchronous condensers or extra compensators. The voltage distortion can be overcome by connecting conventional capacitor banks. On the other hand, the back-to-back converters inject harmonics into the test system which severely affect the dynamics of the system, especially the bus voltages. To tackle this challenge, the inductance of the RL filter of the wind turbine can be increased; however, this action reduces the real power transfer of the PMSG-based wind farm. Thus, the inductance cannot be indefinitely increased. The other alternative is to use an appropriate three-phase harmonic filter to filter voltage and current harmonics.

Synchronous condensers are flexible and effective in reactive power compensation; however, they are expensive. In effect, static capacitors, which are cheaper, can be connected to the CCP to achieve voltage and reactive power regulation. In practice, discrete static capacitors are used for flexibility and economic reasons. Static capacitors can be classified into shunt and series capacitor banks. In this thesis, shunt capacitors are adopted for the following reasons [143]:

- Shunt capacitors reduce the converter currents of the PMSG and hence protecting the back-to-back converters from over current damages.
- They improve the voltage profile of the IEEE 14-bus test system.
- They also reduce the real power loss of the PMSG-based wind farm.
- They enhance the power factor of the PMSG-based wind farm.
- They reduce the load on the PMSG-based wind farm.
- For a practical system, they reduce capital investment per mega-watt.

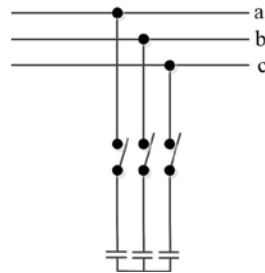


Figure 6.5. Three-phase star-connected shunt capacitor bank

In general, the shunt capacitor bank shown in Figure 6.5 draws a fixed amount of leading current superimposed on the PMSG current reducing the reactive components of the load and hence improving the power factor of the wind power system.

The back-to-back converters of the wind farm generate current harmonics, which in turn produce voltage harmonics across low impedances causing voltage distortion and reducing power factor. A three-phase harmonic filter, a shunt component at the CCP, can be employed to decrease the voltage distortion and correct power factor. The filter is designed to be capacitive at the fundamental frequency in order to produce the reactive power required by the converters and to correct power factor [144].

A number of filter banks may be connected in parallel at the CCP to achieve acceptable voltage distortion and power factor. In this thesis, band-pass filters are used to filter the 11<sup>th</sup>, 13<sup>th</sup> and 24<sup>th</sup> order harmonics. These filters are tuned either at a single frequency (single-tuned filter) or at two frequencies (double-tuned filter). A C-type high-pass filter is used to filter the 3<sup>rd</sup> order harmonics keeping zero losses at 50 Hz frequency. Figure 6.6 shows a combination of a shunt capacitor bank and three typical filters used in this work to tackle voltage distortion and power factor reduction at the CCP.

The filters contain resistive, inductive and capacitive elements. The resistance, inductance, and capacitance values are determined from the following parameters [144]:

- Reactive power at the CCP
- Harmonic frequencies and
- Quality factor ( $Q_f$ ), a measure of the sharpness of the tuning frequency. Quality factor is determined using the resistance value.



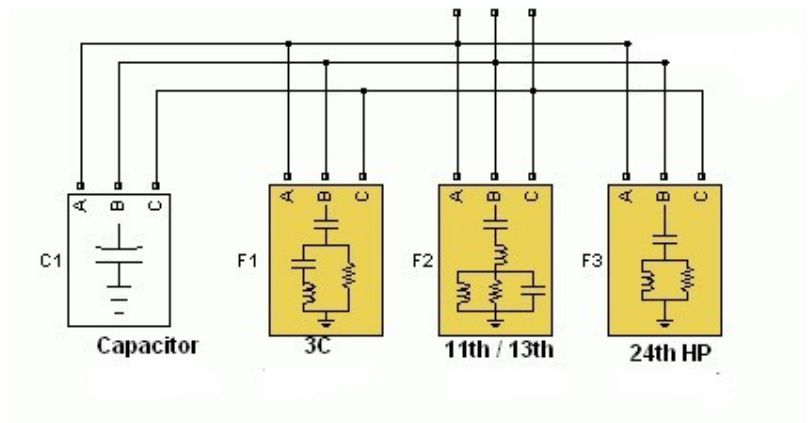


Figure 6.6. A shunt capacitor and three filter banks [144]

In single-tuned frequency filters, where resistance, inductance and capacitance elements are connected in series, the harmonic order (n), quality factor (Q<sub>f</sub>) and the band width (B) of the three-phase harmonic filters are determined as shown in (6.15), (6.16) and (6.17) respectively.

$$\frac{f_n}{f} = \sqrt{\frac{X_C}{X}} \tag{6.15}$$

$$= \frac{1}{Q_f} = \frac{1}{\sqrt{\frac{L}{R^2 C}}} \tag{6.16}$$

$$= \frac{R}{\omega L} \tag{6.17}$$

R, X<sub>C</sub>, and X are the resistance, capacitive reactance, and inductive reactance of the filter and f<sub>n</sub> is n<sup>th</sup> order harmonic frequency.

In double-tuned filters having f<sub>1</sub> and f<sub>2</sub>, both the series circuit and the parallel circuit are tuned approximately to the mean geometric frequency (f<sub>g</sub>) given in (6.18). And the corresponding quality factor is given in (6.19). A double-tuned frequency filter incurs less power loss than a single-tuned frequency filter.

$$f_g = \sqrt{f_1 f_2} \tag{6.18}$$

$$Q_f = \frac{1}{2} \left( \frac{f_2}{f_1} + \frac{f_1}{f_2} \right) \tag{6.19}$$

L and R are the parallel resistance and inductance elements at the mean frequency  $f_m$ .

On the other hand, a high-pass filter is a single-tuned filter where the L and R elements are connected in parallel. This filter has a wide-band having impedance at high frequencies limited by the resistance R. The corresponding quality factor is given as:

$$= \frac{\quad}{2} \quad (6.20)$$

### 6.4.3 FACTS Devices

Pragmatically, shunt FACTS devices are used to improve voltage profile and power factor at a bus. Therefore, in this section, the models of static var compensator (SVC) and static compensator (STATCOM) are discussed.

#### 6.4.3.1 SVC Model

The SVC model in this work assumes a balanced fundamental frequency operation and takes firing angle into consideration. It is given by [145]:

$$- \quad (6.21) \quad \text{---} \quad \text{---} =$$

$$\frac{d\alpha}{dt} = \frac{-K_D\alpha + \frac{KT_t}{(T_r T_M)}(-K_M V + v_M) + K(V_{ref} - v_M)}{T} \quad (6.22)$$

$$= \quad (6.23)$$

where  $T_r$ ,  $T_t$ , and  $T_M$  refer to transient regulator time constant, regulator time constant and measured time delay respectively.  $K_D$ ,  $K$ , and  $K_M$  are regulator gain, integral deviation and measured gain respectively.  $\alpha$  is firing angle,  $v_M$  is measured voltage,  $V$  is terminal voltage at the CCP,  $T$  is firing angle time constant and  $X_{SVC}$  is the reactance of the SVC.  $Q_{SVC}$  is reactive power. The firing angle has maximum and minimum limits.

#### 6.4.3.2 STATCOM Model

In this research, a voltage source converter (VSC)-based STATCOM is used to mitigate the negative impacts of the wind power on the dynamic performances of the IEEE 14-bus test system. Figure 6.7 shows the single line diagram of a STATCOM connected to

bus 1 of the IEEE 14-bus test system. This STATCOM is used to reduce voltage distortion and power factor reduction at the point of common connection. It can also be connected at the mid-point of the line connecting buses 1 and 2. It has three major parts as shown in Figure 6.7: the VSC which is an inverter to convert the DC voltage into an appropriate three-phase AC voltage, the transformer which steps up the VSC output and filters harmonics and the controller which is basically dedicated to control the VSC.

In general, the model of the STATCOM is given as [146]:

$$\begin{aligned}
 \frac{1}{L} \frac{d}{dt} \begin{bmatrix} i_d \\ i_q \end{bmatrix} + \begin{bmatrix} \omega i_q \\ -\omega i_d - \frac{R}{L} i_d \end{bmatrix} &= \begin{bmatrix} -\frac{D_d}{3L} \\ -\frac{D_q}{3L} \end{bmatrix} + \frac{1}{3L} \begin{bmatrix} 1 \\ 0 \\ 0 \end{bmatrix} \\
 \frac{3D_d}{2C} &= \frac{3D_q}{2C}
 \end{aligned}
 \tag{6.24}$$

where  $R$  and  $L$  are equivalent resistance and inductance between the VSC and bus 1.  $i_d$ ,  $i_q$ , and  $D$  are the d-axis current, q-axis current and the DC voltage of the STATCOM respectively.  $D_d$  and  $D_q$  are the d- and q-axis control variables.  $C$  is the capacitance at the terminal of the VSC.

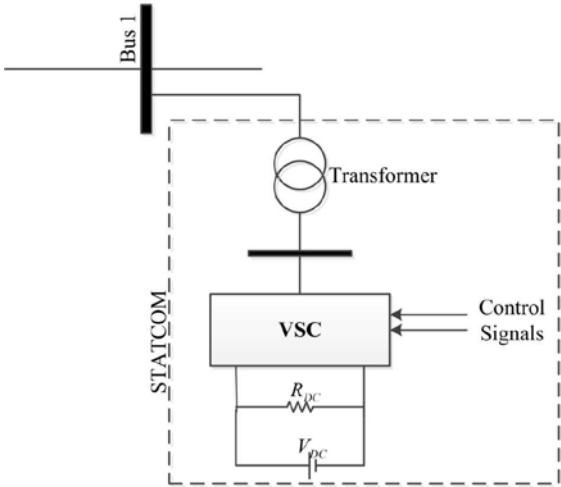


Figure 6.7. A STATCOM connected to the CCP

The controller takes voltage and current measurements and compares them against reference voltages and currents. Based on the error signals, it adjusts the control variables and sends the switching signals to the VSC.

Ideally, the output of the VSC is assumed to be in phase with the voltage at bus 1 and there will be no real power transfer from the STATCOM to bus 1. In this scenario, the battery source in the converter will be unnecessary. However, due to the power loss in the VSC, this cannot happen in real world. Therefore, the power source in Figure 6.7 is added to compensate the power loss in the VSC. Due to this fact, the output voltage of the VSC slightly leads the voltage at bus 1 as the STATCOM is expected to function as a capacitor bank to regulate the voltage and improve the power factor [146]. The STATCOM can also be placed at the midpoint of a transmission line for efficient operation.

## 6.5 Results and Discussion

In this section, all the models including the PMSG-based wind farm model are implemented in MATLAB/Simulink for time domain dynamic simulations. The influences of the PMSG-based wind farm on the dynamic performances of the IEEE 14-bus test system are thoroughly investigated. In Figure 6.1, Generator 1 of the IEEE 14-bus test system is fully replaced by a PMSG-based wind farm. Both the base and modified test systems are simulated for 10 to 13 seconds. In order to include a grid disturbance, a three-phase fault with a fault resistance of 1.0 milliohm is applied at bus 4 of the test system for 150 ms starting from the 5<sup>th</sup> second. The influence of the wind power on the test system increases with the corresponding wind power penetration. However, in this chapter, a 25% PMSG-based wind power penetration is considered. Two sets of wind speed series are also considered: steady wind speed series having 12 m/s magnitude and stochastic wind speed series generated in Chapter 3.

The aim of this section is to assess the impacts of the dynamic characteristics of the PMSG-based wind farm, sharp wind gusts, back-to-back converters, PMSG-based wind power controllers, and stochastic wind speed series on power system dynamics with possible power system faults. Moreover, possible mitigation techniques which can reduce negative impacts are investigated. The dynamic responses of the wind turbine direct-driven PMSG were presented in Chapters 4 and 5. However, in that case, the PMSG was connected to an infinite bus. In this chapter, the equivalent wind turbine direct-driven PMSG representing a PMSGbased wind farm is connected to the IEEE 14-bus test system where the voltage at the

CCP is not as stiff as that of the infinite bus. This will bring its own influences on the dynamic performances of the PMSG. Therefore, as part of the test system itself, the dynamic performances of the PMSG-wind farm should also be investigated.

### 6.5.1 Effects of Dynamic Characteristics of PMSG-Based Wind Farm on Power System Dynamics

One of the challenges of PMSG-based wind power integration into power systems comes from the back-to-back converters. They inject current and voltage harmonics into the power system causing voltage distortion and power factor reduction. Figure 6.8 shows the dynamic responses of the synchronous generator at bus 2 when a conventional generator and a PMSG-based wind farm are connected to bus 1. When the wind farm is used, mitigation methods suggested in Chapters 4 and 5 are not employed, and there is also no conventional compensation method or FACTS device connected to any of the buses. The responses with the wind farm are noisy and messy because of the current and voltage harmonics injected by the converters.

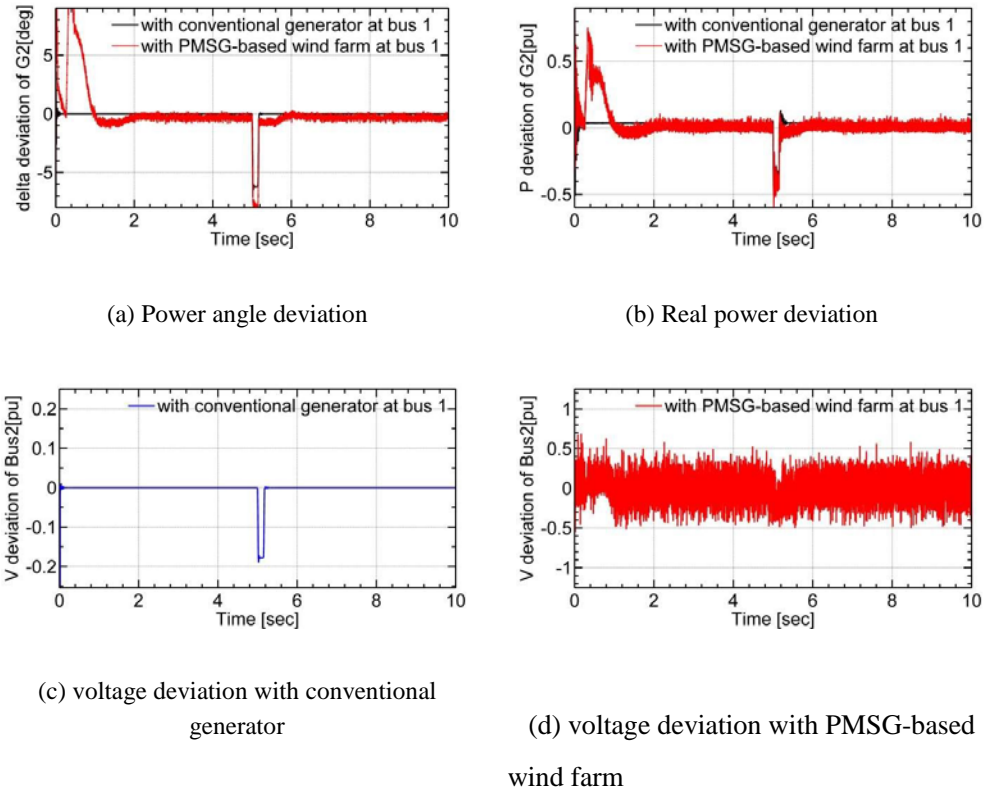
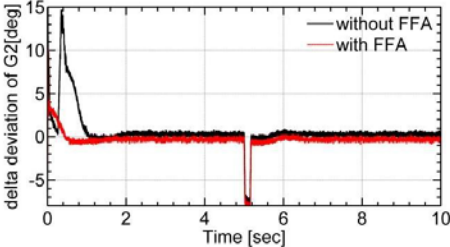


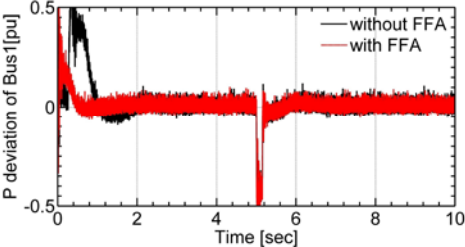
Figure 6.8. Dynamic responses of generator 2

Figure 6.8(a) shows that, during transient periods, the dynamic response of the power angle of synchronous generator 2 is more affected by the wind turbine direct-driven PMSG than by the conventional synchronous generator. This is due to the fact that the wind turbine direct-driven PMSG considered takes more time to settle as discussed in Chapter 4. The real power response in Figure 6.8(b) also shows that the wind farm significantly affects the dynamics of generator 2 compared to the conventional generator. From the two responses, it can be observed that the dynamic performances of synchronous generator 2 deteriorates when a PMSG-based wind farm is connected to bus 1.

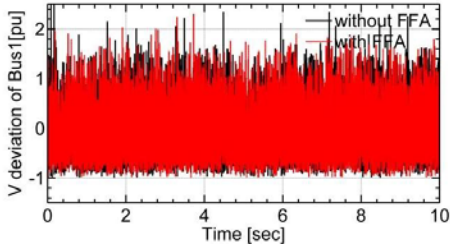
Under any national grid code, a utility company operating a wind farm is usually expected to maintain the voltage at the CCP within a certain error margin. However, with PMSG-based wind farms, unless a mitigation method is employed, the converters lead to the violation of the grid code as depicted in Figure 6.8(d) compared to the one shown in Figure 6.8(c) which employs a conventional generator at bus 1. One can decrease the effects of the back-to-back converters by increasing the inductance of the RL filter of the wind turbine direct-driven PMSGs; nevertheless, increasing the inductance makes the wind farm grid coupling weak and finally may lead to instability.



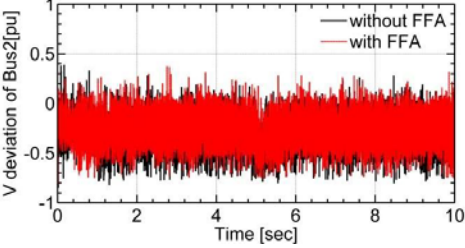
(a) Power angle deviation



(b) Power output deviation



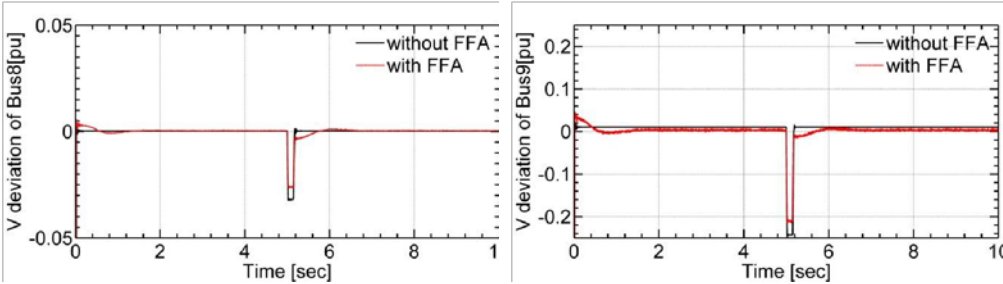
(c) Voltage magnitude deviation at bus 1



(d) Voltage magnitude deviation at bus 2

Figure 6.9. Dynamic responses of test system with FFAs

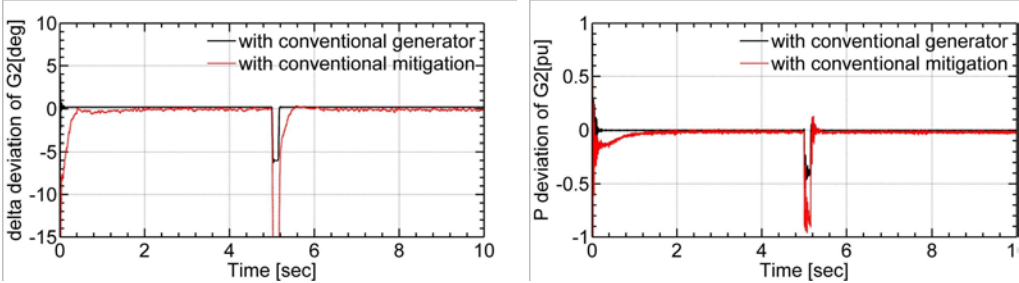
Figure 6.9 illustrates the dynamic responses of the test system when a PMSG-based wind farm with FFAs is connected to bus 1. The results show that the FFAs improve the dynamic responses of synchronous generator 2 particularly during transient periods as shown in Figures 6.9(a) and 6.9(b). It can be observed that overshoots, time constants and settling times are reduced when the FFAs are employed. It can also be deduced that the other mitigation approaches suggested in Chapters 4 and 5 can be used. The effects of the FFAs on the voltage magnitude responses at the CCP, Figure 6.9(c), and bus 2, Figure 6.9(d), are not significantly visible. This is due to the fact that voltage and reactive power have a strong relationship and the reactive power output of the PMSG-based wind farm is maintained at zero by its controller regardless of the presence of the FFAs. The power angle and real power responses are enhanced because they are directly affected by the real power output of the wind farm, which can be controlled by the FFAs.



(a) Voltage magnitude at bus 8

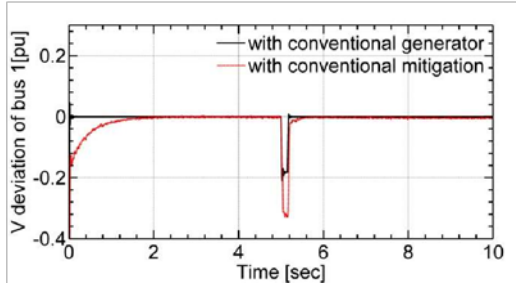
(b) Voltage magnitude at bus 9

Figure 6.10. Effects of the PMSG-based wind farm on bus voltages

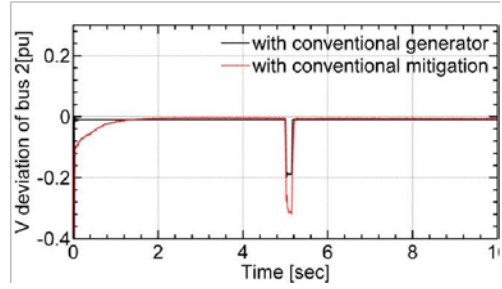


(a) power angle deviation

(b) power output deviation

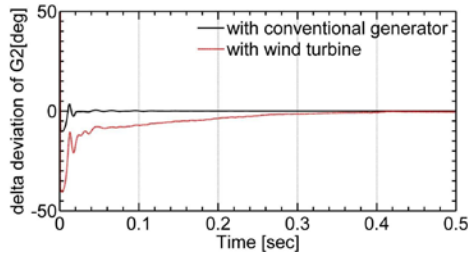


(c) voltage deviation at bus 1

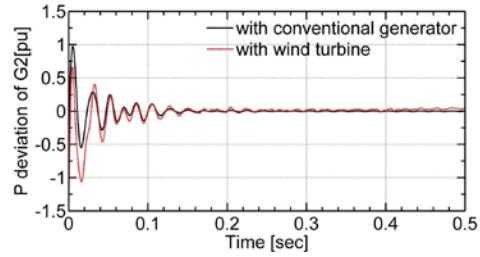


(d) voltage deviation at bus 2

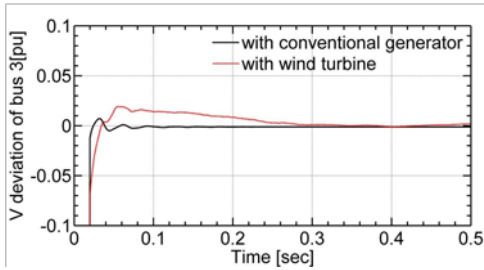
Figure 6.11. Dynamic responses of the test system with capacitor bank and filters connected to bus 1



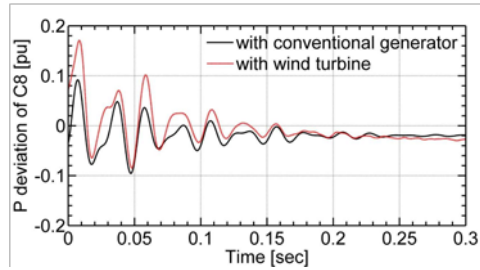
(a) Power angle deviation of G2



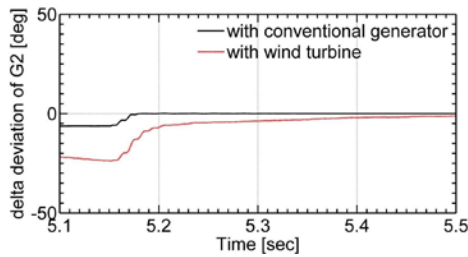
(b) Power output deviation of G2



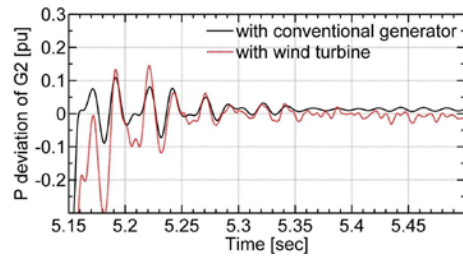
(c) Voltage deviation at bus 2



(d) Power deviation of synchronous condenser at bus 8

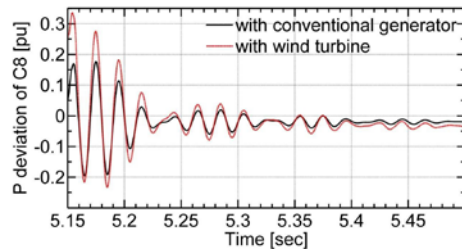


(e) Power angle deviation of G2 after fault



(f) Real power deviation of G2 after fault clearance





(g) Real power deviation of synchronous condenser at bus 8 after fault clearance

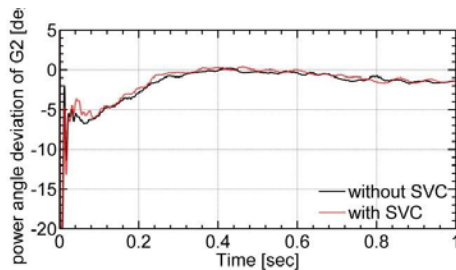
Figure 6.12. Typical dynamic responses

Comparing the dynamic responses in 6.9(c) and 6.9(d) with that of 6.10(a) and 6.10(b) reveals that the dynamics of buses in the vicinity of the CCP are more affected by the PMSG-based wind farm than those of afar buses. The far most buses are slightly affected by the presence and disturbance of the wind. The back-to-back converters inject voltage and current harmonics in the vicinity buses. These problems can be tackled by adopting conventional mitigation methods such as shunt capacitor banks and filters. Therefore, the combination suggested in Figure 6.6 has been connected to bus 1 of Figure 6.1. The simulation results are depicted in Figure 6.11. It can be observed that the current and voltage harmonics causing disturbances in the power angle, power and voltage are appropriately eliminated.

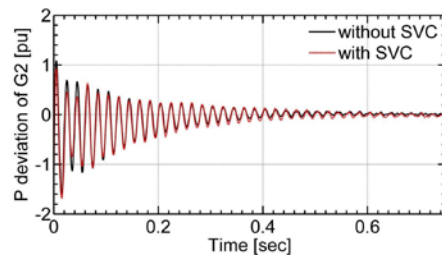
Figure 6.12 presents the comparison of typical dynamic responses of the IEEE 14-bus test system with a conventional generator and a PMSG-based wind farm connected to bus 1. Figures 6.12(a) to 6.12(d) are responses to the connection of the wind farm at a wind speed of magnitude 12 m/s at  $t = 0+$ , whereas the ones from 6.12(e) to 6.12(g) show the responses for a fault at bus 4 at  $t = 5.0$  seconds. In all cases, a qualitative observation demonstrates that the adoption of the wind farm has affected the dynamic performances of the test system. Time constants, settling times and oscillations of the responses have increased. Damping ratios are reduced. In this particular investigation, these deviations of technical specifications in the simulation results are within acceptable ranges of the technical specifications. However, in some critical cases, the parameters may go out of the specified ranges and require further mitigations.

### 6.5.2 Effects of an SVC on the Dynamic performances of the Test System

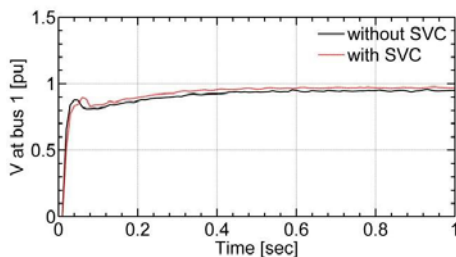
An SVC was connected to bus 1 of the modified IEEE 14-bus test system shown in Figure 6.1. The power angle response of generator 2, real power response of generator 2, and voltage responses at buses 1 and 2 are shown in Figure 6.13. The test system was subjected to a 12 m/s wind speed. The results show that the dynamics of the power angle of the conventional generator connected to bus 2 is slightly improved by the presence of the SVC. From Figure 6.13(a), it can be observed that oscillations in the power angle are reduced, and the new power angle of generator 2 reaches steady state slightly faster than the one without the SVC does. Similarly, in Figure 6.13(b), the same conclusion is reached. In general, the SVC is intended to improve the voltage and reactive power responses of the test system. It indirectly affects the performances of the synchronous generators. In Figures 6.13(c) and 6.13(d), the voltage responses at buses 1 and 2 illustrate the application of the SVC has brought the voltages faster to the corresponding steady states. The use of delta connected passive elements in the SVC has prevented the injection of current and voltage harmonics into the test system.



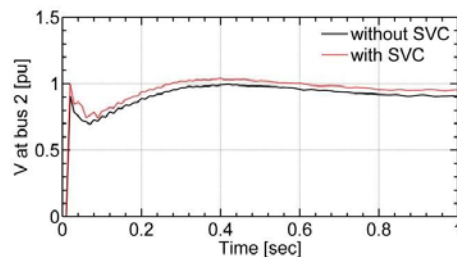
(a) Power angle deviation of G2



(b) Real power deviation of G2



(c) Voltage magnitude at CCP



(d) Voltage magnitude at bus 2

Figure 6.13. Effects of SVC

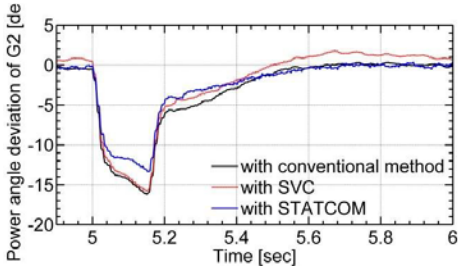
Overall, the SVC is more crucial in enhancing the steady state performances than the dynamic performances of the test system. Since the effects of the SVC on the dynamic

performances of the test system are less significant, a conventional mitigation method such as a three-phase shunt capacitor bank is recommended for economic reasons.

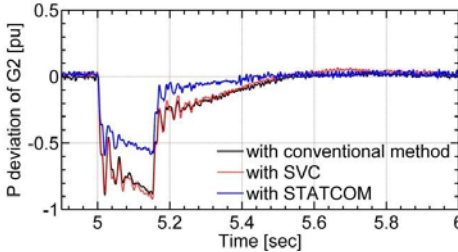
### 6.5.3 Effects of a STATCOM on the Dynamic Performances of the Test System

The STATCOM was placed at the mid-point of the transmission line connecting buses 1 and 2 which are significantly affected by the wind power. The fault was applied at the fifth second. Figure 6.14 presents the comparison of the influences of a shunt capacitor bank (conventional method), SVC and STATCOM on the dynamic performances of the IEEE 14bus test system with the PMSG-based wind farm connected to bus 1 of Figure 6.1. Figure 6.14 shows the dynamic responses of the test system subjected to a 150 ms three-phase fault at bus 4.

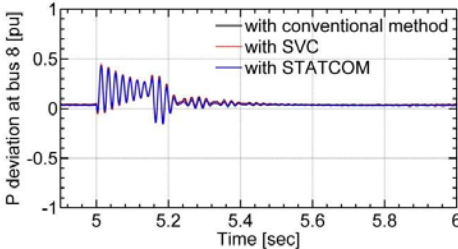
In Figure 6.14(a), the impact of the STATCOM on the power angle dynamic response of the synchronous generator connected to bus 2 is depicted. It is observed that the test system with the STATCOM has dynamically performed better than the ones with shunt capacitor bank and SVC do during the three-phase fault. The inclusion of the STATCOM has reduced the power angle deviation, the corresponding time constant and settling time by injecting the proper amount of reactive power at the appropriate time.



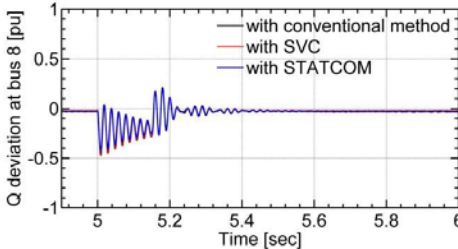
(a) Power angle deviation



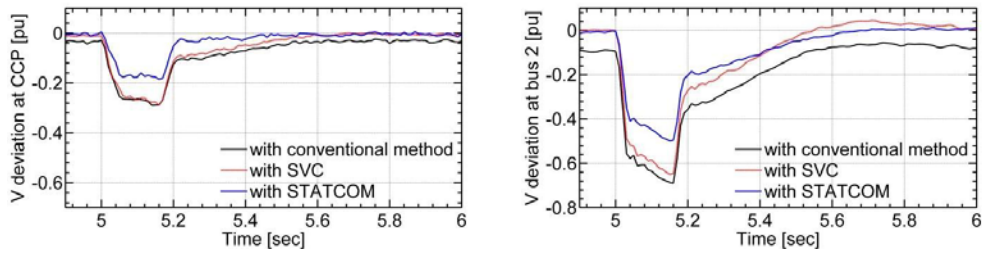
(b) Real power deviation of G2



(c) Real power deviation at bus 8



(d) Reactive power deviation at bus 8



(e) Voltage magnitude deviation at CCP      (f) Voltage magnitude deviation at bus 2

Figure 6.14. Comparison of Effects of Conventional method, SVC and STATCOM on dynamic performances

The STATCOM has also improved the real power dynamic response of the synchronous generator connected to bus 2 as shown in Figure 6.14 (b) during the fault. On the other hand, both the PMSG-based wind farm and the STATCOM have little impact on bus 8 as shown in Figures 6.14(c) and 6.14(d). This is due to the fact that bus 8 is not in the vicinity of the wind farm and the STATCOM. Moreover, bus 8 has its own synchronous condenser which controls the corresponding voltage and reactive power.

Both the dynamics and the steady state bus voltages in the vicinity of the wind farm are improved by the STATCOM as shown in Figures 6.14(e) and 6.14(f). In this case, compared to that of the shunt capacitor bank and the SVC, voltage deviations are reduced and the voltage responses are relatively fast during the three-phase fault. Generally, the system with the STATCOM shows lower overshoots and faster responses than that with the SVC does since the STATCOM has a rapid response to power system disturbances and smooth voltage control capability over a wide range of operating conditions.

In Figures 6.13(a) and 6.14(a) the unit of the power angle deviation of G2 is degree abbreviated as ‘de’.

#### 6.5.4 Effects of Power System Disturbances on the PMSG-Based Wind Farm

Figure 6.15 depicts the effects of a three-phase fault at bus 4 on the dynamic performances of the PMSG-based wind farm. It can be observed that the power system disturbance has no impact on the dynamics of the rotor speed and electromagnetic torque responses as shown in Figures 6.15(a) and 6.15(b). This is due to the decoupling effect of the back-to-back converters. Because of the interaction between the wind farm and the test

system, the steady state rotor speed has slightly increased from that obtained in Chapters 4 and 5.

Similarly, the steady-state electromagnetic torque is reduced from 0.9 to 0.7 per unit.

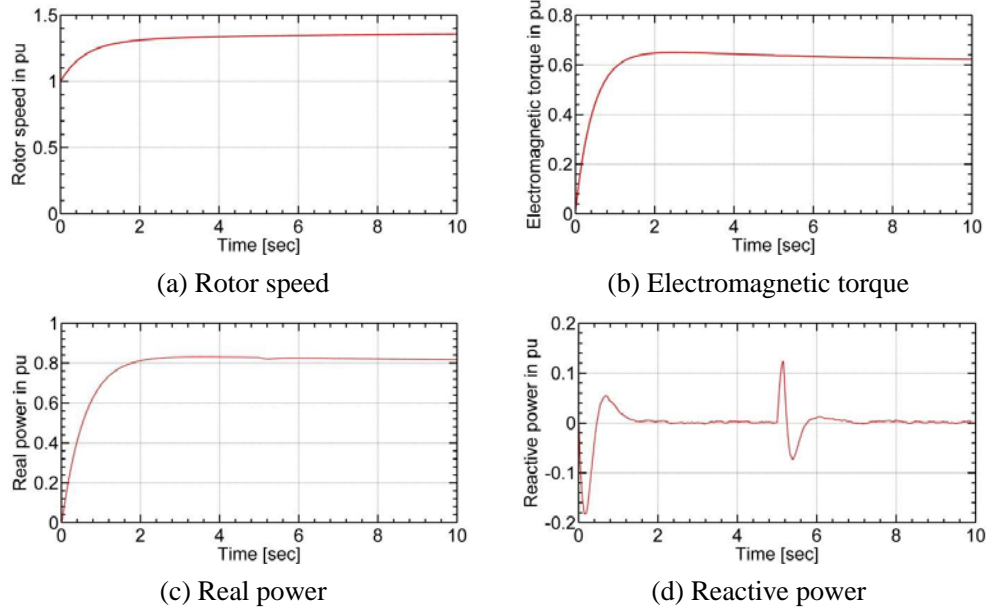


Figure 6.15. Dynamic responses of the PMSG-based wind farm

The real power output of the wind farm is hardly affected by the occurrence of the three-phase fault at the fifth second as the rotor speed remains unaffected as shown in Figure 6.15(c). On the contrary, the reactive power of the farm is highly influenced by the three-phase fault. This is because there is a high correlation between the voltage at bus 1 and the reactive power of the farm. As this voltage is disturbed, the reactive power will also be disturbed. However, the wind turbine controller always tries to maintain the reactive power of the wind farm at zero as shown in Figure 6.15(d) at steady state.

### 6.5.5 Effects of Stochastic Wind Speed Series

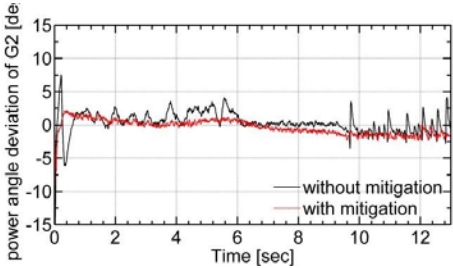
In Chapters 4 and 5, the influences of stochastic wind speed series on the dynamics of a wind turbine direct-driven PMSG had been investigated and mitigation methods were thereof proposed to tackle the detrimental impacts on the dynamic performances of the PMSG. The wind speed extends its impact to a power system consisting of a PMSG-based wind farm. For that reason, this section investigates the effects of stochastic wind speed series generated in Chapter 3 on the dynamics of the modified IEEE 14-bus test system shown in Figure 6.1. Two simulation scenarios are considered. In the first scenario, no mitigation

method except a threephase filter is adopted, whereas in the second case FFA is adopted to improve the local dynamic performances of the PMSG-based wind farm and a STATCOM is employed to tackle the detrimental effects of the stochastic wind speed series on the dynamic performances of the test system. The STATCOM is placed at the mid-point of the transmission line connecting buses 1 and 2.

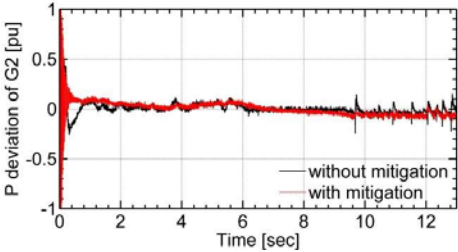
Figure 6.16 shows the simulation results of the test system both with and without the proposed mitigation methods. In the figure, typical dynamic responses such as power angle, real power, reactive power and bus voltage magnitude responses are shown.

In Figure 6.16(a), the power angle response of synchronous generator 2 without any mitigation method (black line) depicts that the stochastic wind speed series significantly affects the power angle. The power angle continuously oscillates together with the wind speed series. This has its own drawback on the real power output of generator 2 which in turn influences the dynamics of the test system. Any nearby synchronous machine is similarly affected.

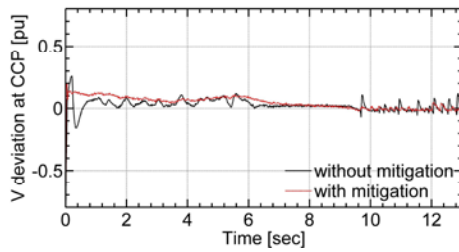
In this scenario, the stochastic wind speed series affects the dynamics of the system by continuously varying the real power output of the wind farm and hence affecting the power balance of synchronous machines, for instance as shown in Figure 6.16(b). From the two figures, after observing the results with the mitigation methods (broken red lines), it can be inferred that the FFA mitigation method proposed in Chapter 5 and the STATCOM are effective in damping power angle and real power oscillations caused by the stochastic wind speed series in the PMSG-based wind farm. Oscillations appearing from the 1<sup>st</sup> to the 6<sup>th</sup> second and from the 10<sup>th</sup> to 13<sup>th</sup> second are damped, and the corresponding time constants and settling times are also reduced by the mitigation methods. Power angle and real power deviations can be maintained within acceptable ranges particularly during stochastic wind disturbances having low variance with the support of the FFA and STATCOM.



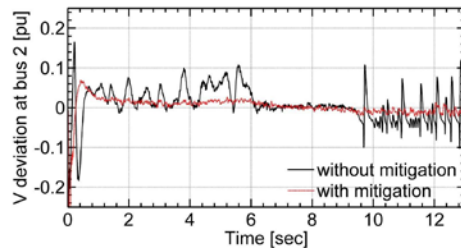
(a) Power angle deviation of G2



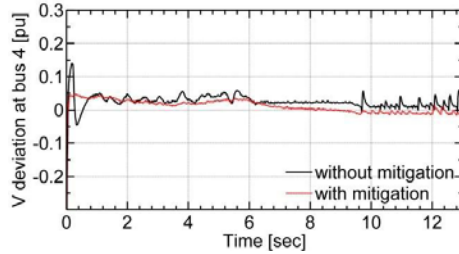
(b) Real power deviation of G2



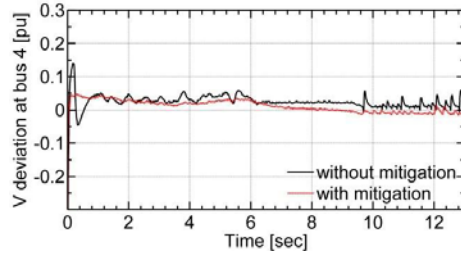
(c) Voltage deviation at CCP



(d) Voltage deviation at bus 2



(e) Voltage deviation at bus 4



(f) Reactive power deviation at bus 4

Figure 6.16. Impact of stochastic wind speed series on power dynamics

The stochastic wind speed series also negatively affects the bus voltages, especially the ones close to the CCP as shown in Figures 6.16(c) and 6.16(d). Even though the converter controller tries to maintain the reactive power of the wind farm at zero, the wind speed fluctuation indirectly affects the reactive power of the buses and thus affecting the bus voltages of the test system. The results have shown that both the FFA and STATCOM can add positive damping to bus voltage fluctuations resulting from the stochastic wind speed series.

Similarly, in Figures 6.16(e) and 6.16(f), the wind speed fluctuations cause the bus voltage and reactive power fluctuations at bus 4 which can be damped by the proposed mitigation methods in this work as shown by the broken red lines. In general, the dynamic performances of the test system deteriorate because of the presence of stochastic wind speed disturbances in the PMSG-based wind farm. And such detrimental effects of the wind farm can be controlled by the mitigation methods suggested in this thesis.

## 6.6 Conclusion

This chapter has analysed the impacts of PMSG-based wind power on power system dynamics using a modified IEEE 14-bus test system where the wind farm is connected to bus

1. Mitigation methods such as FFA, shunt capacitor banks, SVC and STATCOM, which can be employed to tackle detrimental impacts, have also been proposed.

The dynamic characteristics of the PMSG-based wind farm indirectly affect the dynamics of the test system. The dynamics of the synchronous machines, the major dynamic components in the test system, depend on power balance, which is influenced by the power response of the wind farm. Thus, enhancing the dynamic performances of the wind turbine direct-driven PMSGs indirectly improves the dynamic performances of a power system consisting of such wind turbines. Therefore, the mitigation methods suggested in Chapters 4 and 5 are efficient in improving the dynamic performances of a power system containing a PMSG-based wind farm. Moreover, shunt capacitor bank, SVC and STATCOM are proven to be effective in enhancing the dynamic performances of a power system with a PMSG-based wind farm.

Disturbances in a power system can have also their own effects on the dynamic performances of a PMSG-based wind farm. In this case, rotor speed and electromagnetic torque responses are hardly affected by the disturbances. Nevertheless, reactive power and terminal voltage responses of the wind farm are severely affected, whereas the corresponding real power response is slightly affected.

The other important point in this chapter is that stochastic wind speed disturbances result in oscillations (or fluctuations) in power angles, real power, reactive power and bus voltages, affecting the dynamics of a power system. It is also found that the mitigation techniques proposed in Chapters 4 and 5 are efficient in improving the dynamic performances of a power system in fluctuating wind environments. Moreover, SVC and STATCOM along with virtual methods suggested in this thesis can also be used to enhance the dynamic performances of a power system containing a PMSG-based wind farm subjected to stochastic wind speed disturbances.



## CHAPTER 7

### CONCLUSIONS AND RECOMMENDATIONS

#### 7.1 Introduction

The vision of any transmission system operator (TSO) is to serve its customers through a seamless, cost-effective, and dynamically stable power system. In this regard, the types of generators, controllers and the interaction between them determine the dynamic performances of a power system. Because of the challenges related to conventional fuels, the world is shifting its focus towards wind power, among which PMSG-based wind power is promising. However, replacing conventional synchronous generators by wind turbine direct-driven PMSGs is introducing its own challenges, affecting the dynamic stability of a power

system, and hence compelling TSOs to revise their planning and control methods. In line with wind power integration, a new set of disturbances, related to stochastic wind speed series, are being introduced into a power system. The review in Chapter 2 has revealed that wind speed disturbances are often neglected in the investigations of the dynamic performances of a power system having wind power plants. However, as the penetration level grows further, the impacts of the stochastic wind speed disturbances on power system dynamics become significant and can no more be neglected.

Moreover, wind power introduces a new set of controls into a power system, which influences the dynamics of the system differently. Altogether, the impacts of a PMSG-based wind farm on the dynamic stability of a power system can be seen from two perspectives. First, a PMSG-based wind farm has its own (local) dynamic stability issues, which depend on the dynamics of PMSGs, drive-trains and wind power controllers. The local dynamic stability problems are aggravated by the presence of the stochastic wind speed series. Therefore, one of the aims of this thesis has been geared towards investigating the impacts of stochastic wind speed series on the dynamics of a wind turbine direct-driven PMSG. As reviewed in Chapter 2, these local problems can be overcome by enhancing the dynamic performances of PMSGs through mitigation techniques employing real and reactive power controls. In this regard, this thesis has initiated novel techniques called virtual controls stemming from resistors, compensators, and damper windings to enhance the dynamic performances of a wind turbine direct-driven PMSG. Second, the review has also shown that the integration of PMSG-based wind power has both positive and negative impacts on the system-wide dynamic stability of a power system. Considering this, investigations in this thesis have revealed that negative impacts of wind power exist in a power system containing a PMSG-based wind farm, and this thesis suggests that the use of virtual controls along with STATCOM and SVC improves the dynamic performances of such a power system. In short, this thesis has dealt with modelling and analysis of stochastic wind speed series for dynamic simulations of wind farms and the corresponding effects on the dynamic performances of a power system and has also proposed mitigation techniques.

In general, the results from this study have demonstrated that stochastic wind speed disturbances significantly affect the dynamic performances of a power system consisting of high penetration of PMSG-based wind power, and employing virtual controls along with FACTS devices, particularly STATCOM, enhances the dynamic performances. Several

prominent conclusions and recommendations can be drawn from the novel studies done on the impacts of stochastic wind speed series and the corresponding mitigation methods.

## 7.2 Conclusions

This conclusion section hereby presents the conclusions drawn from Chapters 3, 4, 5 and 6 of this thesis.

### 7.2.1 Chapter 3: Modelling and Analysis of Wind Speed Series

This work has presented the characterization of wind speed series and power in Durban for dynamic simulations of a wind turbine direct-driven PMSG. Markov chain and Weibull distribution were employed in the characterization. In developing the Markov model, measured wind speed series from Durban were categorised into sixteen distinct states, and a TPM was formed. This TPM along with its limiting probability vector was used to write a MATLAB code that generated synthetic wind speed series. The median, mean, and standard deviation of the synthetic series were close to those of the measured ones, indicating the accuracy of the model. On the other hand, the shape and scale factors of a Weibull distribution were generated using the measured wind speed series and maximum likelihood estimation method. Comparing the PDFs of the Weibull fit, a widely-employed technique in dynamic simulations of wind turbines, and the Markov model using RMSE methods showed that the latter accurately characterised the wind speed series. Intermediate wind speeds between hours and minutes were also generated using Weibull and Gaussian distributions employing the results of the Markov model. The Markov model could, indeed, generate stochastic wind speed series, which can be used in analysis and simulations of the dynamic behaviour of wind turbines. It could also predict wind speed series for different time horizons. Finally, the analysis of wind power density had revealed that large wind turbines having hub heights greater than 85 m could be effective in Durban and its environs. However, compared to windy areas, wind turbines in this area would have high hub heights.

### 7.2.2 Chapter 4: Modelling a Wind Turbine Direct-Driven PMSG for Dynamic Simulations

Chapter 4 has laid the foundation for the thesis by modelling and analysing the different components of a wind turbine direct-driven PMSG such as the drive train, generator, DC-link, generator and grid side controllers. It has also modelled a power grid considered as

an infinite bus for dynamic analysis. In response to wind speed disturbances, the chapter has proposed the use of virtual compensators, stemming from RLC compensators, along with PI controllers for enhancing the dynamic performances of the PMSG. The compensators have been modelled together with the generator side controller. Simulation results using MATLAB/Simulink showed that increasing amplitudes of wind disturbances reduced the damping ratios of the rotor speed, power and electromagnetic torque responses of the PMSG. The corresponding settling times were also negatively affected. However, the virtual compensators enhanced the dynamic performances of the PMSG by damping local oscillations in the speed, power, and torque responses, caused by stochastic wind speed disturbances. Moreover, the compensators significantly improved the DC-link and the terminal voltage responses. A close observation revealed that lag compensators were more effective than lead compensators. On the other hand, the performances of lead-lag compensators were mainly dominated by the lag components, and they were nearly as effective as lag compensators. Finally, the technique proposed in this section is applicable in smoothing the rotor speed and the output power of a wind turbine

direct-driven PMSG.

### 7.2.3 Chapter 5: Enhancing the Dynamic Performances of a Wind Turbine

#### Direct-Driven PMSG

In taking the characterisation, modelling and analysis begun in Chapter 4 of this thesis further, Chapter 5 has dealt with three novel mitigation approaches to enhance the dynamic performances of a wind turbine direct-driven PMSG in response to stochastic wind speed disturbances: namely VRs, FFAs, and SDCs.

VRs, connected in series and parallel to the stator windings of the PMSG, were implemented in the generator side converter controller. Simulation results showed that series VRs efficiently enhanced the dynamic performances of the PMSG by damping local oscillations. Speed, power, and torque oscillations, caused by stochastic wind disturbances, were well damped. Moreover, the series VRs significantly improved the DC-link and the terminal voltage responses. On the other hand, parallel VRs decreased the damping performances of the PMSG. Hence, for a better performance, VRs should be connected in series to the stator windings.

Likewise, FFA algorithms, stemming from fictitious damper windings, were modelled and realised in the generator side controller. Thereafter, the system was subjected to constant and stochastic wind speed operating conditions to evaluate the effectiveness of the algorithms. The results showed that stochastic wind speed disturbances reduced the damping ratios of the rotor speed, power and electromagnetic torque responses of the PMSG, and the corresponding settling times were also negatively affected without the FFAs. However, it was shown that the FFAs efficiently enhanced the dynamic characteristics of the PMSG by damping local oscillations. Power, and torque oscillations, caused by wind speed disturbances, were well damped. The FFAs also improved the DC-link and terminal voltage responses.

In the SDCs scheme, the d-axis damping controller was a supplementary controller based on the rotor speed deviation, and the q-axis controller was a supplementary controller based on the DC-link voltage deviation. Both SDCs were implemented in the generator-side controller and their influences on the dynamic performances of the PMSG were investigated. Simulation results showed their effectiveness in damping local oscillations. In the presence of the SDCs, the rise and settling times of the rotor speed, electromagnetic torque, active power and reactive power responses were further reduced and the corresponding damping ratios were increased. Nevertheless, SDCs were poor in smoothing the rotor speed and power of the PMSG during rapid wind speed variations. More interestingly, it is concluded that FFAs are superior to VRs, virtual compensators and SDCs in most of the dynamic performance indices of the PMSG.

Like the mitigation technique proposed in Chapter 4, the techniques proposed here are applicable in smoothing the rotor speed and output power of a wind turbine direct-driven PMSG under stochastic win disturbances. Apart from improving the dynamic stability of a power system, the mitigation techniques suggested in this thesis reduce stresses in drive-trains, over currents and over voltages which may damage solid state switches, DC-link capacitors and windings.

#### 7.2.4 Chapter 6: Impacts of a PMSG-Based Wind Farm on Power System Dynamics

Chapter 6 has investigated the influences of high penetration of PMSG-based wind power on power system dynamics. The investigation, based on a modified IEEE 14-bus test system, showed that the dynamic performances of the test system deteriorated with the inclusion of wind power. This was due to the dynamic characteristics of the wind farm and

stochastic wind speed series which indirectly affect the dynamics of the system by influencing the real power balance. Indeed, the dynamics of the synchronous machines, the major dynamic components in the test system, depend on power balance, which is influenced by the power response of the wind farm. The stochastic wind speed series resulted in oscillations (or fluctuations) in power angles, real power, reactive power and bus voltages, affecting the dynamics of the test system. On the other hand, disturbances in a power system can have also their own effects on the dynamic performances of a PMSG-based wind farm. In this case, rotor speed and electromagnetic torque responses were hardly affected. However, reactive power and terminal voltage responses of the wind farm were severely affected, while the real power response was slightly influenced.

Mitigation techniques for poor dynamic performances are, therefore, definitely compulsory. In doing so, enhancing the dynamic performances of the wind turbine directdriven PMSG directly improved the dynamic performances of the test system. Thus, the novel mitigation techniques suggested in this thesis are efficient in improving the dynamic performances of such a power system. Moreover, shunt capacitor banks, SVCs and STATCOMs when employed with the virtual controls were found effective to enhance the dynamic performances of the test power system with a PMSG-based wind farm. To this end, it is concluded that the mitigation techniques proposed in this thesis are crucial in improving the dynamic performances of a power system having wind farms and operating in fluctuating wind environments.

### 7.3 Suggestions for Future Research

Based on the investigations done in this thesis, the following future research areas have been suggested:

- The wind speed modelling in this work has been based on the wind speed data collected from Durban. A further study is recommended following this same trend for larger geographical areas, including wider datasets, for dynamic simulations of different types of wind turbines and farms.
- In this research, a constant time spacing between two wind speed states has been considered due to the behaviour of the hourly mean wind speed data obtained from SAWS; however, in practice, the time duration between wind speed states

is stochastic in nature. Therefore, a higher order Markov chain model which includes a stochastic time duration is recommended for further study.

- In future, the effect of compensators, implemented along with advanced converter controllers instead of PI controllers, on the dynamic performances of a wind turbine direct-driven PMSG can be studied.
- Further research on virtual control emulating conventional power plants and control systems will be beneficial.
- This thesis has employed the IEEE 14-bus test system for dynamic performance investigation of a power system consisting of PMSG-based wind farms. Further research including larger power systems will be important to validate the results obtained in this research.
- Finally, in this work, field experimental work on a wind turbine direct-driven PMSG has not been conducted as the system was not available at hand. Therefore, the simulation results here can be supported by field experiments on real wind turbines in a practical power system.

## REFERENCES

- [1] R. W. Shortridge, "Some early history of hydroelectric power," *Hydro Review*, June 1988.
- [2] M. Asif and T. Muneer, "Energy supply, its demand and security issues for developed and emerging economies," *Renewable and Sustainable Energy Reviews*, vol. 11, pp. 1388–1413, 2007.

- [3] G. J. Herberta, S. Iniyan, E. Sreevalsan and S. Rajapandian, "A review of wind energy technologies," *Renewable and Sustainable Energy Reviews*, vol. 11, pp. 1117–1145, 2007.
- [4] M. Haque, M. Negnevitsky and K. Muttaqi, "A novel control strategy for a variable speed wind turbine with a permanent magnet synchronous generator," *IEEE Transactions on Industry Applications*, vol. 46, pp. 331 – 339, 2010.
- [5] M. Mayouf and R. Abdessemed, "Comparative study of a small size wind generation system efficiency for battery charging," *Serbian Journal of Electrical Engineering*, vol. 10, pp. 261 – 274, 2013.
- [6] A. Rolan, A. Luna, G. Vazquez, D. Aguilar and G. Azevedo, "Modeling of a variable speed wind turbine with a permanent magnet synchronous generator," in *IEEE International Symposium on Industrial Electronics*, Seoul, 2009.
- [7] L. Shi, L. Kang, L. Yao, S. Qin, R. Wang and J. Zhang, "Effects of wind generation uncertainty and volatility on power system small-signals Stability," *Journal of Electrical Engineering Technology*, vol. 9, pp. 60 – 70, 2014.
- [8] H. Espen, I. Norheim and K. Uhlen, "Large-scale wind power integration in Norway and impact on damping in the Nordic grid," *Wind Energy 2005*, vol. 8, pp. 375 – 384, 2005.
- [9] M. Mahmud, M. Hossain, H. Pota and C. Zhang, "Investigation of critical factors affecting dynamic stability of wind generation systems with permanent magnet synchronous generators," in *The International Federation of Automatic Control*, Cape Town, South Africa, August 2014.
- [10] E. Mahersi, A. Khedher and M. Mimouni, "The wind energy conversion system using PMSG controlled by vector control and SMC strategies," *International Journal of Renewable Energy Research*, vol. 3, pp. 41 – 50, 2013.
- [11] K. Zhao, G. Li, B. Wang and M. Zhou, "Grid-connected topology of PMSG wind power system based on VSC-HVDC," in *International Conference on Electric Utility Deregulation and Restructuring and Power Technologies (DRPT)*, Weihai, China, July 2011.
- [12] N. Abdolghani, J. Milimonfared and G. Gharehpetian, "A direct torque control method for CSC based PMSG wind energy conversion systems," in *International*



Conference on Renewable Energies and Power Quality, Santiago de Compostela, Spain, March 2012.

- [13] S. Y. Kong, R. C. Bansal and Z. Y. Dong, "Comparative small-signal stability analyses of PMSG-, DFIG- and SCIG-based wind farms," *International Journal of Ambient Energy*, vol. 33, no. 2, pp. 87-97, 2012.
- [14] P. Kundur, *Power system stability and control*, New York: McGraw Hill, Inc., 1994.
- [15] X. F. Wang, Y. Song and M. Irving, *Modern power system analysis*, Springer Science+Business Media, LLC, 2008.
- [16] D. Gautam, V. Vittal and T. Harbour, "Impact of Increased Penetration of DFIG-Based Wind Turbine Generators on Transient and Small Signal Stability of Power Systems," *IEEE Transactions on Power Systems*, vol. 24, no. 3, pp. 1426-1434, 2009.
- [17] M. Jafarian and A. Ranjbar, "The impact of wind farms with doubly fed induction generators on power system electromechanical oscillations," *Renewable Energy Elsevier*, vol. 50, pp. 780-785, 2013.
- [18] T. Ayodele, A. Jimoh, J. Munda and J. Agee, "The influence of wind power on the small signal stability of a power system 2007 quality," in the international conference on renewable energies and power tech, 2011.
- [19] J. L. Rueda and I. Erlich, "Impacts of large scale integration of wind power on power system small-signal stability," in *Electric Utility Deregulation and Restructuring and Power Technologies (DRPT), 2011 4th International Conference on*, 2011.
- [20] G. Tsourakis, B. M. Nomikos and C. D. Vournas, "Contribution of Doubly Fed Wind Generators to Oscillation Damping," *IEEE Transactions on Energy Conversion*, vol. 24, no. 3, pp. 783-791, 2009.
- [21] D. Gautam and V. Vittal, "Impact of DFIG based Wind Turbine Generators on Transient and Small Signal Stability of Power Systems," in *Power & Energy Society General Meeting, 2009. PES '09. IEEE, 2009*.
- [22] S. Ravichandran, S. B. Dasan and R. Devi, "Small Signal Stability Analysis of Grid Connected Wind Energy Conversion Systems," in *IEEE International Conference on Recent Advancements in Electrical, Electronics and Control Engineering*, 2011.
- [23] N. Modi, T. K. Saha and N. Mithulananthan, "Effect of Wind Farms with Doubly Fed Induction Generators on Small-Signal Stability; A Case Study on Australian Equivalent System," in *Innovative Smart Grid Technologies Asia (ISGT), 2011 IEEE PES, 2011*.

- [24] J. Rueda and F. Shewarega, "Small signal stability of power systems with large scale wind power integration," in Proceedings of the XIII Encuentro Regional Iberoamericano de CIGRÉ, no. XIII/PI-C1-22, Puerto Iguazú, Argentina, 2009.
- [25] P. S. Georgilakis, "Technical challenges associated with the integration of wind power into power systems," *Renewable and Sustainable Energy Reviews*, vol. 12, no. Elsevier, pp. 852–863, 2008.
- [26] G. Tsourakisa, B. Nomikosb and C. Vournasa, "Effect of wind parks with doubly fed asynchronous generators on small-signal stability," *Electric Power Systems Research*, vol. 79, no. Elsevier, pp. 190–200, 2009.
- [27] A. Mendonca and J. P. Lopes, "Impact of large scale wind power integration on small signal stability," in International Conference on IEEE Future Power Systems, Amsterdam, 18-18 Nov. 2005.
- [28] T. Ackermann, *Wind power in power systems*, Stockholm, Sweden: John Wiley and Sons, Ltd, 2005.
- [29] Domínguez-García, J. Luis, OriolGomis-Bellmunt, F. D.Bianchi and A. Sumper, "Power oscillation damping supported by windpower: A review," *Renewable and Sustainable Energy Reviews*, vol. 16, pp. 4994–5006, 2012.
- [30] S. Yuanzhang, W. Lixin, L. Guojie and L. Jin, "A review on analysis and control of small signal stability of power systems with large scale integration of wind power," in IEEE International Conference on Power System Technology (POWERCON), Hangzhou, 24-28 Oct. 2010.
- [31] B. Safari, "Modeling wind speed and wind power distributions in Rwanda," *Renewable and Sustainable Energy Reviews*, vol. 15, pp. 925–935, 2011.
- [32] J. G. Slootweg, *Wind Power Modelling and Impact on Power System Dynamics*, Ridderkerk, the Netherlands: Delft University of Technology, 2003.
- [33] A. Feijóo and D. Villanueva, "Assessing wind speed simulation methods," *Renewable and Sustainable Energy Reviews*, vol. 56, pp. 473–483, 2016.
- [34] L. Freris, *Wind energy conversion systems*, Cambridge, UK: Prentice Hal, 1990.
- [35] T. Arslan, Y. M. Bulut and A. A. Yavuz, "Comparative study of numerical methods for determining Weibull parameters for wind energy potential," *Renewable and Sustainable Energy Reviews*, vol. 40, pp. 820–825, 2014.

- [36] H. Nfaoui, H. Essiarab and A. Sayigh, "A stochastic Markov chain model for simulating wind speed time series at Tangiers, Morocco," *Renewable Energy*, vol. 29, pp. 1407-1418, 2004.
- [37] A. Shamshad, M. Bawadi, W. W. Hussin, T. Majid and S. Sanusi, "First and second order Markov chain models for synthetic generation of wind speed time series," *Energy*, vol. 30, pp. 693-708, 2005.
- [38] H. Kantza, D. Holsteina, M. Ragwitzb and N. K. Vitanov, "Markov chain model for turbulent wind speed data," *Physica A*, vol. 342, pp. 315-321, 2004.
- [39] F. Y. Ettoumi, H. Sauvageot and A. Adane, "Statistical bivariate modeling of wind using first-order Markov chain and Weibull distribution," *Renewable Energy*, vol. 28, pp. 1787-1802, 2003.
- [40] A. Sanchez, M. Molina and A. Lede, "Dynamic model of wind energy conversion systems with PMSG-based variable-speed wind turbines for power system studies," *International Journal of Hydrogen Energy*, vol. 37, pp. 10064-10069, 2012.
- [41] A. Westlake, J. R. Bumby and E. Spooner, "Damping the power-angle oscillations of a permanent-magnet synchronous generator with particular reference to wind turbine applications," *IEE Proceedings - Electric Power Applications*, vol. 143, no. 3, pp. 269 - 280, May 1996.
- [42] C. Jauch, T. Cronin, P. Sørensen and B. Jensen, "A fuzzy logic pitch angle controller for power system stabilization," *Wind Energy*, vol. 10, pp. 19-30, 2007.
- [43] H. Geng, D. Xu, B. Wu and G. Yang, "Active damping for PMSG-based WECS with DC-Link current estimation," *IEEE Transactions on Industrial Electronics*, vol. 58, no. 4, pp. 1110-1119, 2011.
- [44] Xu, H. Geng and Dewei, "Stability analysis and improvements for variable-speed multipole PMSG-based wind energy conversion system," *IEEE Transactions on Sustainable Energy*, vol. 2, no. 4, pp. 459-466, 2011.
- [45] B. Han, H. L. Y. Wang and X. Zhang, "Supplementary power control of PMSG-based wind farms for system dynamic stability," in *IEEE international conference on electrical machines and systems*, Busan, Korea, 2013.
- [46] S. Rodrigues, R. T. Pinto, P. Bauer and J. Pierik, "Multi-objective optimization of a PMSG control system through small-signal analysis," in *IEEE ECCE Asia Downunder (ECCE Asia)*, Melbourne, VIC, 3-6 June 2013.

- [47] A. Adameczyk, R. Teodorescu and P. Rodriguez, "Control of full-scale converter based wind power plants for damping of low frequency system oscillations," in IEEE PowerTech, Trondheim, 2011.
- [48] X. Zhang, Y. Wang and H. Li, "Control of PMSG-based wind turbines to damp the power system oscillations," in IEEE PEDS 2011, Singapore, December 2011.
- [49] C. Jauch, S. M. Islam, P. Sørensen and B. B. Jensen, "Design of a wind turbine pitch angle controller for power system stabilisation," *Renewable Energy*, vol. 32, pp. 2334–2349, 2007.
- [50] Y. Zhang, X. Liu and B. Qu, "Distributed Model Predictive Load Frequency Control of Multi-Area Power System with DFIGs," *IEEE/CAA Journal of Automatica Sinica*, vol. 4, no. 1, pp. 125-131, 2017.
- [51] F. Díaz-González, M. Haub, A. Sumpera and O. Gomis-Bellmunt, "Participation of wind power plants in system frequency control: Review of grid code requirements and control methods," *Renewable and Sustainable Energy Reviews*, vol. 34, pp. 551–564, June 2014.
- [52] H. Shao, X. Deng and F. Cui, "Short-term wind speed forecasting using the wavelet decomposition and AdaBoost technique in wind farm of East China," *IET Generation, Transmission & Distribution*, vol. 10, no. 11, pp. 2585 - 2592, 2016.
- [53] R. Zárate-Miñano, M. Anghel and F. Milano, "Continuous wind speed models based on stochastic differential equations," *Applied Energy*, vol. 104, pp. 42–49, 2013.
- [54] G. S. Hawker, W. A. Bukhsh and S. Gill, "Synthesis of wind time series for network adequacy assessment," in *IEEE Power Systems Computation Conference (PSCC)*, 2024 June 2016.
- [55] Y. Wang, V. Silva and M. Lopez-Botet-Zulueta, "Impact of high penetration of variable renewable generation on frequency dynamics in the continental Europe interconnected system," *IET Renewable Power Generation*, vol. 10, no. 1, pp. 10 - 16, 2016.
- [56] O. AL-Masari and M. AL-Masari, "Influence of a Wind Farm on Power System Oscillatory Stability," *International Journal of Inventive Engineering and Sciences (IJIES)*, vol. 2, no. 9, pp. ISSN: 2319–9598, 2014.
- [57] K. Li, S. L. Bao, N. Y. Xin, Y. L. Zhong and M. Bazargan, "Small signal stability analysis with penetration of grid-connected wind farm of PMSG type," in IEEE

- International Conference on Advanced Power System Automation and Protection, 2011.
- [58] M. Polikarpova, P. Ponomarev and P. R oytt , “Direct liquid cooling for an outer-rotor direct-drive permanent-magnet synchronous generator for wind farm applications,” *IET Electric Power Applications*, vol. 9, no. 8, pp. 523 - 532, 2015.
- [59] Y. Alexandrova, S. Semken and M. Polikarpova, “Defining proper initial geometry of an 8 MW liquid-cooled direct-drive permanent magnet synchronous generator for wind turbine applications based on minimizing mass,” in *International Conference on Electrical Machines (ICEM)*, 2-5 Sept. 2012, DOI: 10.1109/ICEIMach.2012.6350036.
- [60] D. P. Kothari and I. J. Nagrath, *Modern Power System Analysis*, ISBN: 0070494894, 9780070494893: Tata McGraw-Hill Education, 2003.
- [61] IEEE, *IEEE Standard Dictionary of Electrical and Electronic Terms*, New York: IEEE, 1972.
- [62] S. Pan, T. Morris and U. Adhikari, “Classification of Disturbances and Cyber-Attacks in Power Systems Using Heterogeneous Time-Synchronized Data,” *IEEE Transactions on Industrial Informatics*, vol. 11, no. 3, pp. 650 - 662, 2015.
- [63] R. C. B. Hink, J. M. Beaver and M. A. Buckner, “Machine learning for power system disturbance and cyber-attack discrimination,” in *7th International Symposium on Resilient Control Systems (ISRCS)*, DOI: 10.1109/ISRCS.2014.6900095, 19-21 Aug. 2014.
- [64] M. S. Manikandan, S. R. Samantaray and I. Kamwa, “Simultaneous denoising and compression of power system disturbances using sparse representation on overcomplete hybrid dictionaries,” *IET Generation, Transmission & Distribution*, vol. 9, no. 11, pp. 1077 - 1088, August 2015.
- [65] IEEE, *IEEE Recommended Practice for Monitoring Electric Power Quality: IEEE Std 1159™-2009 (Revision of IEEE Std 1159-1995)*
- [66] J. F. Manwell and J. G. McGowan, *Wind Energy Explained: Theory, Design and Application*, Washington DC: John Wiley & Sons Ltd, 2009.
- [67] T. Al-Shemmeri, *Wind Turbines*, ISBN: 978-87-7681-692-6: Ventus Publishing ApS, 1<sup>st</sup> edition.
- [68] D. Pimentel, M. Herz, M. Glickstei, D. Pimentel, M. Herz, M. Glickstein, M. Zimmerman, R. Allen, K. Becker, J. Evans, B. Hussain, R. Sarsfeld, A. Grosfeld and

- T. Seidel, "Renewable Energy: Current and Potential Issues," *BioScience*, vol. 52, no. 12, pp. 1111-1120, 2002.
- [69] M. Lei, L. Shiyang, J. Chuanwen, L. Hongling and Z. Yan, "A review on the forecasting of wind speed and generated power," *Renewable and Sustainable Energy Reviews*, vol. 13, no. 4, pp. 915–920, 2009.
- [70] V. Romero-Ternero, "Influence of the fitted probability distribution type on the annual mean power generated by wind turbines. A case study at the Canary Islands," *Energy Conversion and Management*, vol. 49, no. 8, pp. 2047–2054, 2008.
- [71] J. Carta and D. Mentado, "A continuous bivariate model for wind power density and wind turbine energy output estimations," *Energy Conversion and Management*, vol. 48, no. 2, pp. 420–432, 2007.
- [72] T. Chang, "Estimation of wind energy potential using different probability density functions," *Applied Energy*, vol. 88, no. 5, pp. 1848–1856, 2011.
- [73] Z. Qin, W. Li and X. Xiong, "Estimating wind speed probability distribution using kernel density method," *Electr Power Systems Research*, vol. 81, no. 12, pp. 2139–2146, 2011.
- [74] D. Villanueva and A. Feijóo, "A genetic algorithm for the simulation of correlated wind speeds," *International Journal of Electrical Power and Energy Systems*, vol. 1, no. 2, pp. 107–112, 2009.
- [75] G. D'Amico, F. Petroni and F. Praticco, "First and second order semi-Markov chains for wind speed modeling," *Physica A*, vol. 392, pp. 1194-1201, 2012.
- [76] A. Otto, "Wind Atlas for South Africa," SANEDI, June 2004.
- [77] L. Herbst and J. Lalk, "A case study of climate variability effects on wind resources in South Africa," *Journal of Energy in Southern Africa*, pp. 2-10, August 2014.
- [78] T. C. Mosetlhe, A. A. Yusuff, Y. Hamam and A. A. Jimoh, "Estimation of Wind Speed Statistical Distribution at Vredendal, South Africa," *International Journal of Power and Energy Systems*, pp. DOI: 10.2316/P.2016.839-017, 2016.
- [79] Committee, Academy's Engineering Policy, WIND ENERGY implications of largescale deployment on the GB electricity system, Royal Academy of Engineering, April 2014.
- [80] P. Ji, C. B. Dai and S. Y. Wu, "A scheme on adaption detection of large-capacity wind turbines to the power grid," in *International Conference on Advanced Power System*

- Automation and Protection (APAP), DOI: 10.1109/APAP.2011.6180721, 16-20 Oct. 2011.
- [81] H. Li, Z. Chen and H. Polinder, "Optimization of Multibrid Permanent-Magnet Wind Generator Systems," *IEEE Transactions on Energy Conversion*, vol. 24, no. 1, pp. 82 - 92, 2009.
- [82] E. Kulunk, *Aerodynamics of Wind Turbines*, ISBN: 978-953-307-508-2: Available from: <http://www.intechopen.com/books/fundamental-and-advanced-topics-in-windpower/aerodynamics-of-windturbines>, 2011.
- [83] R. Gasch and J. Twele, *Wind Power Plants: Fundamentals, Design, Construction and Operation*, London: Springer, 2012.
- [84] I. Al-Bahadly, *Wind Turbines*, Rijek, Croatia: InTech, 2011.
- [85] B. Fox, D. Flynn, L. Bryans, N. Jenkins, D. Milborrow, M. O'Malley, R. Watson and O. Anaya-Lara, *Wind Power Integration Connection and system operational aspects*, London, United Kingdom: The Institution of Engineering and Technology, 2007.
- [86] S. Li, T. A. Haskew, R. P. Swatloski and W. Gathings, "Optimal and Direct-Current Vector Control of Direct-Driven PMSG Wind Turbines," *IEEE Transactions on Power Electronics*, vol. 27, no. 5, pp. 2325-2337, May 2012.
- [87] D. Vowles, C. Samarasinghe, M. Gibbard and G. Ancell, "Effect of Wind Generation on Small-Signal Stability - A New Zealand Example," in *Power and Energy Society General Meeting - Conversion and Delivery of Electrical Energy in the 21st Century*, 2008 IEEE, 2008.
- [88] R. Fernandez, R. Mantza and P. Battaiottoa, "Impact of wind farms on a power system: An eigenvalue analysis approach," *Renewable Energy-Elsevier*, vol. 32, pp. 1676- 1688, 2007.
- [89] L. Fan, Z. Miao and D. Osborn, "Impact of Doubly Fed Wind Turbine Generation on Inter-Area Oscillation Damping," in *Power and Energy Society General Meeting - Conversion and Delivery of Electrical Energy in the 21st Century*, 2008 IEEE, 2008.
- [90] F. Wu, X.-P. Zhang and P. Ju, "Impact of Wind Turbines on Power System Stability," in *2007 iREP Symposium- Bulk Power System Dynamics and Control - VII, Revitalizing Operational Reliability*, Charleston, SC, USA, August 19-24, 2007.
- [91] C. Wang, L. Shi, L. Wang and Y. Ni, "Small Signal Stability Analysis Considering Grid-Connected Wind Farms of DFIG Type," in *Power and Energy Society General*

- Meeting - Conversion and Delivery of Electrical Energy in the 21st Century, 2008  
IEEE, 2008.
- [92] W. Liu, R. Ge, H. Li and J. Ge, "Impact of Large-Scale Wind Power Integration on Small Signal Stability Based on Stability Region Boundary," *Sustainability*, vol. 6, no. ISSN 2071-1050, pp. 7921-7944, 2014.
- [93] F. Wu, X. P. Zhang and P. Ju, "Small signal stability analysis and control of the wind turbine with the direct-drive permanent magnet generator integrated to the grid," *Electric Power Systems Research*, vol. 79, no. 12, pp. 1661–1667, December 2009.
- [94] Y. Chen, P. Pillay and A. Khan, "PM wind generator topologies," *IEEE Transactions on Industrial Applications*, vol. 41, no. 6, pp. 1619–1626, Nov./Dec. 2005.
- [95] L. Lin, L. Song, W. Li and S. Jing, "Moda lanalysis concerning the control mode of doubly-fed induction generator," in *international conference on sustainable power generation and supply*, 2009.
- [96] H. Geng, D. Xu, W. B and G. Yang, "Comparison of oscillation damping capability in three power control strategies for PMSG-based WECS," *Wind Energy*, vol. 14, pp. 389–406, 2011.
- [97] R. Wang, L. Shi, L. Yao and Y. Ni, "Small-signal stability analysis with high penetration of grid-connected wind farm of PMSG type considering the wake effect," in *IEEE PES General Meeting | Conference & Exposition, National Harbor, MD*, 2014.
- [98] H. Ahmadi, H. Ghasemi and H. Lesani, "A comparative small-Signal stability analysis of PMSG and SCIG-based wind farms," in *25th International Power System Conference, Iran*, 2010.
- [99] N. Ullah, *Wind power—added value for network operation*, Ph. D Thesis: Chalmers University of Technology, 2008.
- [100] P. He, F. Wen, G. Ledwich and Y. Xue, "Small-signal stability analysis of power systems with high penetration of wind power," *Journal of Modern Power Systems and Clean Energy*, vol. 1, no. 3, pp. 241-248, 2013.
- [101] N. P. W. Strachan and D. Jovcic, "Stability of a variable-speed permanent magnet wind generator with weak AC grids," *IEEE Transactions on Power Delivery*, vol. 25, no. 4, pp. 2779-2787, 2010.



]

]

- [102] T. Knuppel, J. Nielsen and K. Jensen, "Small-signal stability of wind power system with full-load converter interfaced wind turbines," *IET Renewable Power Generation*, vol. 6, no. 2, pp. 79–91, 2012.
- [103] W. Hu, C. Su and Z. Chen, "Impact of wind shear and tower Shadow effects on power system with large-scale wind power penetration," in *IEEE Power Systems Delivery*, Melbourne, VIC, 2011.
- [104] H. Huang, C. Mao, J. Lu and D. Wang, "Small-signal modelling and analysis of wind turbine with direct drive permanent magnet synchronous generator connected to power grid," *IET Renewable Power Generation*, vol. 6, no. 1, pp. 48-58, 2012.
- [105] Z. Wei and S. Shaojian, "The small-signal stability analysis of a power system integrated with PMSG-based wind farm," in *IEEE Innovative Smart Grid Technologies - Asia (ISGT ASIA)*, Kuala Lumpur, Malaysia, 2014.
- [106] J. G. Venkatesh, M. Thirunavukkarasu and G. Sundar, "Damping enhancement of multi Parallel offshore PMSG-based wind turbine- using STATCOM," *Research Journal of Applied Sciences*, vol. 9, no. 8, pp. 496-502, 2014.
- [107] L. Wang and D.-N. Truong, "Dynamic stability improvement of four parallel-operated PMSG-based offshore wind turbine generators fed to a power system using a STATCOM," *IEEE Transactions on Power Delivery*, vol. 28, no. 1, pp. 111-119, January 2013.
- [108] C. Jauch, "Transient and dynamic control of a variable speed wind turbine with synchronous generator," *Wind Energy*, vol. 10, pp. 247–269, 2007.
- [109] Z. Miao, L. Fan, D. Osborn and S. Yuvarajan, "Control of DFIG-based wind generation to improve inter area oscillation damping," *IEEE Transaction on Energy Conversion*, vol. 24, pp. 415–422, 2009.
- [110] L. Fan, H. Yin and Z. Miao, "On active/reactive power modulation of DFIG-based wind generation for inter area oscillation damping," *IEEE Transactions on Energy Conversion*, vol. 26, pp. 513–521, 2011.

]

]

- [111] G. Delille, B. François and G. Malarange, “Dynamic frequency control support: A virtual inertia provided by distributed energy storage to isolated power systems,” in IEEE PES. on Innovative Smart Grid Technologies Conference Europe (ISGT Europe), 2010.
- [112] M. F. M. Arani and E. F. El-Saadany, “Implementing virtual inertia in DFIG-based wind power generation,” IEEE Transactions on Power Systems, vol. 28, no. 2, pp. 1373-1384, 2013.
- [113] H. T. Ma and B. H. Chowdhury, “Working towards frequency regulation with wind plants: Combined control approaches,” IET Renewable Power Generation, vol. 4, pp. 308–316, 2010.
- [114] Z. Zhang, Y. Wang, H. Li and Z. Su, “Comparison of inertia control methods for DFIGbased wind turbines,” in Proceeding of IEEE ECCE Asia Downunder (ECCE Asia), 2013.
- [115] Y. Wang, J. Meng, X. Zhang and L. Xu, “Control of PMSG-based wind turbines for system inertial response and power oscillation damping,” IEEE Transactions on Sustainable Energy, vol. 6, pp. 565–574, 2015.
- [116] Q. Shi, G. Wang, Y. Chen, L. j. Fu, W. Jiang and H. Huang, “Frequency Response Control of D-PMSG Based on the Active Disturbance Rejection Controller,” in 17th International Conference on Electrical Machines and Systems (ICEMS), Hangzhou, China, Oct. 22-25, 2014.
- [117] S. Wang, J. Hu and X. Y. Yuan', “Virtual synchronous control for grid-connected DFIG-based wind turbines,” IEEE Journal of Emerging and Selected Topics in Power Electronics, vol. 3, no. 4, pp. 932-944, 2015.
- [118] S. Heier, Grid Integration of Wind Energy Conversion Systems, Chichester: John Wiley & Sons, 2005.
- [119] S. Meyn and R. Tweedie, Markov Chains and Stochastic Stability, Springer-Verlag, 2005.

]

]

- [120] F. O. Hocaoglu, O. N. Gerek and M. Kurban, "The Effect of Markov Chain State Size for Synthetic Wind Speed Generation," in Proceedings of the 10th International Conference on Probabilistic Methods Applied to Power Systems, 2008. PMAPS '08, May 2008.
- [121] M. Scott, Characterizations of strong ergodicity for continuous time Markov chains, PhD thesis: Iowa State University Ames, 1979.
- [122] H. Aksoy, Z. F. Toprak, A. AYTEK and N. E. Unal, "Stochastic generation of hourly mean wind speed data," *Renewable Energy*, vol. 29, pp. 2111–2131, 2004.
- [123] E.-S. C. Agustín, "Estimation of Extreme Wind Speeds by Using Mixed Distributions," *Ingeniería, Investigación y Tecnología*, vol. 14, no. 2, pp. 153–162, 2013.
- [124] P. Ramirez and J. Carta, "Influence of the data sampling interval in the estimation of the parameters of the Weibull wind speed probability density distribution: a case study," *Energy Conversion and Management*, vol. 46, no. 15-16, pp. 2419–38, 2005.
- [125] R. Datta and V. T. Ranganathan, "A Method of Tracking the Peak Power Points for a Variable Speed Wind Energy Conversion System," *IEEE Transaction on Energy Conversion*, vol. 18, no. 1, pp. 163-168, 2003.
- [126] T. Ramachandra, D. Subramanian and N. Joshi, "Wind energy potential assessment in Uttaranada district of Karnataka, India," *Renewable Energy*, vol. 10, no. 4, pp. 585–611, 1997.
- [127] B. Bhaskar, *Energy Security and Economic Development in India: a holistic approach*, The Energy and Resources Institute (TERI), 2013.
- [128] X. H. Ma, D. Tian and Z. H. Zhang, "Combined wind speed model based on real wind data," in *International Conference on Renewable Power Generation (RPG 2015)*, 2015.
- [129] W. Gullvik, L. Norum and R. Nilsen, "Active damping of resonance oscillations in LCL-filters based on virtual flux and virtual resistor," in *European Conference on Power Electronics and Applications*, Aalborg, Denmark, 2007.

]

]

- [130] C. Bottasso, A. Crose, C. Riboldi and Y. Nam, “Multi-layer control architecture for the reduction of deterministic and non-deterministic loads on wind turbines,” *Renewable Energy*, vol. 51, pp. 159–169, 2013.
- [131] E. Bossanyi, “Individual blade pitch control for load reduction,” *Wind Energy*, vol. 6, p. 119–128, 2002.
- [132] S. K. Yun, Y. C. Il and I. M. Seung, “Tuning of the PI controller parameters of a PMSG wind turbine to improve control performance under various wind speeds,” *Energies*, vol. 8, pp. 1406-1425, 2015.
- [133] K. Ogata, *Modern Control Engineering*, New Jersey: Prentice Hall, 2002.
- [134] D. J. Inman, *Engineering Vibration*, Upper Saddle: NJ: Pearson Education, Inc., 2008.
- [135] University of Illinois Board of Trustees, “Illinois Centre for a Smarter Electric Grid (ICSEG),” Information Trust Institute, 01 01 2013. [Online]. Available: <http://icseg.iti.illinois.edu/ieee-14-bus-system/>. [Accessed 01 01 2017].
- [136] S. K. M. Kodsi and C. A. Cañizares, “Modelling and simulation of IEEE 14 bus system with FACTS controllers,” Department of Electrical and Computer Engineering, University of Waterloo, Waterloo, 2003.
- [137] N. Mithulananthan, *Hopf Bifurcation Control and Indices for Power System with Interacting Generator and FACTS Controllers*, Canada: PhD dissertation, Department of Electrical and Computer Engineering, University of Waterloo, 2002.
- [138] V. Akhmatov and H. Knudsen, “An aggregate model of a grid-connected, large-scale, offshore wind farm for power stability investigations—importance of windmill mechanical system,” *International Journal of Electrical Power & Energy Systems*, vol. 25, no. 9, pp. 707-719, 2002.
- [139] J. T. Bialasiewicz and E. Muljadi, “Analysis of Renewable-Energy Systems Using RPM-SIM Simulator,” *IEEE Transactions on Industrial Electronics*, vol. 53, no. 4, pp. 1137-1143, 2006.

]

]

- [140] N. Fischer, G. Benmouyal and S. Samineni, "Tutorial on the Impact of the Synchronous Generator Model on Protection Studies," SEL Journal of Reliable Power, vol. 3, no. 1, pp. 1-12, 2012.
- [141] E. W. Kimbark, Power System Stability: Synchronous Machines, New York: Publications, Inc., 1956.
- [142] IEEE Power Engineering Society, "IEEE Xplor Digital Library," 21 April 2006. [Online]. Available: <http://ieeexplore.ieee.org/stamp/stamp.jsp?arnumber=1626480>. [Accessed 06 January 2017].
- [143] N. Muromba and D. Pudney, "Shunt capacitor banks increase capacity of distribution networks," Energize, vol. May, pp. 30-33, 2011.
- [144] MathWorks, "Three-phase harmonics," MathWorks, [Online]. Available: <https://www.mathworks.com/help/phymod/sps/examples/three-phase-harmonicfilters.html>. [Accessed 08 01 2016].
- [145] F. Milano, Power System Analysis Toolbox documentation, Federico Milano, 2005.
- [146] P. V. Kishore, S. R. Reddy and P. V. Kishore, "Modelling and simulation of 14-bus system with D-STATCOM for power quality improvement," Indian Journal of Science and Research, vol. 3, no. 1, pp. 73-79, 2012.

## APPENDIX A

Table A1. Wind turbine driven PMSG parameters [144]

Parameter	Value
Terminal voltage	575 V
+	0.0377 mΩ
Rated power	1.5 MW
Rated frequency	60 HZ
Filter resistance	0.003 p.u.
Filter inductance	0.3 p.u.
DC-link voltage	1150 V
Number of pole pairs	48
,	0.3 mH
,	1.48 V.s.
Moment of inertia	35000 kgm <sup>2</sup>

Table A2. Control parameters of the PMSG

Parameter	Value	Parameter	Value
,	0.14 pu	,	0.001 s <sup>-1</sup>
,	2.72 s <sup>-1</sup>	,	1.0 pu
,	0.84 pu	Lag pole	-10.0
,	0.25 pu	Lead pole	-25.0
,	200 pu	Lag zero	-25.0
,	8.0 pu	Lead zero	-23.0
,	400 s <sup>-1</sup>	Lead-lag zeroes	-23.0, -25.0
,	0.83 pu	Lead-lag poles	-25.0, -10.0
,	5.0 s <sup>-1</sup>	,	,
,	1.0 pu	,	,

Table A3. Virtual control and SDC parameters

Parameter	Value
R <sub>v</sub>	3.0 p.u.
R <sub>d</sub>	50.0 p.u.
L <sub>D</sub>	1.0 p.u.
L <sub>Q</sub>	1.0 p.u.
L <sub>Qsd</sub>	0.1 p.u.

$L_{qsq}$	0.1 p.u.
N	1
$L_{Qq}$	9.10 p.u.
$L_{Qd}$	9.10 p.u.
Phai_D	0.5 p.u.
SDC d-axis filter gain	0.5
SDC d-axis filter time constant	0.5 sec
SDC q-axis filter gain	100/3
SDC q-axis filter time constant	100/3 sec
SDC d-axis proportional gain	80
SDC d-axis integral gain	12 sec
SDC q-axis proportional gain	0.2
SDC q-axis integral gain	0.2 msec

## APPENDIX B

Table B1. IEEE-14 bus line data

Branch name	From bus	To bus	Resistance (pu)	Reactance (pu)	MVA rating
Line1-2	1	2	0.01937	0.05916	120.0
Line1-5	1	5	0.05402	0.22300	65.0
Line2-3	2	3	0.04697	0.19794	36.0
Line2-4	2	4	0.05810	0.17628	65.0
Line2-5	2	5	0.05693	0.17384	50.0
Line3-4	3	4	0.06700	0.17099	65.0
Line4-7	4	7	0.00000	0.20900	45.0
Line4-9	4	9	0.00000	0.55618	55.0
Line4-5	4	5	0.01335	0.04209	32.0
Line5-6	5	6	0.00000	0.25020	45.0
Line6-11	6	11	0.09495	0.19887	18.0
Line6-12	6	12	0.12285	0.25575	32.0
Line6-13	6	13	0.06613	0.13024	32.0
Line7-8	7	8	0.00000	0.17615	32.0
Line7-9	7	9	0.00000	0.11000	32.0
Line9-10	9	10	0.03181	0.08448	32.0
Line9-14	9	14	0.01270	0.27033	32.0
Line10-11	10	11	0.08203	0.19202	12.0
Line12-13	12	13	0.22087	0.19985	12.0
Line13-14	13	14	0.17089	0.34795	12.0

Table B2. IEEE-14 bus data

Bus Number	Bus Voltage		Generation		Load		Reactive Power Limits	
	Magnitude (p.u.)	Phase Angle (deg)	Real Power (MW)	Reactive Power (MVAR)	Real Power (MW)	Reactive Power (MVAR)	Q <sub>min</sub> (MVAR)	Q <sub>max</sub> (MVAR)



1	1.06	0	91.0	0	0	0	0	10.0
2	1.045	0	91.0	-16.9	21.7	12.7	-42.0	50.0
3	1.01	0	0	0	94.2	19.1	23.4	40.0
4	1.00	0	0	0	47.8	-3.9	-	-
5	1.00	0	0	0	7.6	1.6	-	-
6	1.00	0	39.0	0	11.2	7.5	-	-
7	1.00	0	0	0	0	0	-	-
8	1.00	0	0	0	0	0	-	-
9	1.00	0	0	0	29.5	16.6	-	-
10	1.00	0	0	0	9.0	5.8	-	-
11	1.00	0	0	0	3.5	1.8	-	-
12	1.00	0	0	0	6.1	1.6	-	-
13	1.00	0	0	0	13.8	5.8	-	-
14	1.00	0	0	0	14.9	5.0	-	-

Table B3. Synchronous machine parameters

Parameter	Value
Inertia constant	4.0 s
Damping coefficient	0
Impedance	0.22/15+j 0.22 p.u.
Synchronous speed	314 rad/sec

Table B4. Governor and turbine model parameters

Parameter	Value
R	0.05
$K_d$	0
$T_1$	0
$T_2$	2.67 s
$T_3$	1.2 s

Table B5. Exciter model parameters

Parameter	Value
K	300
$T_A$	0.001 s
$T_B$	0.02 s
$T_E$	0 s

Table B6. Capacitor and filter banks parameters

Parameter	SCB	Filter 1	Filter 2	Filter 3
Nominal Reactive power (p.u.)	-1.0	0.5	0.5	0.5
Quality Factor	-	2	20	7
Tuning Frequencies (Hz)	50	150	[550, 650]	1200

Table B7. SVC parameters

Parameter	Value
	1000

	0.001
	1.0
	0 s
	10 s
	0.01 s
	0.001 s
	0.1 p.u.

Table B8. STATCOM parameters

Parameter	Value	Parameter	Value	Parameter	Value
R	0.0017 p.u.	L	0.05 p.u.	C	3.8e-8 F